ARL

The University of Texas at Austin

TECHNICAL REPORT

ARL-TR-97-3
15 April 1997

Copy Number 8

Development and Tests of a Low Cost Passive Millimeter Wave Sensor

Final Report under Contract N00039-91-C-0082
TD No. 04A1003, Passive Millimeter Wave Sensor
2 March 1992 - 31 December 1997

Robert L. Rogers
David L. Fisher
Heinrich D. Foltz

Prepared for: Defense Special Weapons Agency
Alexandria, VA 22310-3398

Monitored by: Naval Sea Systems Command
Department of the Navy • Washington, DC 20362-5101

Applied Research Laboratories•The University of Texas at Austin•Post Office Box 8029•Austin, Texas 78713-8029

REPORT DOCUMENTATION PAGE

Form Approved
OMB No. 0704-0188

1. AGENCY USE ONLY (Leave blank)	2. REPORT DATE	3. REPORT TYPE AND DATES COVERED
	15 Apr 97	final 2 Mar 92 - 31 Dec 97

4. TITLE AND SUBTITLE

Development and Tests of a Low Cost Passive Millimeter Wave Sensor, Final Report under Contract N00039-91-C-0082, TD No. 04A1003, Passive Millimeter Wave Sensor

5. FUNDING NUMBERS

N00039-91-C-0082
TD No. 04A1003

6. AUTHOR(S)

Rogers, Robert L. Fisher, David L. Foltz, Heinrich D.

7. PERFORMING ORGANIZATION NAMES(S) AND ADDRESS(ES)

Applied Research Laboratories
The University of Texas at Austin
P.O. Box 8029
Austin, Texas 78713-8029

8. PERFORMING ORGANIZATION REPORT NUMBER

ARL-TR-97-3

9. SPONSORING/MONITORING AGENCY NAME(S) AND ADDRESS(ES)

Defense Special Weapons Agency
Alexandria, VA 22310-3398

Naval Sea Systems Command
Department of the Navy
Washington, DC 20362-5101

10. SPONSORING/MONITORING AGENCY REPORT NUMBER

11. SUPPLEMENTARY NOTES

12a. DISTRIBUTION/AVAILABILITY STATEMENT

Approved for public release; distribution is unlimited.

12b. DISTRIBUTION CODE

13. ABSTRACT (Maximum 200 words)

(see reverse side)

14. SUBJECT TERMS

millimeter waves
millimeter wave integrated circuit
passive sensor
physical security
radiometer
security sensor
total power radiometer

15. NUMBER OF PAGES

84

16. PRICE CODE

17. SECURITY CLASSIFICATION OF REPORT	18. SECURITY CLASSIFICATION OF THIS PAGE	19. SECURITY CLASSIFICATION OF ABSTRACT	20. LIMITATION OF ABSTRACT
UNCLASSIFIED	UNCLASSIFIED	UNCLASSIFIED	SAR

13. This report describes an effort to develop and test a passive millimeter wave (PMMW) sensor for application as a physical security sensor. It also describes the successful implementation of a total power radiometer at 27.7-GHz center frequency as the sensor. The sensor that was demonstrated was completely fabricated from printed circuit board components. The architecture of the down-converter was coplanar waveguide. This means that no via-holes were required for the rf section. All the critical elements of the receiver were demonstrated with low cost components. The thermal resolution of the radiometer was better than 0.1 K.

Testing showed that the sensor performed comparably to a passive infrared (PIR) sensor in most interior environments. Tests were conducted with simultaneous measurements by colocated sensors so that direct comparisons could be made between the PIR and the PMMW sensor. The PMMW sensor was less susceptible to evasive efforts, especially simple techniques. The PMMW sensor appeared to perform much better in an exterior environment. Reliable exterior target detections were made at a range of 200 ft with a single sensor. Furthermore, the sensor still detected targets at 200 ft when the ambient temperature was 99°F. This has significant application in areas such as desert and coastal environments.

Estimates for the probability of detection and probability of false alarm which are based on the measured data are provided for both the PIR sensor and the PMMW sensors. These estimates show that the PMMW sensor can provide good probability of detection with a low probability of false alarm in both the interior and the exterior environment. The PIR sensor, in contrast, can provide good detections only in the interior environment and made no detections in the exterior environment testing performed.

TABLE OF CONTENTS

This page intentionally left blank.

LIST OF FIGURES

LIST OF TABLES

This page intentionally left blank.

PREFACE

This is the final report on work that Applied Research Laboratories, The University of Texas at Austin (ARL:UT), was tasked to perform under Contract N00039-91-C-0082, TD No. 04A1003, Passive Millimeter Wave Sensor.

This page intentionally left blank.

1. INTRODUCTION

This report documents the results of a project intended to develop the technology and demonstrate the proof of concept for using millimeter wave radiometers as passive sensors for physical security. Millimeter wave radiometers have been in use for many years. However, they have traditionally been expensive and bulky primarily because they utilize waveguide components. Recent developments in microwave/millimeter wave integrated circuits (MMICs) using both silicon (Si) and gallium arsenide (GaAs) have resulted in the fabrication of these radiometers (at least in some frequency bands) at a much lower cost than was possible in the past. The development of this technology was driven in the early stages by the U.S. Department of Defense. It is now rapidly being adopted in the commercial sector and used in many commercial communications applications, such as satellite networks and wireless communications. Good performance amplifiers and down-converters have been fabricated for use at millimeter wave frequencies[1,2] although many of these chips are not widely available yet. However, the development of low noise, high gain Si-based MMICs has made possible the realization of wideband, low noise, high gain amplifiers that have sufficiently good performance for radiometers. The overall outlook is good for the production of these types of sensors at costs acceptable for physical security sensors in both the civilian and military environments.[3,4,5]

The work reported here describes the development of a radiometer using MMICs in conjunction with a low cost down-converter fabricated on printed circuit board and using coplanar waveguide architecture that was initially studied at Applied Research Laboratories, The University of Texas at Austin.[6] This design resulted in a radiometer in which the major rf components, including the down-converter module, were fabricated on printed circuit boards. This means that a low cost sensor utilizing this technology can be built and will function very effectively as an intrusion detection sensor.

1.1 POTENTIAL

Passive millimeter wave (PMMW) sensors detect the thermally emitted radiation from a target in the millimeter wave part of the electromagnetic

spectrum (typically, the wavelengths that range from 1 mm to 1 cm). The sensor documented in this report operated at 27 GHz, which corresponds to a wavelength slightly longer than 1 cm. This type of sensor is similar to radiometers that have been used for remote sensing for many years.[7] However, the application here requires a much lower cost of fabrication and has as good or better thermal sensitivity than that offered by remote sensing radiometers. In contrast, passive infrared (PIR) sensors usually detect wavelengths ranging from 8 to 14 μm. The longer wavelengths at millimeter wave frequencies can penetrate non-metallic substances with low moisture content. This includes most types of clothing, most plastics, and commonly used construction materials, such as Sheetrock (gypsum wallboard) and plywood. Furthermore, a PMMW receiver is essentially a very sensitive rf receiver.[8] This means that it directly detects the electromagnetic fields from the target, so no elements (i.e., piezoelectric) are used in the sensor that are inherently sensitive to mechanical vibration. In contrast, to detect infrared radiation typical PIR sensors use thermally sensitive pyroelectric materials that are inherently sensitive to mechanical vibrations because all pyroelectric materials are also piezoelectric materials. These features give the PMMW sensor several advantages over the common passive infrared sensors: long-range passive exterior detection, even when the ambient temperature exceeds the target temperature; low susceptibility to vibration-induced false alarms; absolute radiometric signal output; long wavelength detection; and penetration through heavy clothing, drywall, some types of doors, fog, mist, and other atmospheric obscurants.

Test results included in this report demonstrate these enhanced capabilities. The passive millimeter wave sensor prototype fabricated in this work demonstrated during our testing a number of significant advantages over current infrared sensors. Test results showing superior performance were obtained in five areas:

(1) Superior detection range was demonstrated by the PMMW sensor in the exterior environment; detection ranges of 200 ft with high signal-to-noise ratios (SNRs) were achieved with human targets.

(2) The PMMW sensor is not affected nearly as strongly by exterior environmental fluctuations; detection ranges of 200 ft were achieved even in ambient temperatures of 37°C (99°F).

(3) The PMMW sensor demonstrated the ability to sense targets through clothing and wall materials such as Sheetrock, plywood, and Styrofoam.

(4) The PMMW sensor demonstrated the ability to sense through heavy clothing, and hence sense the whole body as a detection; this is an important advantage for long range detection.

(5) The PMMW sensor demonstrated superior response time to a target moving rapidly across the field of view of the sensor.

Measurements with the PMMW sensor colocated with a PIR sensor show that the PMMW sensor can penetrate wall material, such as Sheetrock and plywood, as well as Styrofoam and heavy clothing. Furthermore, the PMMW sensor very effectively covers long corridors. The maximum interior detection range was 115 ft. As previously stated, our results indicate that the PMMW sensor is extremely effective in an exterior environment and has measured detection ranges of as much as 200 ft with the proof-of-concept sensor. Perhaps the most remarkable feature of this sensor is that it can detect human targets at ranges of as much as 200 ft when the ambient temperature is 37°C (99°F). This means that the PMMW sensor is effective in an exterior environment at high ambient temperatures when infrared sensors are, for all practical purposes, blind. This is a significant advantage in desert and coastal environments where ambient temperatures are often at or above human skin temperature.

From the results reported here, several possible applications of the PMMW sensor are apparent:

(1) as a covert or hidden interior sensor;

(2) as a sensor used in conjunction with a conventional sensor to reduce nuisance alarms and aid in target discrimination;

(3) for detecting targets from moving platforms and identifying human targets;

(4) as a long-range exterior detection sensor;

(5) for detecting swimmers or small craft on the water surface.

These applications stem from the way in which the sensor operates and the fact that the long wave passive detection permits an assessment of the target when combined with the output from conventional infrared sensors.

Before fabricating the sensor, two configurations of radiometers were considered: total power radiometer and Dicke-switched radiometer. Total power radiometers are very simple and inexpensive to build. However, they can suffer from 1/f noise problems and thermal drift. Dicke-switched radiometers (named after the inventor of the technique, R. H. Dicke) have very good thermal stability and few or no problems with 1/f noise.[9] At the time this technique was developed (in 1946), the state of microwave devices was such that the direct total power radiometer was not a practical configuration. In the last 15 years, substantial improvements in solid state microwave devices have allowed the construction of devices that make the total power radiometer a practical configuration for some applications. In this application, where a highly sensitive "trip wire" radiometer is needed, a total power radiometer is the best choice. It is the simplest and least expensive to build. When sensor cost is a major factor, keeping the component cost as low as possible while making the sensor as sensitive as possible makes the total power radiometer an attractive option. The PMMW sensor has one other important advantage over the Dicke-switched radiometer as well, and that is its radiometric temperature resolution. In principle, the total power radiometer provides twice as much thermal resolution and, hence, twice the sensitivity of a Dicke radiometer for a given noise level that can practically be attained in a receiver. In security sensors, it is important to have very low false alarm rates. For a given probability of detection, the probability of a false alarm decreases as the sensitivity of the sensor increases.

The following report consists of four sections. Section 2 describes the sensor design and some of the salient features of the sensor. Section 3 gives the performance calculations for the probabilities of false alarms and detections. Section 4 describes the results from a number of tests that were run with the sensor. Section 5 summarizes the test results and gives an outline for future development.

2. SENSOR DESCRIPTION

2.1 INTRODUCTION

A block diagram of the sensor is shown in Fig. 2.1. As mentioned previously, the sensor is a total power radiometer. This section will describe the components of the sensor and how the performance of those components can affect the overall sensor performance. The most difficult component to fabricate is the high frequency down-converter. A major portion of the development effort was spent on designing this component so that it would be very inexpensive to build. The entire down-converter circuit board has only one transistor for the local oscillator and a diode pair for the balanced mixer. All the circuit designs use a coplanar waveguide (CPW), which has the important characteristic of allowing the construction of the circuit board without via-holes in the substrate.[10] Furthermore, the substrate is not required to be extremely thin, which makes fabrication much simpler. This configuration is believed to be the best choice for a low cost sensor intended for target detection.

2.2 DOWN-CONVERTER AND RADIOMETER PERFORMANCE

The most important parameters for the performance of the radiometer are the mixer noise, the conversion loss, and the amplifier noise. In this section, two down-converter modules that were built and tested are discussed. The conversion loss shown for the down-converter module is the ratio of the signal going into the rf port of the mixer to the signal leaving the intermediate frequency (IF) port. If the mixer noise is omitted, the overall noise figure of the receiver is approximately the noise figure of the first IF amplifier plus the conversion loss. The mixer noise is estimated from measurements to add about 1 dB to the overall receiver noise figure. The mixer designed and fabricated for this sensor was a single-balanced mixer, which balanced the local oscillator (LO) signal with respect to the rf signal. This minimizes the leakage of the LO signal from the rf port. Figure 2.2 shows a block diagram of the down-converter module with the filters for the diplexer. The transistor used in the LO was a Fujitsu FHX-14X high electron mobility (HEMT) transistor. The diodes used in the down-converter mixer were Hewlett Packard HSCH-9201 gallium arsenide (GaAs) mixer diodes. Figure 2.3 shows a photograph of a down-converter board.

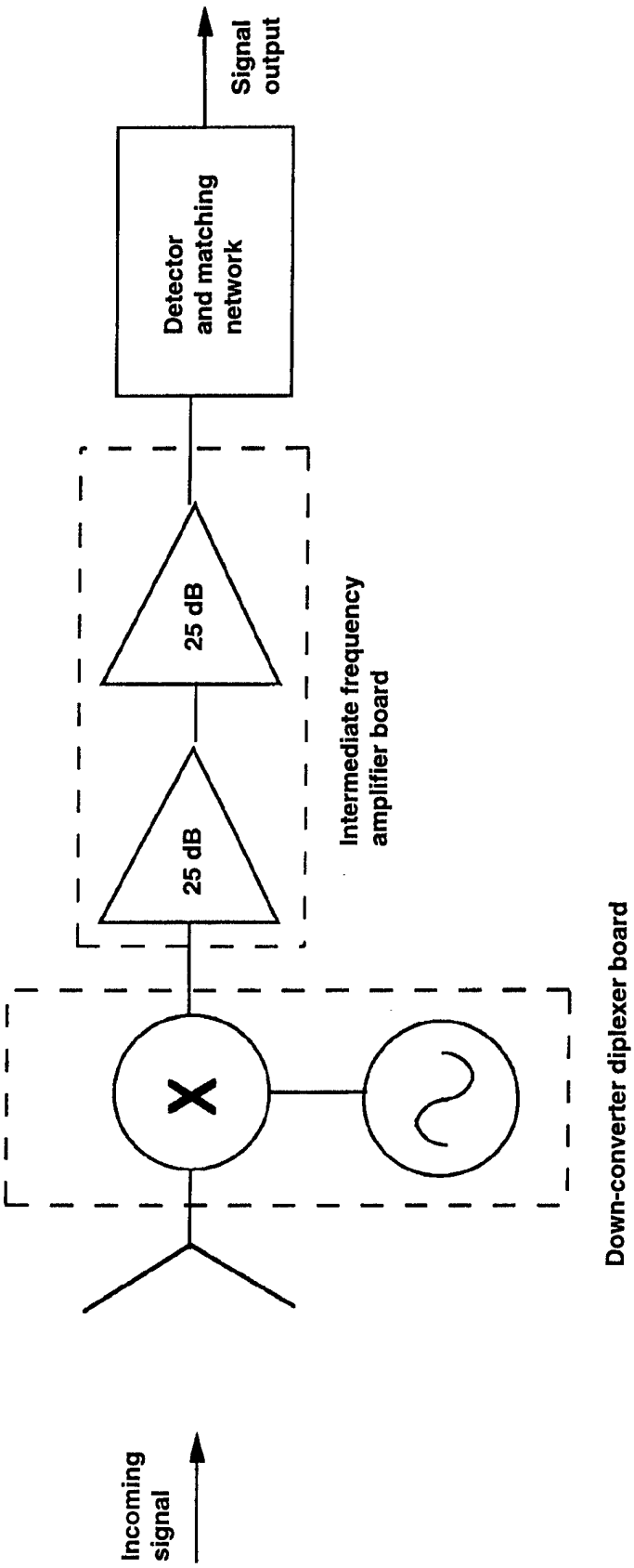

Figure 2.1
Block diagram of the sensor.

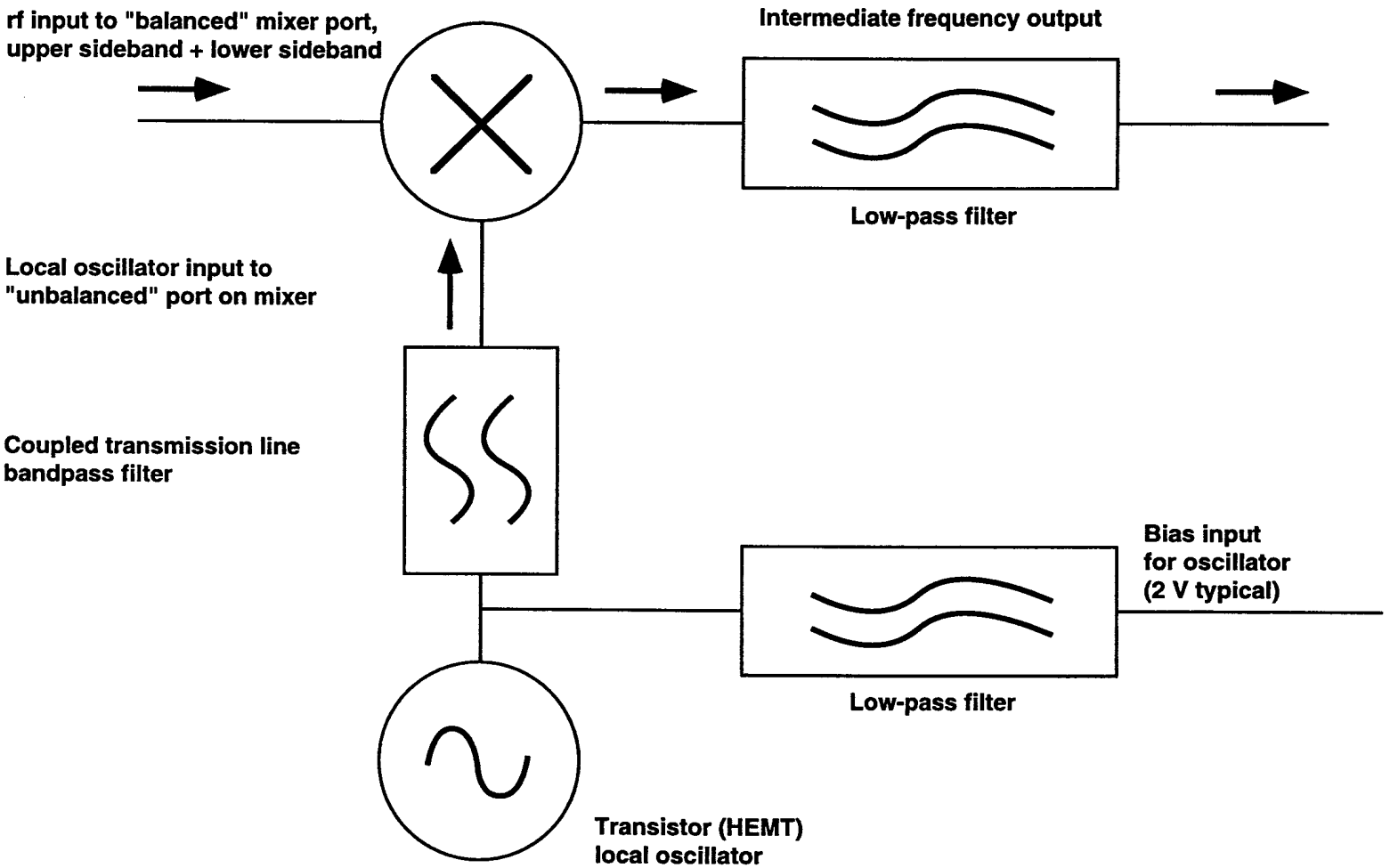

Figure 2.2
Block diagram of down-converter diplexer board.

ARL:UT
AS-97-97
RLR - rfg
4-97

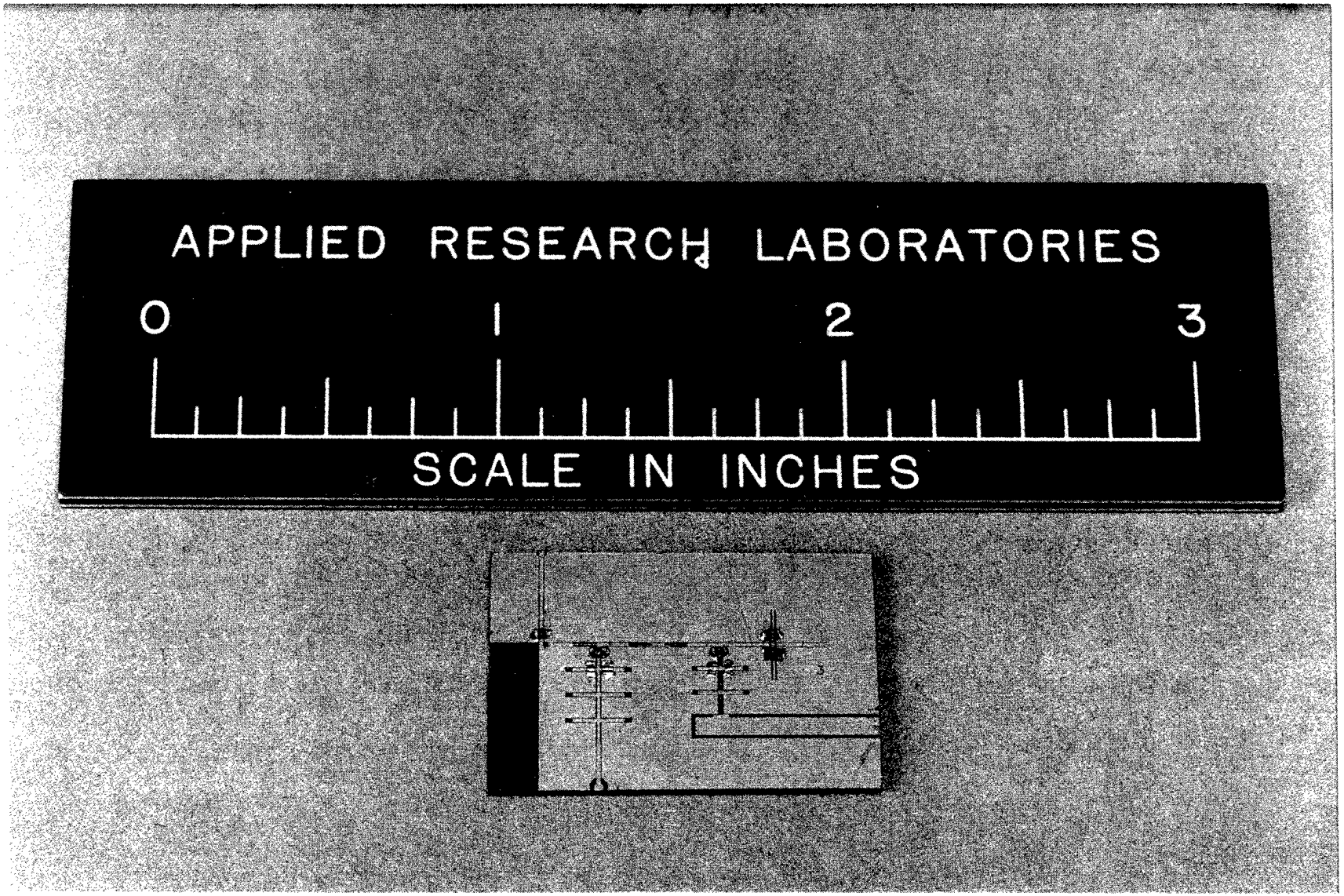

Figure 2.3
Photograph of down-converter diplexer board.

Figure 2.4 shows the conversion loss of a down-converter module with a LO frequency of 31.4 GHz. The conversion loss is approximately the same for both the upper and the lower sidebands. The conversion loss varies from about 9 to 11 dB. It is not known how much signal loss the discontinuity of the package connector transition to the CPW ground plane adds to the conversion loss. At this frequency, it is assumed to be 1 dB. Calculations indicate that this conversion loss is a little higher than was expected. By measuring the conversion loss of the mixer at very low signal levels and then increasing the signal input power until the IF output from the mixer begins to saturate, we can approximately determine the LO drive level.[11] These measurements indicate that this unit had about 1 dBm of LO drive. This suggests that part of the conversion loss may be due to low LO drive. We believe that the problem is most likely the low frequency arms of the diplexer absorbing some of the LO power. If this is correct, then this problem should be easy to correct. Current versus voltage measurements indicate that the diode resistance at dc is near manufacturer specifications. The temperature resolution of the radiometer is the measure of performance that we use to determine how well the overall sensor works.

The thermal resolution, ΔT, is the minimum observable shift in temperature at the output of the sensor. For the radiometer we are considering here this can be calculated from[8]

$$\Delta T = K\frac{T_{sys}}{\sqrt{B \bullet \tau}} \quad , \tag{2.1}$$

where T_{sys} is the system noise temperature in kelvin, B is the radiometer bandwidth in Hz, and τ is the averaging time in seconds. K is a constant, which is 1 for a total power radiometer. If we were considering a Dicke-switched radiometer, the constant would be 2, which effectively doubles the noise level. This difference in sensitivity as well as the greater simplicity is why we have considered only a total power radiometer for this effort.

If an average value of the conversion loss is assumed to be about 10 dB across the band and is used to estimate performance, the approximate value of the front-end noise of this down-converter is about 13.5 dB. This corresponds to a minimum estimated front-end noise temperature of about 6500 K. For a

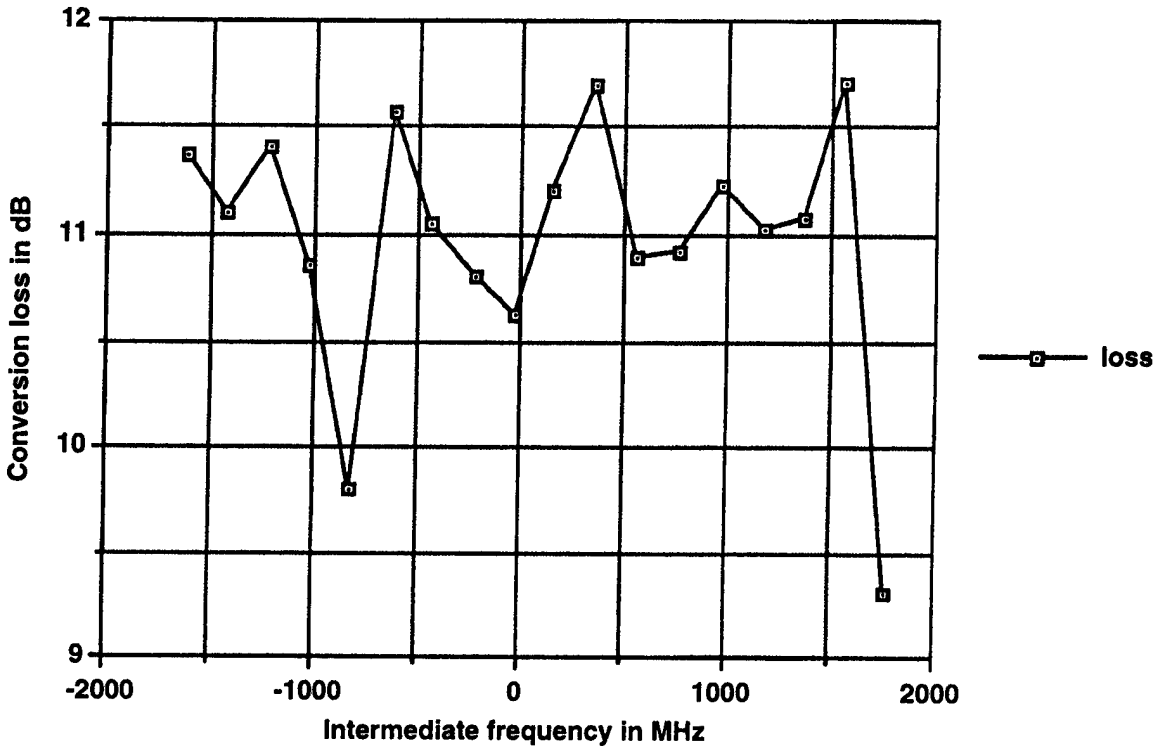

Figure 2.4
Conversion loss of a down-converter module with a local oscillator frequency of 31.4 GHz.

ARL:UT
AS-97--99
RLR - rfg
4-97

1.5-GHz bandwidth receiver with a 1-s integration time, the radiometric temperature resolution is about 0.16 K.

Figure 2.5 shows the conversion loss curve for a down-converter board operating at 27.7 GHz. The upper sideband has a lower conversion loss than the lower sideband. An interesting feature of the conversion loss in the upper sideband is that, at certain frequencies, the conversion loss drops close to 5 dB. The ideal conversion loss for a down-converter is 3 dB. For a down-converter with an integrated LO on a uniplanar circuit board, this is very respectable performance. The average value of the conversion loss in the lower sideband is about 10 dB, while the average value for the conversion loss in the upper sideband is about 7 dB. Thus, the overall conversion loss is around 8 dB. This corresponds to a minimum estimate for noise figure for the same receiver, as discussed in the previous paragraph, of about 10.5 dB, or a noise temperature of about 3200 K. The temperature resolution, ΔT, of the radiometer (total power) will be about 0.08 K, again with a 1.5-GHz bandwidth and a 1-s integration time. This is very close to what was actually measured.

It is estimated that with improvements in transistors and the use of thicker copper on the circuit board, the conversion losses could be reduced an average of about 1 dB. The performance of this mixer could be improved to about 7 dB over the band of interest with the present components.

If much better performance is desired, then a low noise amplifier could conceivably be added to the front end of the receiver. The advantage of doing this is that the front-end amplifier noise figure is better than the mixer front-end noise performance. For example, a front-end amplifier with a 5-dB noise figure will have noise temperature of about 920 K. The radiometric temperature resolution will then be about 0.023 K. This is more than three times the resolution that can be obtained with a mixer front-end sensor. In addition, this reduces the LO leakage out of the antenna.

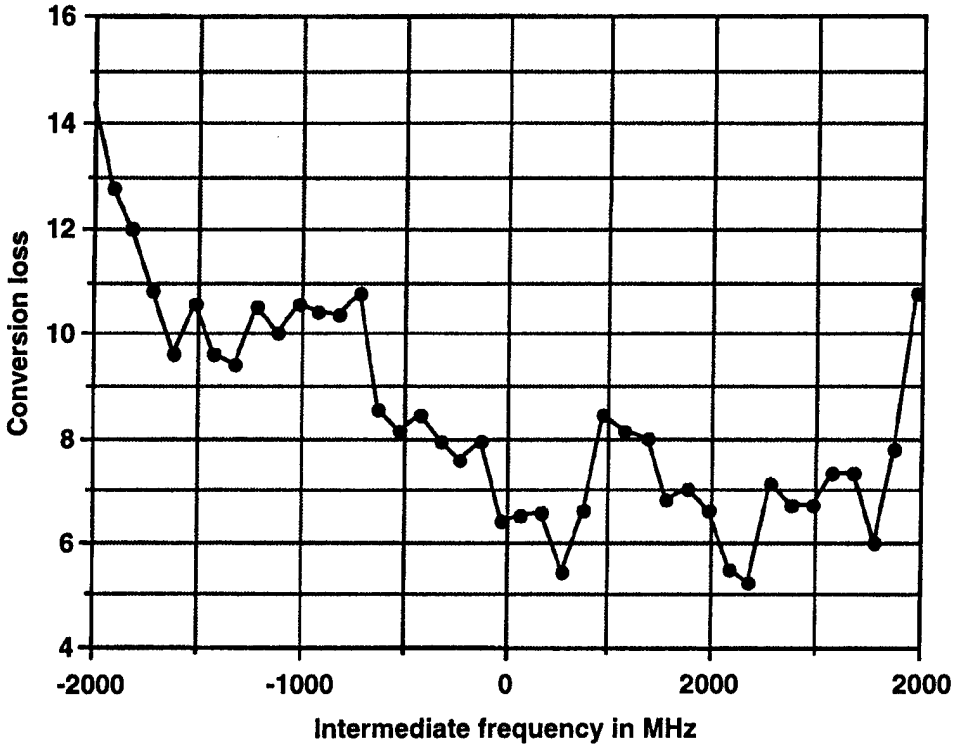

Figure 2.5
Conversion loss curve of a down-converter board operating at 27.7 GHz.

2.3 INTERMEDIATE FREQUENCY AMPLIFIERS AND DETECTOR

The IF amplifier section provides the necessary gain to bring the signal from the down-converter output up to the level that the detector diode can sense. Figure 2.6 shows a diagram of the IF amplifier section. For the test model, a small resistor heater was used to provide a very small heat input with a feedback from a temperature sensor to help thermally stabilize the amplifier. The average power consumption was small and will be smaller if the amplifier housing is insulated.

The amplifiers used were Hewlett Packard Avantek INA-03 amplifiers, which cost about $4 per unit in small quantities. The noise figure of these amplifiers is about 2.5 dB, and the usable frequency band is from about 100 MHz to 1.5 GHz. Thus, the IF amplifier stage is very low cost. The whole assembly was made on standard FR4 printed circuit board, and standard low cost printed circuit fabrication techniques were used. The collector resistors were metal film surface mount resistors, which provided low cost adequate performance for the amplifiers. Furthermore, the coupling capacitors and the bypass capacitors were surface mount capacitors. The coupling capacitors were microwave capacitors, which had a lower impedance at the upper frequencies of the amplifier response. The bias voltage used for this prototype design was 8 V, and the current was approximately 30 mA. Much of the energy was dissipated in the bias resistors. The bias voltage could be substantially reduced if the resistors were replaced with inductors.

The detector was a Schottky diode, which was used because of its good 1/f noise performance. A simple matching network was used to match the diode to the amplifier output. The output from the diode was amplified by an operational amplifier, the Linear Technologies LTC 1051. The resultant amplified signal was sent to an ac-coupled amplifier with a time constant of about 200 s, as well as a differencing amplifier that removed the dc component from the diode output. The resultant signal without the bias provides the dc-coupled output for the sensor. Figure 2.7 shows a photograph of the PPMW sensor with a standard gain horn antenna attached. In an actual sensor, the two modules shown connected together here would be fabricated in a single package.

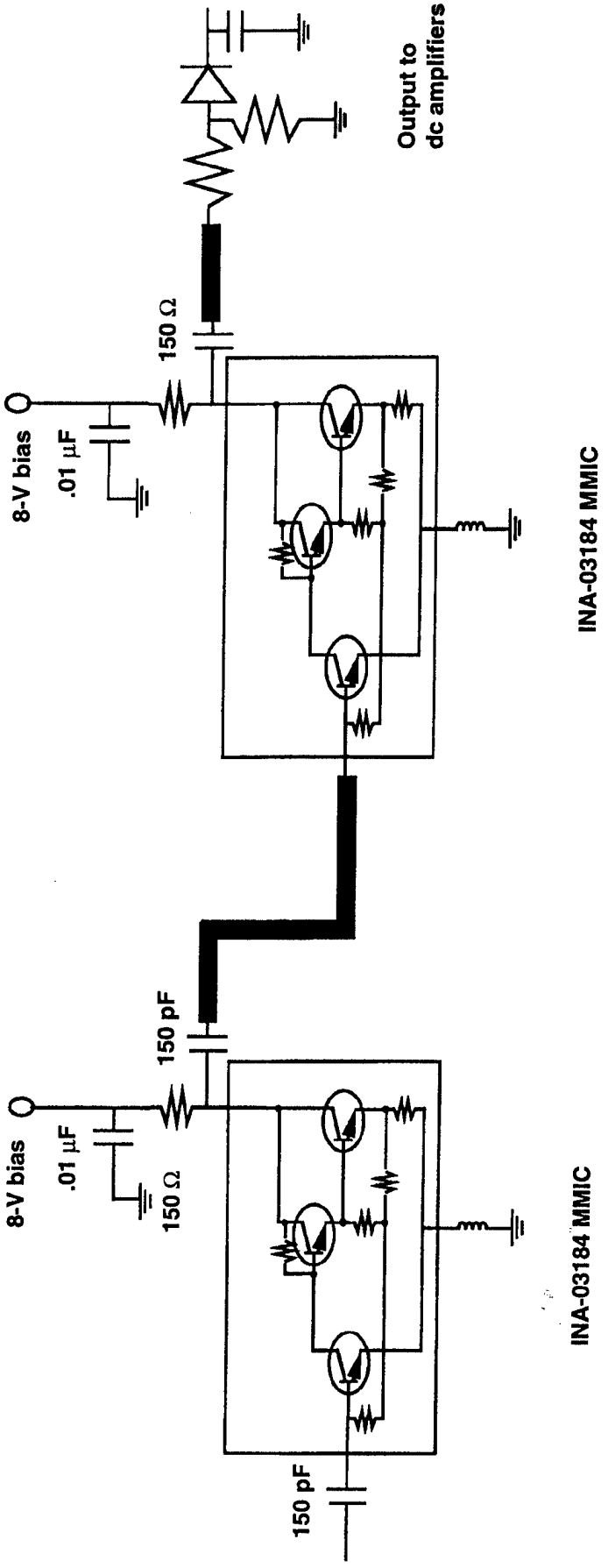

Figure 2.6
Diagram of the intermediate frequency amplifier section.

ARL:UT
AS-97-101
RLR - rfg
4-97

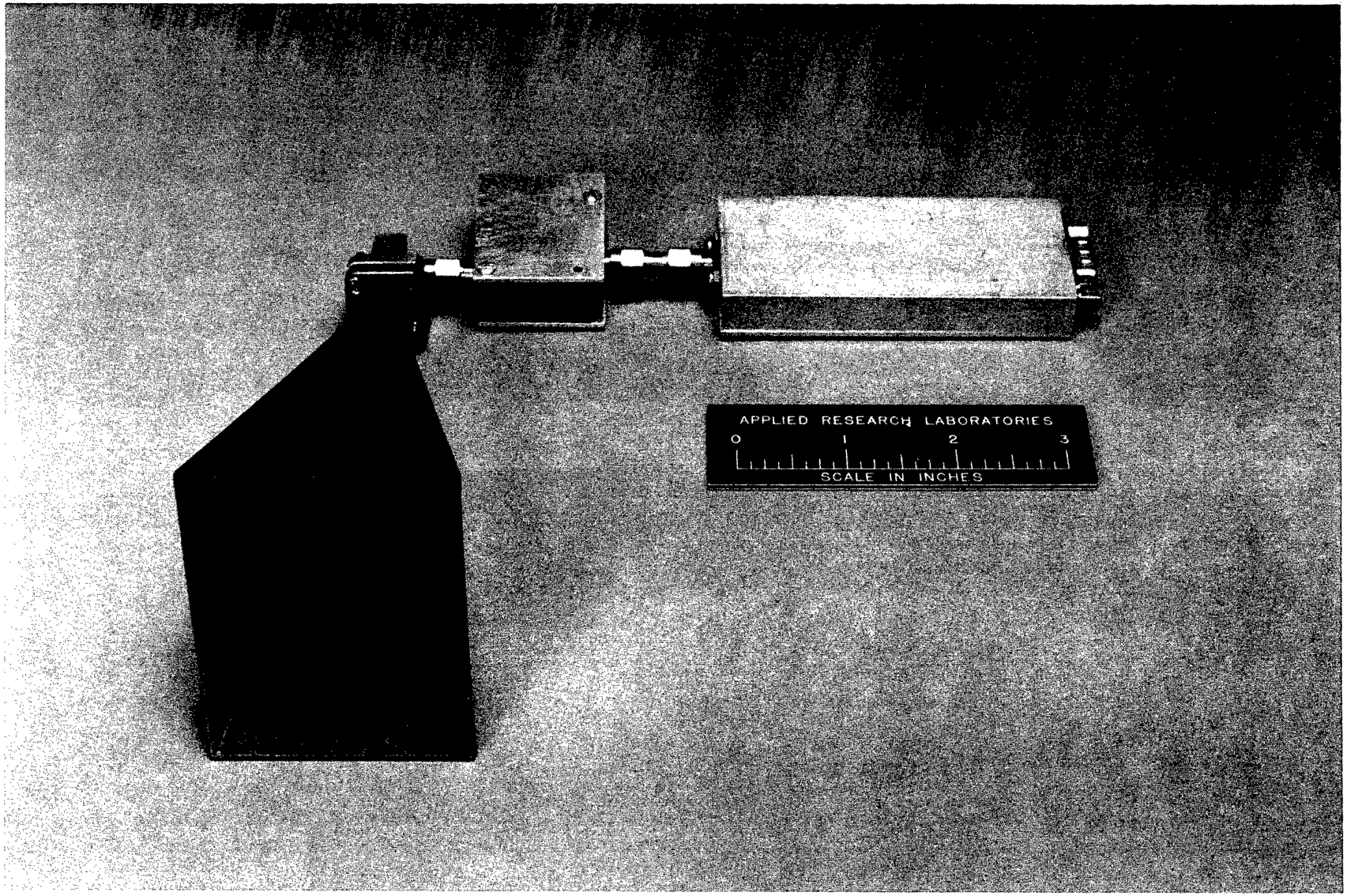

Figure 2.7
Photograph of prototype passive millimeter wave sensor attached to a standard gain horn.

2.4 SUMMARY

The design developed for the PMMW sensor is a low cost design, which utilizes high performance commercial components to provide a very low cost, high performance sensor. The total power configuration makes this a very simple design and also provides the maximum available sensitivity of the receiver with the components available.

3. SENSOR PERFORMANCE CHARACTERISTICS

It is well known that the presence of noise in a sensor or a receiver of any type degrades the performance of the receiver. This is manifested by the appearance of false alarms in the receiver. To reduce false alarms caused by the internal noise in the receiver or by external sources, most sensors or receivers are equipped with a "thresholding" device, such as a comparator, which allows the sensor to indicate a detection or alarm only when a predetermined threshold value has been exceeded. Thus, any real signal that is smaller than the threshold value will be missed. For most security sensors, the trade-off is made to reduce the probability of false alarms to very small values. The discussion here is found in more detail in Ref. 12.

For a given signal strength and a given noise level, the threshold value chosen represents a trade-off between the probability of a false alarm and the probability of a detection. The receiver signals an alarm whenever the signal goes above the threshold value set by the user. When no signal is present, the noise distribution is centered about zero. The chance that a false alarm will occur is calculated from the small portion of the curve that is above the threshold value. In the case for which the signal is present, only the signal values above the threshold values will trigger the alarm. The chance that a detection occurs is then calculated from the area under the curve above the threshold setting. These cases are illustrated in Fig. 3.1.

The two most important parameters for the sensor are the probability of false alarm and the probability of detection. A random variable, X, is designated as the output voltage of the sensor, which is the sum of the signal plus noise:

$$X = S + n \quad . \tag{3.1}$$

The signal, S, is also a random variable, which is considered to have only two values, conveniently 0 and 1. S will take on a value of 0 when there is no signal present and 1 when there is a signal or target present. For the analysis presented here, n is assumed to be a Gaussian random variable with standard deviation of σ_n. Strictly speaking, the SNR should be defined as the ratio of the

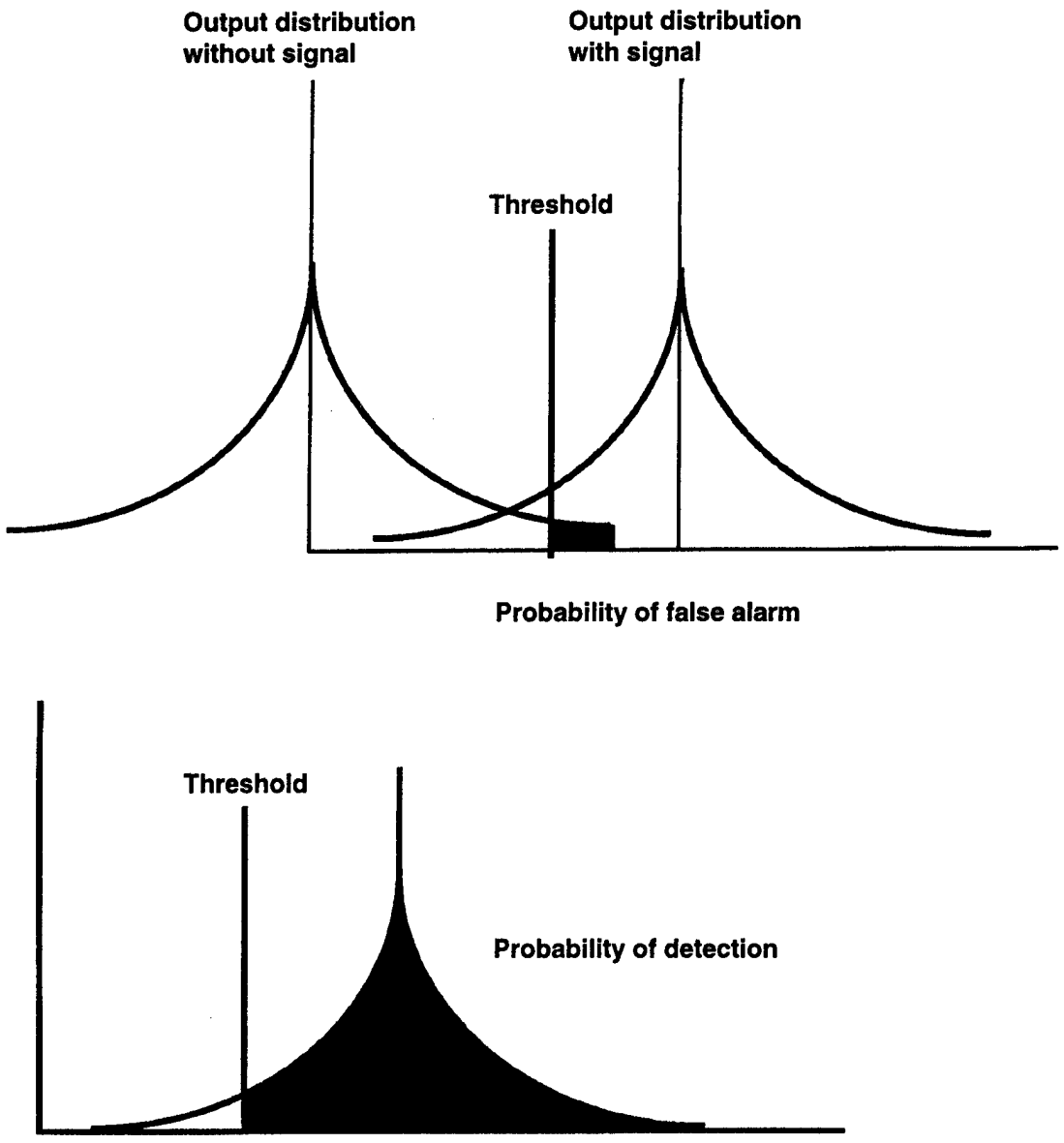

Figure 3.1
Probability density functions for S = 0 and S = 1.

maximum value of the signal amplitude, S, to the standard deviation of the noise, σ_n:

$$SNR = \frac{S}{\sigma_n} \quad . \tag{3.2}$$

However, when we examine the data, all we can actually measure is the combination of the signal and noise, X. When the SNR is high, as it is for nearly all cases of interest in this report and in intrusion sensors in general, it can be assumed that maximum value of S is about the same as the maximum value of X. Therefore, the actual calculation will use the maximum value of X instead of S. This will be used in Section 4, where the probabilities of false alarms for sensors using the measured sensor outputs will be calculated.

A false alarm occurs when the sensor output voltage X exceeds the threshold value T. The probability that this occurs is

$$P(X > T|S = 0) = \int_T^\infty p(x|S = 0)dx \quad . \tag{3.3}$$

If P_f is the probability of a false alarm, then

$$P_f = P(X > T|S = 0) \quad . \tag{3.4}$$

A detection occurs when S = 1 and the output voltage X is greater than the threshold. The probability that a detection occurs is

$$P(X > T|S = 1) = \int_T^\infty p(x|S = 1)dx \quad . \tag{3.5}$$

If P_d is the probability of a detection, then

$$P_d = P(X > T|S = 1) \quad . \tag{3.6}$$

The integrands in Eqs. 3.3 and 3.5 are the conditional probability density functions (pdfs). The left-hand sides of Eqs. 3.3 and 3.5 are conditional

probabilities. The conditional pdfs are the same function; the only difference is that the mean is shifted. The pdfs are

$$p(x|S=0) = e^{-\left(\frac{x}{\sigma_n}\right)^2} \quad , \tag{3.7}$$

$$p(x|S=1) = e^{-\left(\frac{x-1}{\sigma_n}\right)^2} \quad . \tag{3.8}$$

The probability of a miss is the probability that an undetected target is in the beam. This will not be discussed in detail because it is simply related to the probability of detection. The probability of a miss, P_M, can be calculated by

$$P_M = 1 - P_d \quad . \tag{3.9}$$

When Gaussian random variables are assumed, then Eqs. 3.3, 3.6, and 3.7 become

$$P_f = Erfc\left(\frac{T}{\sigma_n}\right) \quad , \tag{3.10}$$

$$P_f = Erfc\left(\frac{T-1}{\sigma_n}\right) \quad , \tag{3.11}$$

where Erfc is the usual complementary error function.

In security systems, it is important to keep the false alarm rate as low as possible. Plots of the error function and the complementary error function are shown in Figs. 3.2 and 3.3. An important feature of Gaussian random variables is that they have a "tail" that diminishes very rapidly as the value of X increases. To keep false alarm rates low, the threshold will be set at least several standard deviations (σ_n) above the average value of the sensor noise. A case of special interest is that of the threshold, T, being set exactly to the value of the signal, S. In this case, P_d is equal to 0.5.

For a given SNR, the probability of detection and the probability of false alarm have a fixed relationship. That is, when a threshold value is selected, P_f and P_d are also uniquely selected. It is possible to look at how the trade-off

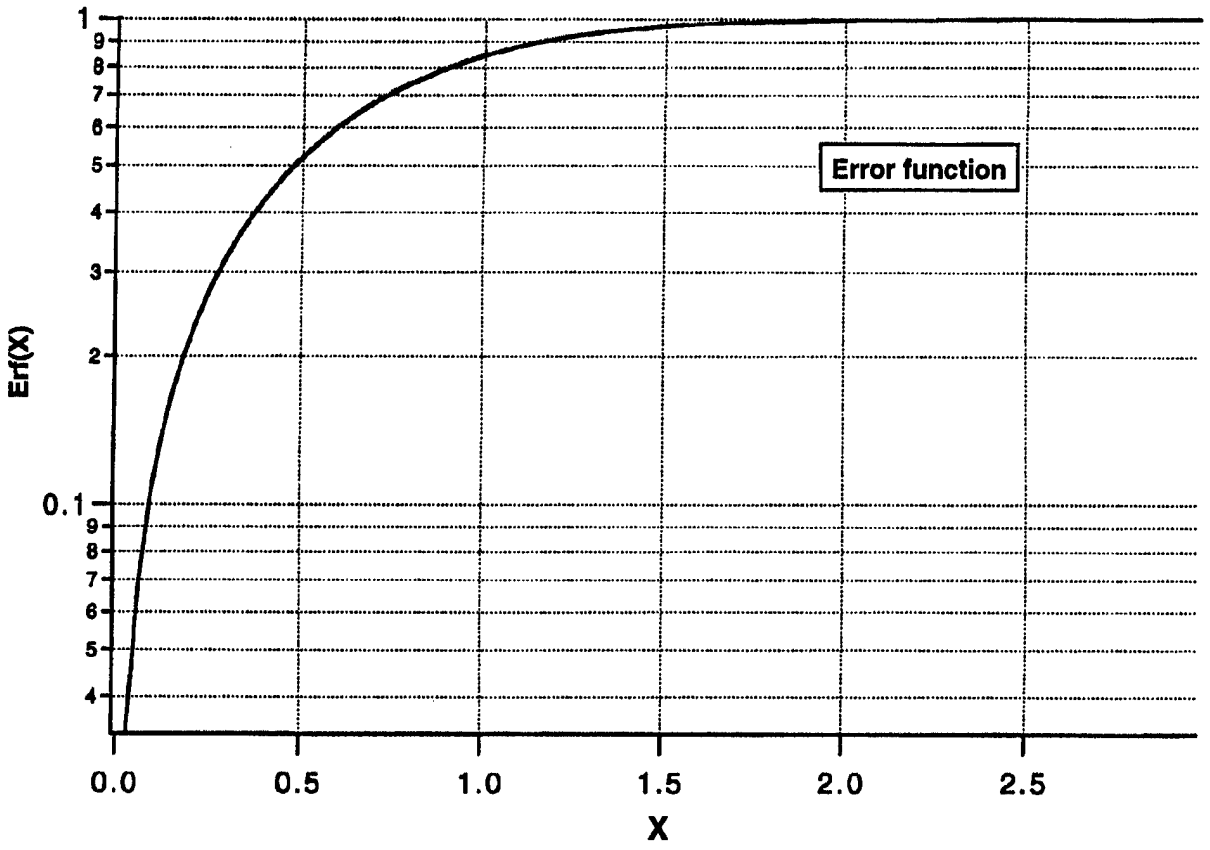

Figure 3.2
Plot of the error function, Erf, as a function of X/σ_n.

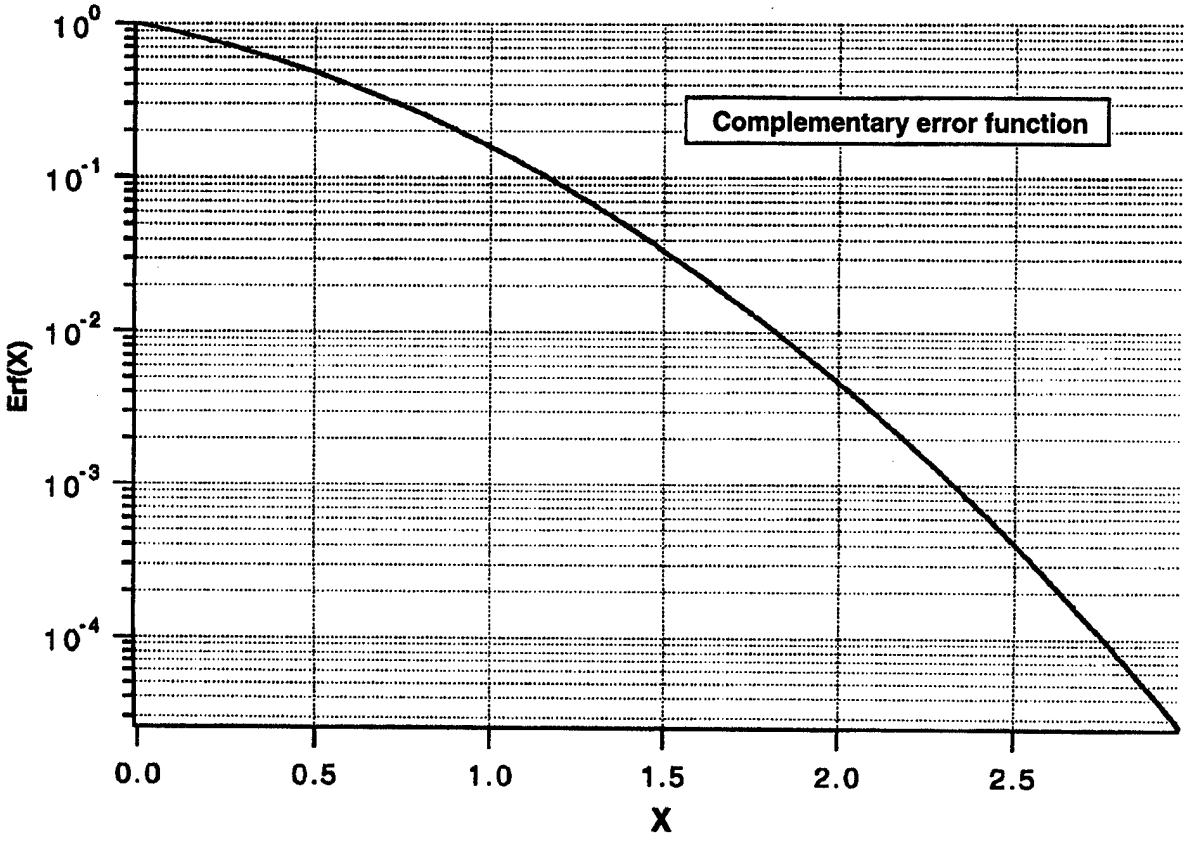

Figure 3.3
Plot of the complementary error function, Erfc, as a function of X/σ_n.

ARL:UT
AS-97-105
RLR - rfg
4-97

between choosing a P_f and a P_d is made for different available SNR values. Figure 3.4 shows a plot of P_d versus P_f for several different SNR values. We can see that if we have a high SNR, such as 7, it is relatively easy to find a high value for P_d and a low value for P_f. On the SNR = 7 curve, we can achieve a P_d of 0.9 with a corresponding P_f of 10^{-16}. At the other extreme, for SNR = 3, we do not achieve a P_d of 0.9 until the P_f is raised to 10^{-3}. For physical security applications, this is a very high false alarm rate. The most important aspect of Fig. 3.4 is that once the SNR is known for a sensor and its environment, then P_f and P_d have a fixed relationship; knowing one is equivalent to knowing the other.

Caution should be used when considering very low false alarm rates for sensors based on the sensor noise alone. Environmental fluctuation and spurious signals can cause false alarms more frequently than one would predict from the estimates based on sensor noise alone. However, because this is unique to each environment, no attempt will be made to characterize these effects. The departure from Gaussian statistics usually becomes apparent in the tail of the pdfs, which is precisely the region of interest. The calculations performed here should be viewed as a tool to help make comparisons and to determine the minimum values of acceptable SNR. For a thermal sensor such as a PMMR sensor or a PIR sensor, the "signal" is the apparent radiometric temperature of the target. The noise value is the apparent temperature fluctuations at the output of the receiver or sensor, which result from either background temperature fluctuations or the internal sensor noise. For the purpose of this discussion here, it is assumed that most of the noise occurs in the receiver. This is a reasonable assumption for interior sensors.

The temperature difference of the target and the background depends on the environment. Standard conditions are assumed for this discussion and make the apparent target temperature a function of the range from the sensor to the target. A background of 290 K (17°C) and a target temperature of 35°C will be assumed. The emissivity used will be 0.8 for infrared frequencies and about 0.6 for millimeter wave frequencies. The difference between the target and the background temperatures can be calculated from the formula

$$T_{rad} = e \cdot (T_T - T_B) \quad , \tag{3.12}$$

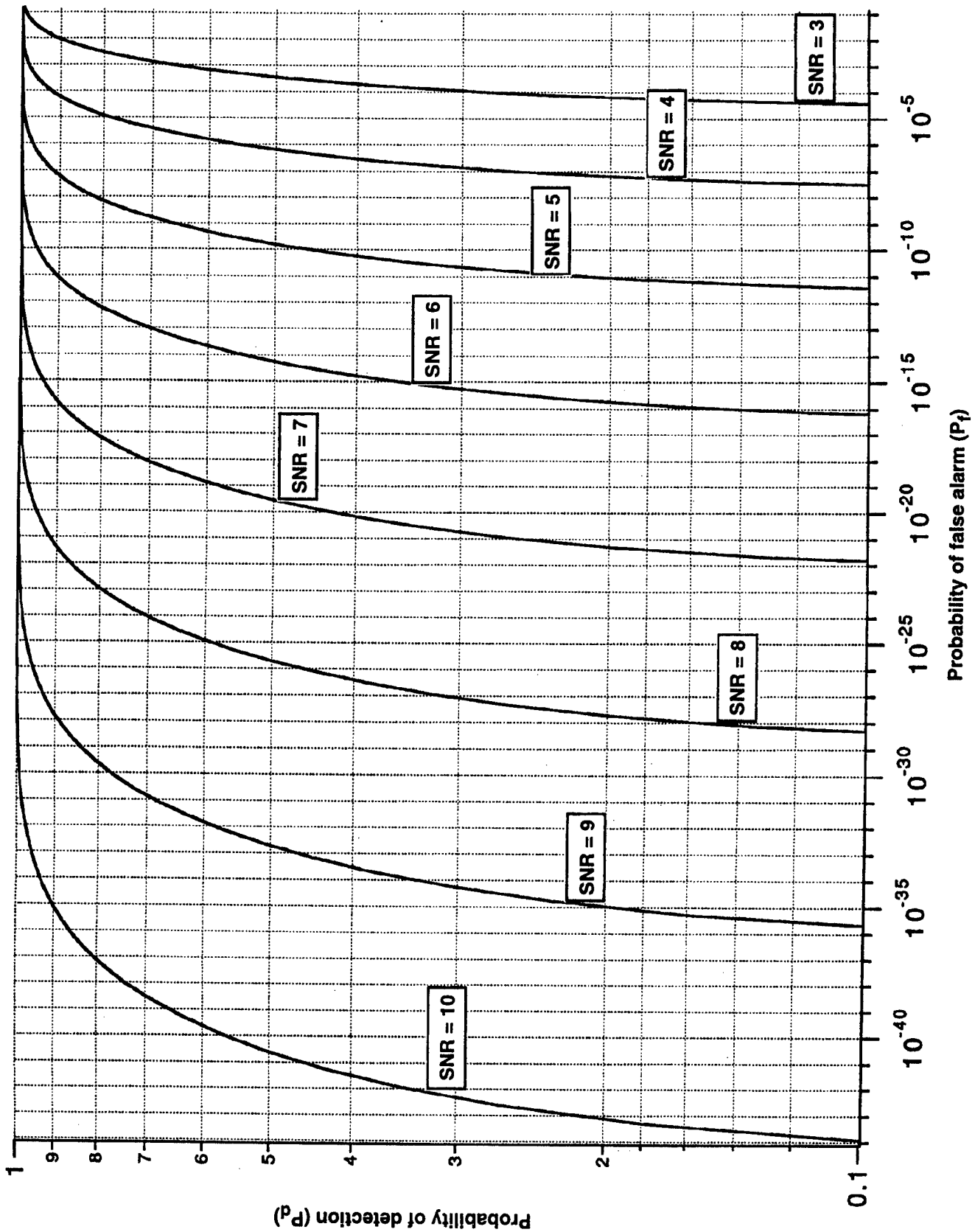

Figure 3.4
Receiver-operating characteristics calculated assuming Gaussian noise for signal-to-noise ratios from 3 to 10.

ARL:UT
AS-97-106
RLR- rfg
4-97

where e is the emissivity, T_T is target radiometric temperature, and T_B is background radiometric temperature. Thus the radiometric target temperature contrast at millimeter wave frequencies is about 11°C, and the radiometric target temperature contrast at infrared frequencies is about 9°C. As will be shown later in this report, the apparent temperature of the target, especially a human target, is not simply related to the emissivity of the skin. Exterior clothing greatly affects the apparent temperature of the target at infrared wavelengths.

The temperature that the sensor actually detects is determined by relative size of the target in the antenna footprint. For example, if an antenna has a beam that is 10° wide and is circularly symmetric, it has a solid angle of about 0.024 sr (steradians). At a range of 20 m, this is an area of about 9.6 m^2. For a human target, the area is approximately 0.5 m^2. The apparent temperature change at the receiver is determined by the relative fraction of the total beam area that the target occupies:

$$T_{antenna} = \frac{A_{target}}{A_{beam}} * (T_{rad}) \quad , \tag{3.13}$$

where A_{target} is the area of the target, A_{beam} is the area of the cross-section of the beam at the range indicated, and $T_{antenna}$ is the radiometric temperature sensed at the antenna.

Now the receiver-operating characteristics can be used to determine the number of false alarms. In a good passive sensor, the noise level will give a Δ of about 0.1 K. If a target produces a 0.8°C radiometric temperature shift at the sensor, the SNR for this range is about 0.8/0.1, or about 8 for the sensor. If the ΔT is 0.25, then the SNR is 3.2. An important assumption will be made that the receiver noise is Gaussian. Thus, if the threshold is set to just detect the presence of the target at that range, the probability of a false alarm, P_f, can be calculated, and detection, P_d, can be determined from Eqs. 3.9 and 3.10 by setting S = 1 and using $\Delta T = \sigma_n$. The SNR at the receiver is X/σ_n. Thus, the P_f for the SNR of 1.56 is about 0.06, while the probability of a false alarm for an SNR of 7 is about 3.3×10^{-12}. If the thresholds are set to detect only these signals, then the probability of detection in both cases is 0.5. Thus, because of the different SNR values of the receivers result in drastically different probabilities

of false alarm for a given probability of detection. If the threshold is changed, the probability of false alarm is decreased as well as the probability of detection.

Plots of Eqs. 3.9 and 3.10 are shown in Figs. 3.2 and 3.3. This is the false alarm rate of a receiver with the threshold set above the noise by the number of standard deviations of the noise. Many sensors will be used in a large security system. Each time a sensor indicates an alarm, it will require some response by the system operator. Too many false alarms may cause the operator to disregard the system alarms. Thus, each individual sensor must have a very low false alarm rate. A typical sensor false alarm rate is one false alarm in 1 month. For the purposes of this discussion, the sensor can be assumed to sample once each second. There are approximately 2.7×10^6 seconds in 1 month, so the false alarm rate must be lower than 4×10^{-7}. From Figs. 3.2 and 3.3, this puts the required X/σ_n at about 5. Thus, the threshold for detection must be set so that the sensor will not indicate an alarm until the target signature is at least five times as great as the radiometric temperature resolution of the sensor. Note that the effects of the background fluctuations have not been considered for the effective range of the sensor.

The probability of detection of a target increases as the target strength increases above the threshold. For a target that has a strength of 6 (in X/σ_n units) with the threshold set at 5, probability of detection is approximately 0.84. Thus, in a system with a large number of sensors, the probability of detection on at least one sensor is 0.974 if the target passes by two sensors. A large system will typically have many sensors that cover many different areas. Thus, the false alarm rate of the system as a whole will be no better than the collective false alarm rate of the sensors. If a system of N identical sensors has independent noise processes and each sensor has a probability of false alarm, P_f, then the probability of at least one sensor having a false alarm, P_{fs}, is

$$P_{fs} = 1 - P_{nf}^N \quad , \tag{3.14}$$

where $P_{nf} = 1\text{-}P_f$ is the probability that there is no false alarm for an individual sensor. For the case where P_f is very small, for example 10^{-7}, and hence P_{nf} is very close to 1, the P_{fs} for the overall system is simply the probability of a false alarm of a single sensor multiplied by the number of sensors. Therefore, if the

probability of a false alarm from one sensor is 10^{-7}, the probability of a false alarm with 30 sensors is simply 30×10^{-7}. Thus, the collective probability of a false alarm for a large system increases approximately in proportion to the number of sensors. Sensor data along with an estimate of the noise statistics based on measured signals will be presented in the next section. The estimates of the variances of the noises will be used to calculate the probabilities of a false alarm.

Since the assumption of a Gaussian process is important for accurate calculation for probability of false alarm and probability of detection for the PMMW sensor (or any sensor), it is important to verify the validity of the Gaussian model. Data were collected from the PMMW sensor for 2.6 days with no targets in front of the sensor. The data were sampled at 10 Hz, and 2.3×10^{6} data points were collected. The false alarm rate was computed for the sensor as a function of threshold setting and compared to the false alarm rate predicted by the Gaussian model by using the complementary error function. The data were high-pass filtered at 0.0013 Hz, and no other filtering was used for this calculation. Figure 3.5 shows that the result from the calculation of probability of false alarm using Erfc and the measured data agree very well over more than five decades of probability. This calculation and measurement strongly suggest that the Gaussian model will be accurate for the calculation of probability of false alarm and probability of detection.

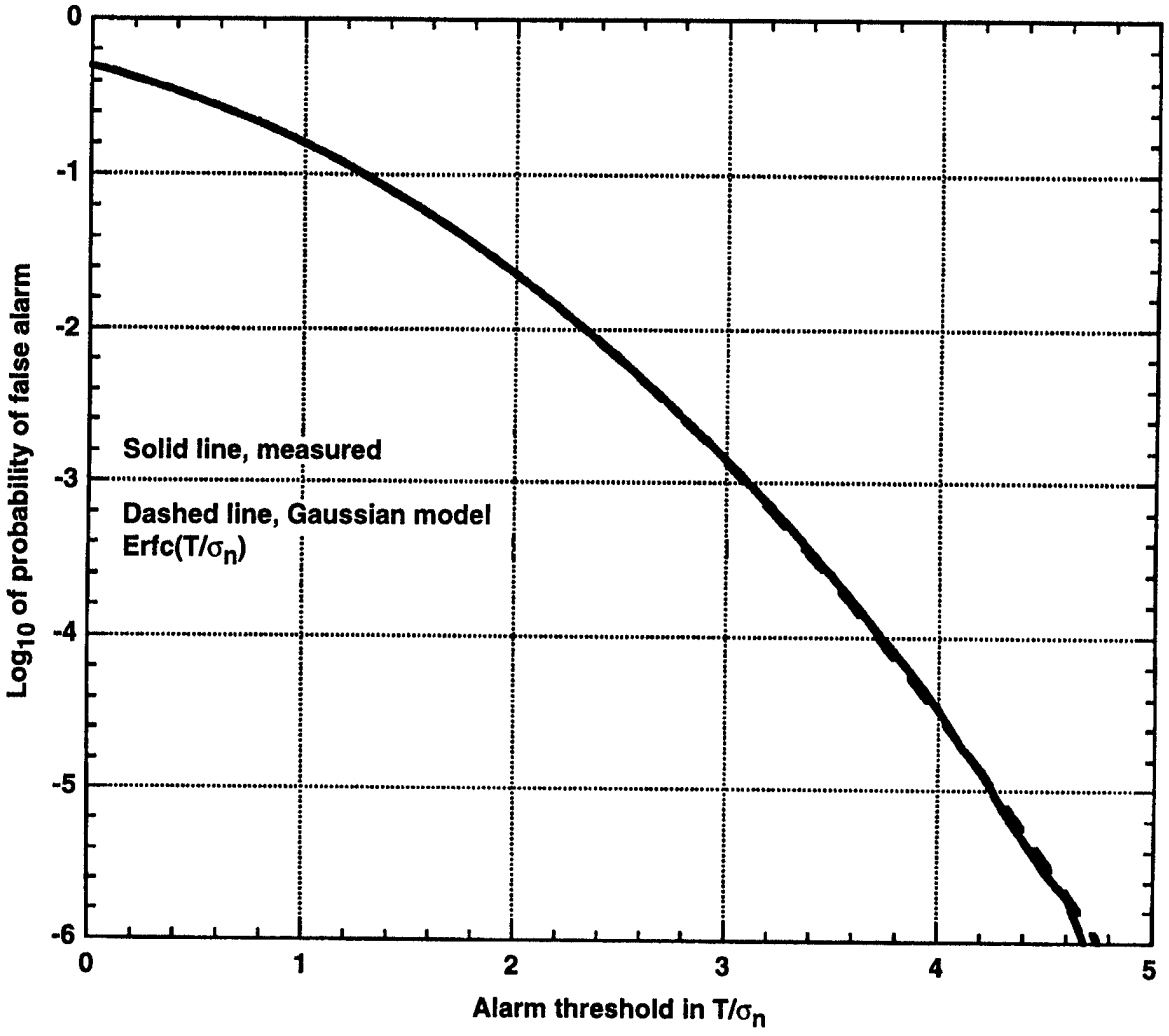

Figure 3.5
Probability of false alarm, Gaussian model calculation and measurements.

ARL:UT
AS-97-107
RLR - rfg
4-97

This page intentionally left blank.

4. RESULTS

4.1 INTRODUCTION TO RESULTS

Every effort was made to be consistent in the presentation and the analysis of the sensor data. Because the PMMW sensor and the PIR sensor have different characteristics in the way that they sense the target, different signal-processing methods are needed to make the sensors operate well. The PIR sensor operates by allowing the target to move past a grated lens focused on the pyroelectric material. The received signal from the target "winks" on and off as it passes across the field of view. The PMMW sensor, on the other hand, has a single broad beam that detects the target. Thus, the target produces a single, slower rising and falling signal on the sensor output. Furthermore, when the analog filters are used, they must be set before the tests. The sensor configuration does not change for the PIR sensor, so the analog filters work reasonably well for most of the tests. However, when the antenna on the PMMW sensor was changed as during the testing scenario, we found that the filtering was not optimal for several of the scenarios tested.

Because both the PIR and the PMMW are best suited for detecting lateral targets, most of the testing was performed with this type of target motion. The target moves across the field of view of the sensor and produces a positive voltage spike on the PMMW sensor and multiple spikes on the PIR sensor. The reason for this difference is, as previously discussed, that the PMMW sensor is a single beam sensor, whereas the lens for the PIR sensor is a multibeam "fly's-eye" lens. Although the millimeter wave antennas used here have a single beam, it is possible to build millimeter wave antenna structures that have a similar beam pattern to the PIR lens.[13]

Results were obtained by recording the output of sensors simultaneously pointed at the same target area. Figure 4.1 is a sensor configuration diagram. Data were collected directly from a PIR sensor and passed through a filter that was reasonably typical of the time constants used in these types of sensors. Data were recorded from an infrared pyrometer, a device that gives an absolute radiometric output in approximately the same band of wavelengths as those of

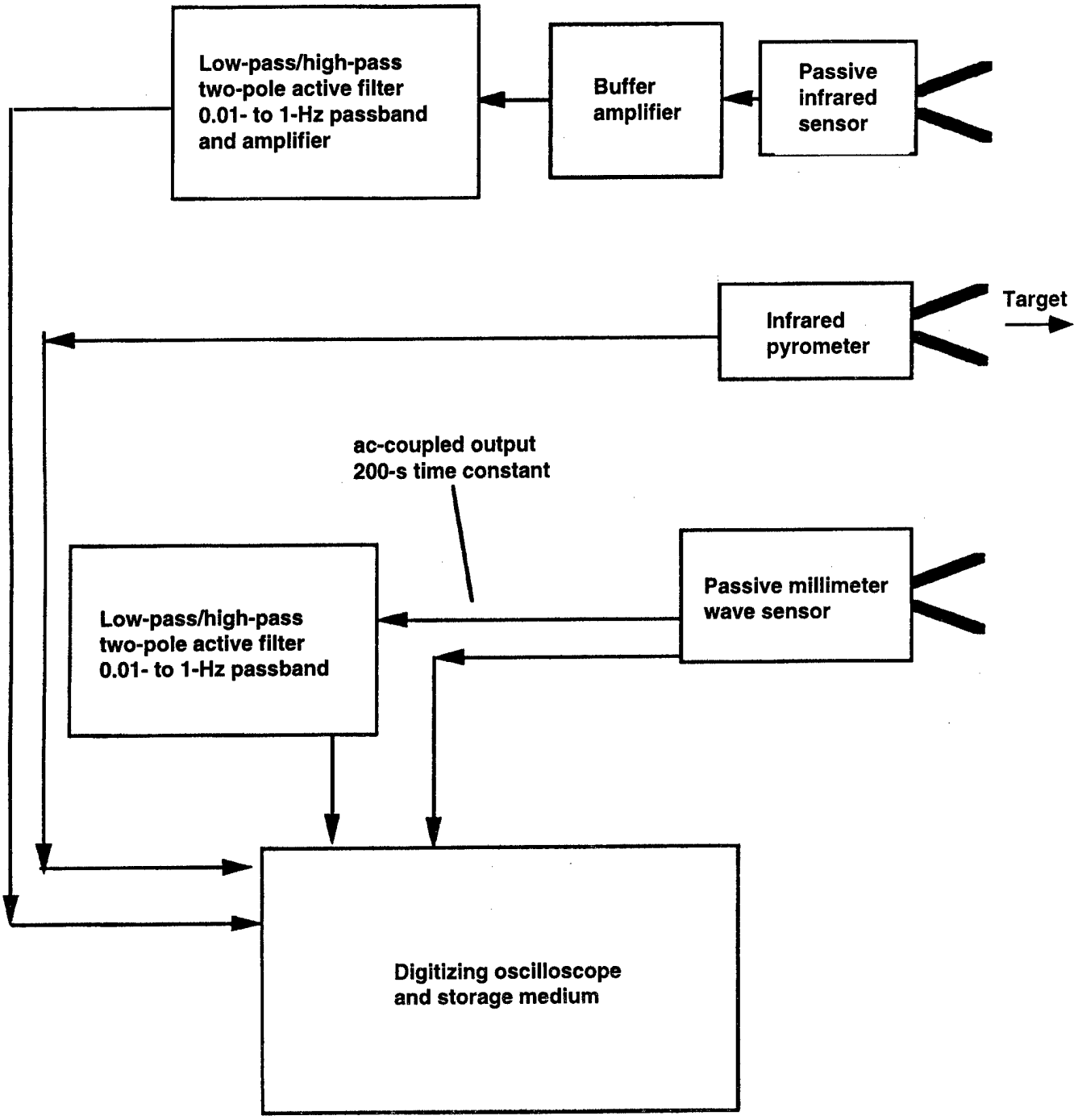

Figure 4.1
Diagram of sensors and data acquisition system.

ARL:UT
AS-97-108
RLR - rfg
4-97

the PIR sensor (8–14 μm). Finally, the PMMW sensor provided two outputs that could be used. The first was an ac-coupled output fed to the same filter as that used on the PIR sensor. The second was the dc-coupled detector output that removed the offset and amplified the result.

Typical background radiometric measurements for the close-range tests are shown in Figs. 4.2 and 4.3. The pyrometer and the PMMW sensor show similar background changes in temperature. The scaling factor on the pyrometer is 1 mV/°C of radiometric temperature shift. The PMMW sensor must be calibrated as shown in Fig. 4.4. The typical calibration factor for the sensor when the standard gain horn antenna was used was approximately 15°C/V, while the typical calibration factor when the reflector antenna was used was approximately 18°C/V. The target standing at successively increasing ranges is shown in Fig. 4.5. Note that at the closest range, the signal is approximately 6°C above the background. Although this is typical signal strength for a human target in an interior environment, it is considerably smaller than the temperature contrast for a human target in an exterior environment. An important feature of this result is that the entire body surface area contributes to the target signature. Most clothing is nearly transparent to the 1-cm wavelength radiation and will not block any of the signal.

The interior tests were conducted in two different environments. The short range tests were conducted in the laboratory at a typical range of 25 ft. A second test was conducted in a long hallway with ranges as great as 115 ft. The background fluctuations measured by the PMMW sensor in each environment along with a reference measurement made looking at a piece of absorber are shown in Table 4.1. The hall had a slightly greater fluctuation in the background temperature than did the laboratory environment, probably because a larger area is being covered by the single beam of PMMW sensor. The environmental fluctuations caused by air conditioning and the presence of people at the end of the hall added to the fluctuations from the sensor noise.

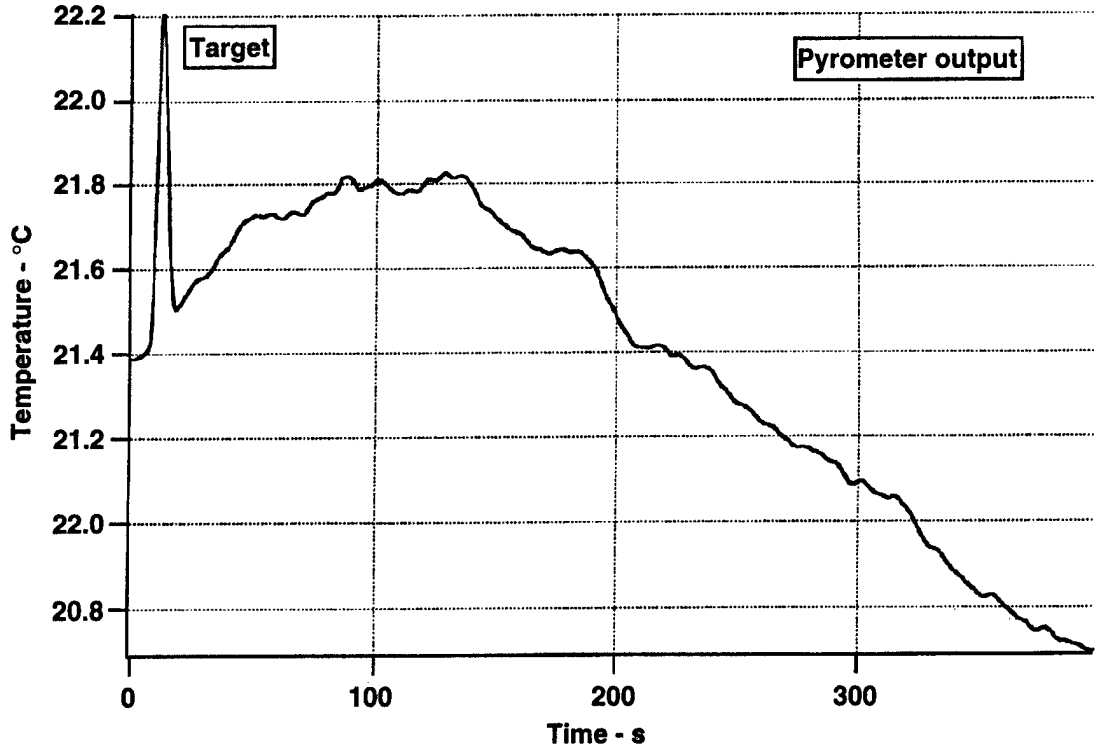

Figure 4.2
Background measurements taken with the infrared pyrometer and the passive millimeter wave sensor – pyrometer sensor output. Target passing in the field of view of the sensor is positive-going spike at about 10 s.

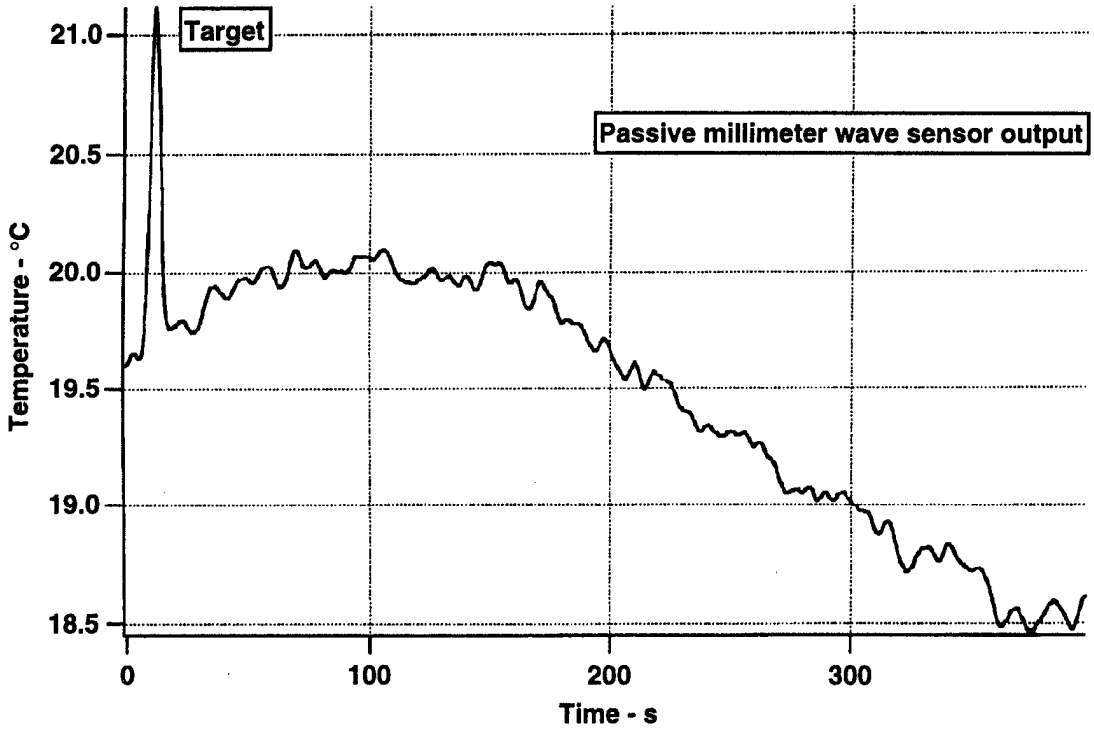

Figure 4.3
Background measurements taken with the infrared pyrometer and the passive millimeter wave sensor – passive millimeter wave sensor output. Target passing in the field of view of the sensor is positive-going spike at about 10 s.

ARL:UT
AS-97-110
RLR - rfg
4-97

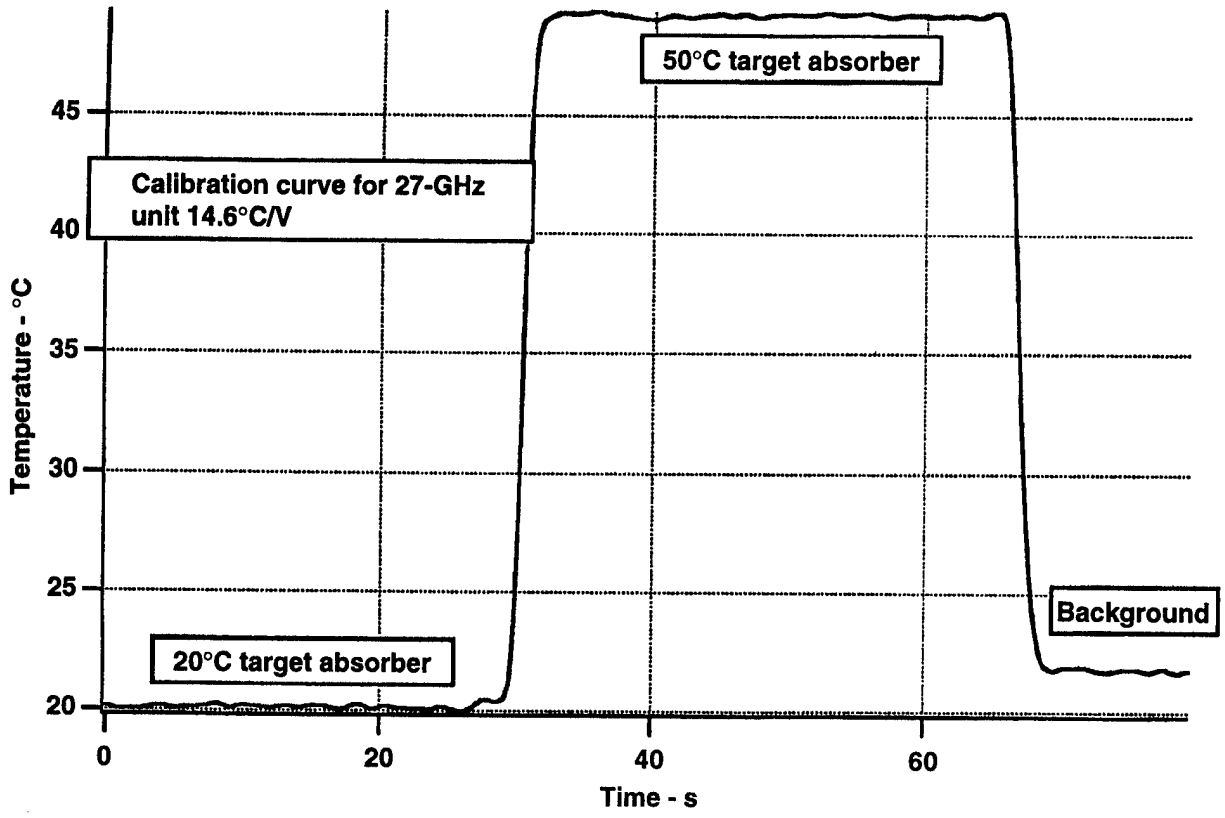

Figure 4.4
Calibration of the passive millimeter wave sensor with a standard gain horn antenna. All data smoothed with 2.8-s triangle filter.

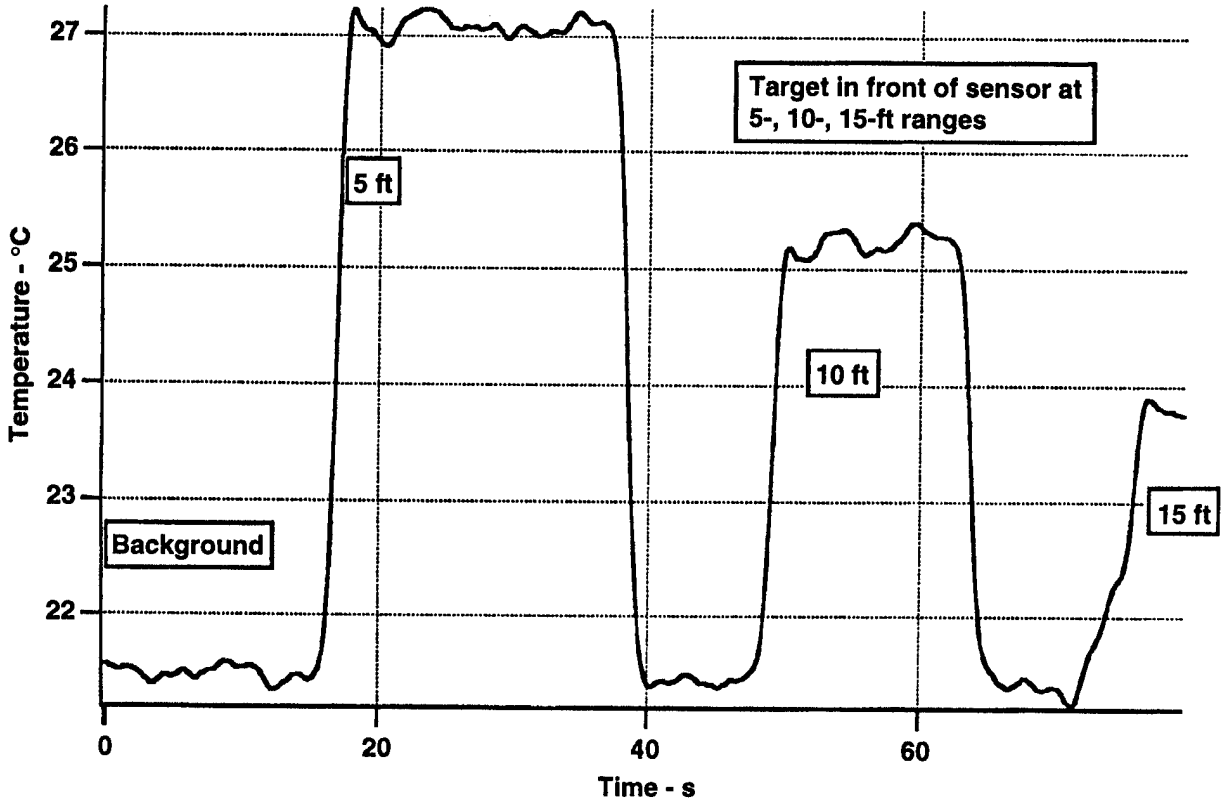

Figure 4.5
Target measurements of the passive millimeter wave sensor with a standard gain horn antenna. All data smoothed with 2.8-s triangle filter – target at 5-, 10-, and 15-ft ranges.

ARL:UT
AS-97-112
RLR - rfg
4-97

Table 4.1
Measured noise levels at the output of the sensor.

Location	PMMW unfiltered and unsmoothed	PMMW unfiltered and smoothed	PMMW filtered
Hallway	0.027 V	0.023 V	0.024 V
Absorber	0.014 V	0.009 V	0.012 V
Short range test	0.015 V	0.009 V	0.013 V

Results of an exterior test are shown in Figs. 4.6 and 4.7, where the range to the target is 100 ft and the air temperature is 37°C is (99°F). Figure 4.6 shows the output from the PMMW sensor and Fig. 4.7 shows the output of the pyrometer. Note that the background radiometric temperature measured by the infrared sensor is close to the air temperature of 37°C (99°F). Data smoothing was used on the output of the PMMW sensor and that of the PIR sensor. The details are discussed in Section 4.2.

For the interior test, the dc-coupled output was available from the PMMW sensor. The data from this output are presented in this report and scaled to units of temperature. This was done to show how large the target signal was in degrees C above the background. This temperature difference is dependent upon the scaling factors mentioned earlier in this section and are reliable measurements. However, the absolute temperature of the output is not reliable. The absolute temperature was set using the pyrometer measurement as a reference. Therefore, the absolute temperature, hence the background, measurements by the PMMW sensor cannot generally be compared against the infrared measurement from the pyrometer. The PMMW sensor was designed to be an effective "trip wire" sensor, as opposed to a precision instrument. Therefore the minimization of long-term drift was not a major performance consideration. In the exterior tests, only the ac-coupled output was available. Therefore the output from the sensor was left in volts for the exterior tests. The only exception to this was a test specifically conducted to show the difference in the background seen by infrared and millimeter wave sensors (Figs. 4.59 and 4.60, shown on page 62).

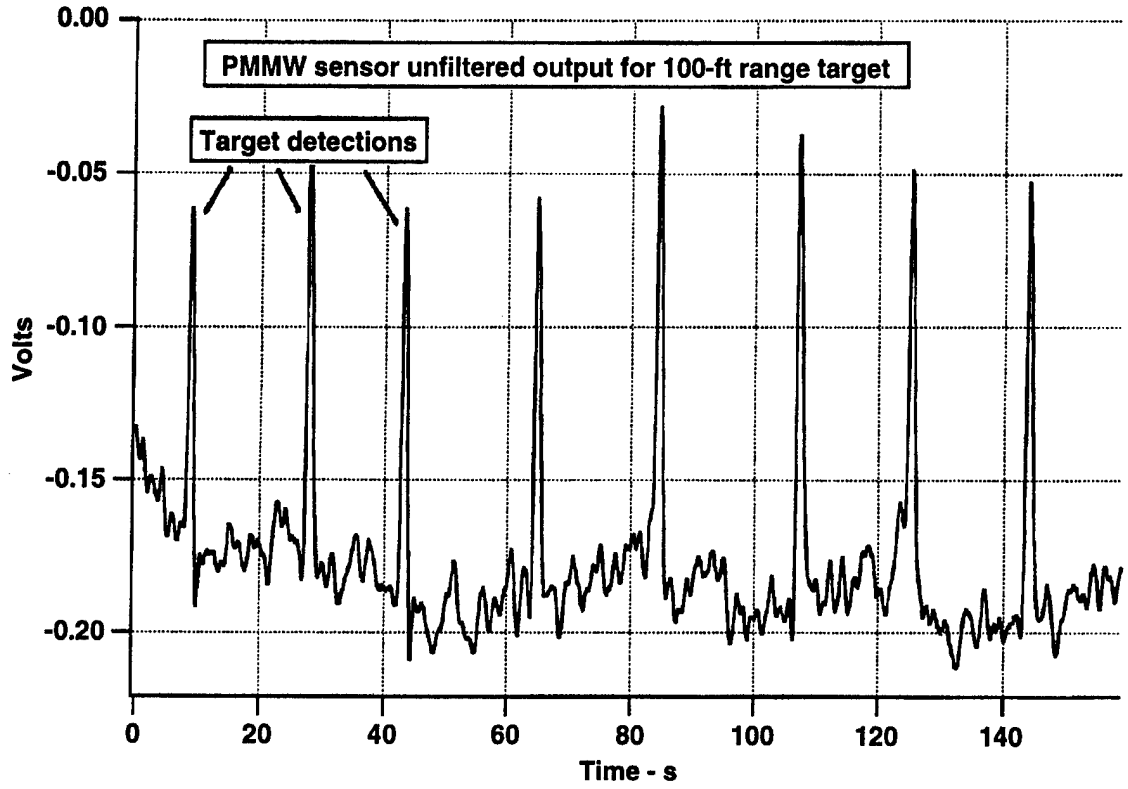

Figure 4.6
Passive millimeter wave sensor unfiltered output.

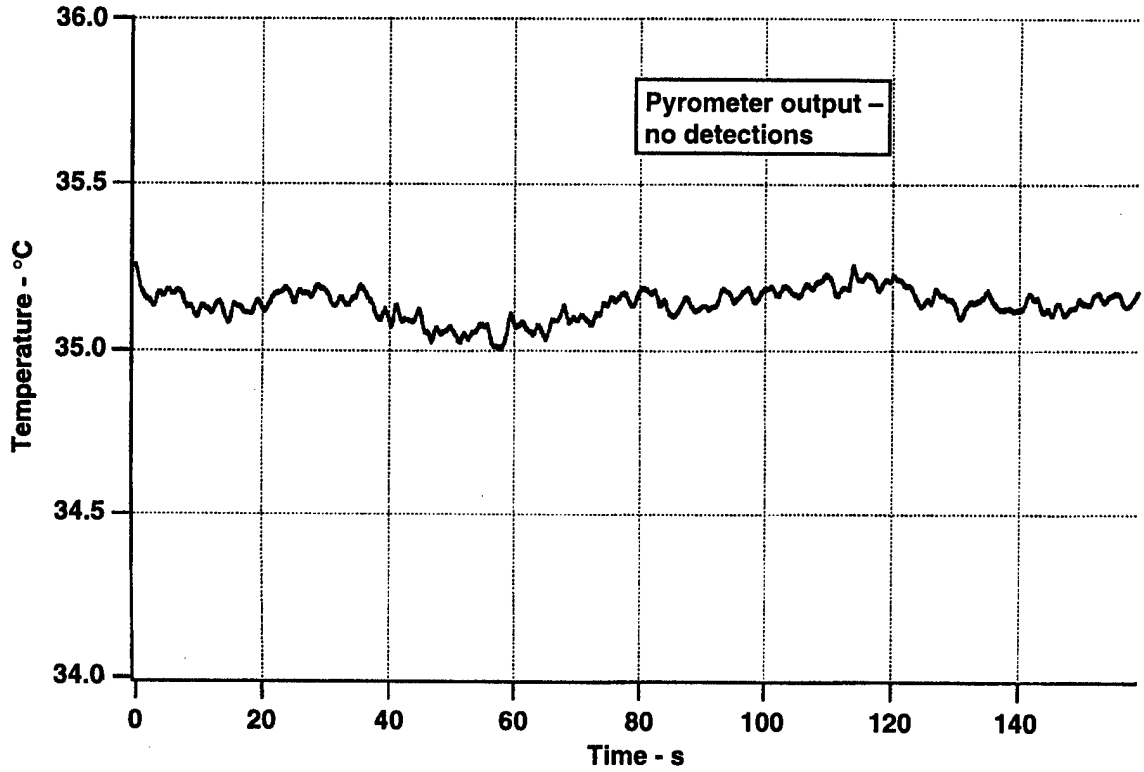

Figure 4.7
Pyrometer output (no detections).

Example of a target detection at 100-ft range in an exterior environment when the ambient air temperature is near 100°F (1.4-s triangle filter smoothing applied to both signals). Target passing in the field of view of the sensor is positive-going spike at approximately 20-s intervals. There are no detections on the pyrometer.

ARL:UT
AS-97-113
RLR - rfg
4-97

4.2 SIGNAL ANALYSIS

Processing the post-detection data from all the sensors used in these tests is a matter of considerable importance. The performance of the sensor can be substantially degraded below its theoretical level if the post-detection processing is mismatched to the signals that are being detected. In the past, only simple passive or active filters could be included in the sensor because of cost, size, and power consumption. Now, microcomputer chips that include analog-to-digital sampling, such as the Motorola MC68HC705B5, are available for a cost of around $11 and can perform digital filter functions such as smoothing with moving averages, high-pass filtering, or other types of event detection with better performance than could be obtained using only simple analog filters. Furthermore, this type of processor is programmable, so the sensor can be quickly reconfigured to adapt to a new environment when it is redeployed. It is conceivable that a temperature sensor, or some other environmental sensor, could be used continuously to update the settings of the post-detection processing.

The typical scenario for the PMMW sensor, as well as for some types of infrared sensors, is shown in Fig. 4.8. The signal produced by the target as it crosses the beam is influenced by the target velocity, target size, range, angle of approach, beam size, environment, and the lateral velocity of the target. Anticipating all of these signal variables is not practical. For the purpose of this discussion, the circumstances will be simplified to perform the comparison. It will be assumed that the target moves laterally across the beam of the antenna with a velocity, v, typical of a normal walking speed. As shown in Fig. 4.8, the closer the target moves toward the sensor, the more rapidly the target moves in and out of the beam. However, the signal from the target is also stronger as it moves closer, so detection does not necessarily need to be optimal for a very close target. The strategy is to optimize the smoothing of the output of the sensor for a target near the limit of the detection range. If an assumption can be made that targets closer in range will continue to be detected because the signals are stronger, then using a smoothing window with a time constant optimized for a target at the extreme range of detection of the sensor results in a close target continuing to be detected because its signature is much larger.

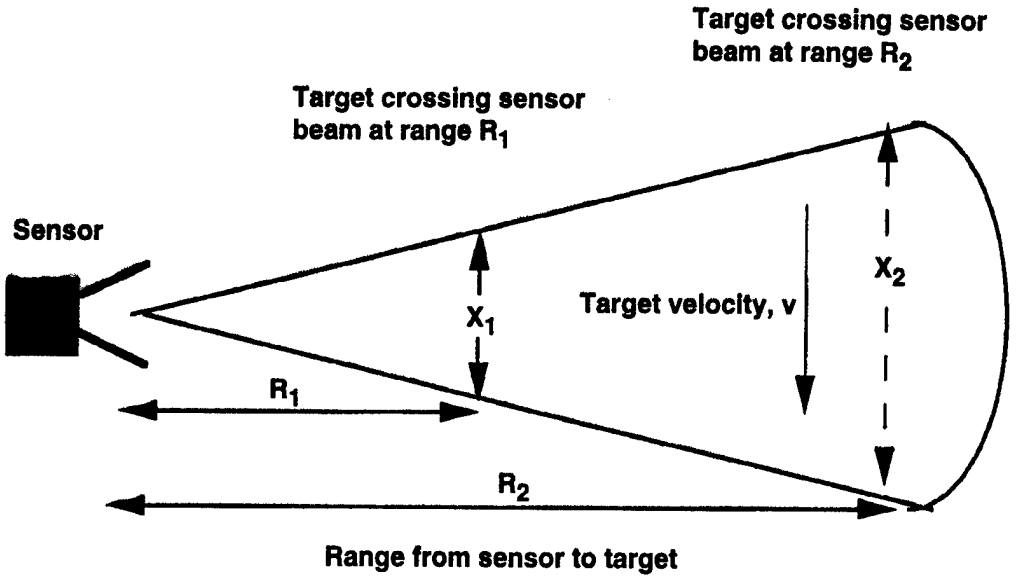

Time in beam at range R_1, $T_1 = \frac{X_1}{v}$

Time in beam range R_2, $T_2 = \frac{X_2}{v}$

Figure 4.8
Time characteristics of target signal as a function of range from the sensor.

ARL:UT
AS-97-114
RLR - rfg
4-97

When the reflector antenna is connected to the sensor, the filter length is 70 data points, or approximately 1.4 s. When the standard gain horn is connected, the filter length is approximately 150 data points, or approximately 2.8 s. Figures 4.9 and 4.10 show plots of the filter coefficients. Figures 4.11 and 4.12 show the results of the application of this technique for an exterior test at 200 ft range. Figure 4.13 shows a typical interior detection with a widebeam antenna and Fig. 4.14 illustrates the effect of the application of a triangle-weighted smoothing function.

Generally, no smoothing was applied to the data from the PIR sensor because the type of lens used created signals in such a way that the smoothing actually decreased the SNR. Our approach was to use only analog filtering for the output of the PIR sensor. The time constants for the analog filters seemed to be nearly optimal for the PIR sensor.

4.3 INTERIOR TESTS

The interior tests were conducted in two scenarios. One test was a short range test in a metal-walled room. The second was a longer range test in a long hallway with Sheetrock walls. Typical results for the close range test are shown in Figs. 4.15–4.26. The typical level of noise for the PMMW sensor is about 8 mV, or about 0.1°C, with the standard gain horn antenna, and for the PIR sensor, noise level is 2 mV. Note also that the pyrometer makes very reliable detections, and its standard deviation after smoothing is 0.02°C. The noise level of the pyrometer is difficult to discern from the background temperature fluctuations.

A short summary of the detections made on the short range tests is given in Table 4.2. This table shows the measured SNR for the PMMW sensor and the PIR sensor under normal interior conditions with a range of 25 ft. The PIR sensor performed well when a lens was used with the sensor but suffered a significant reduction in signal strength when a running target was presented to the sensor. Both sensors were improved when a high gain lens or antenna was used to focus the electromagnetic energy on the detector.

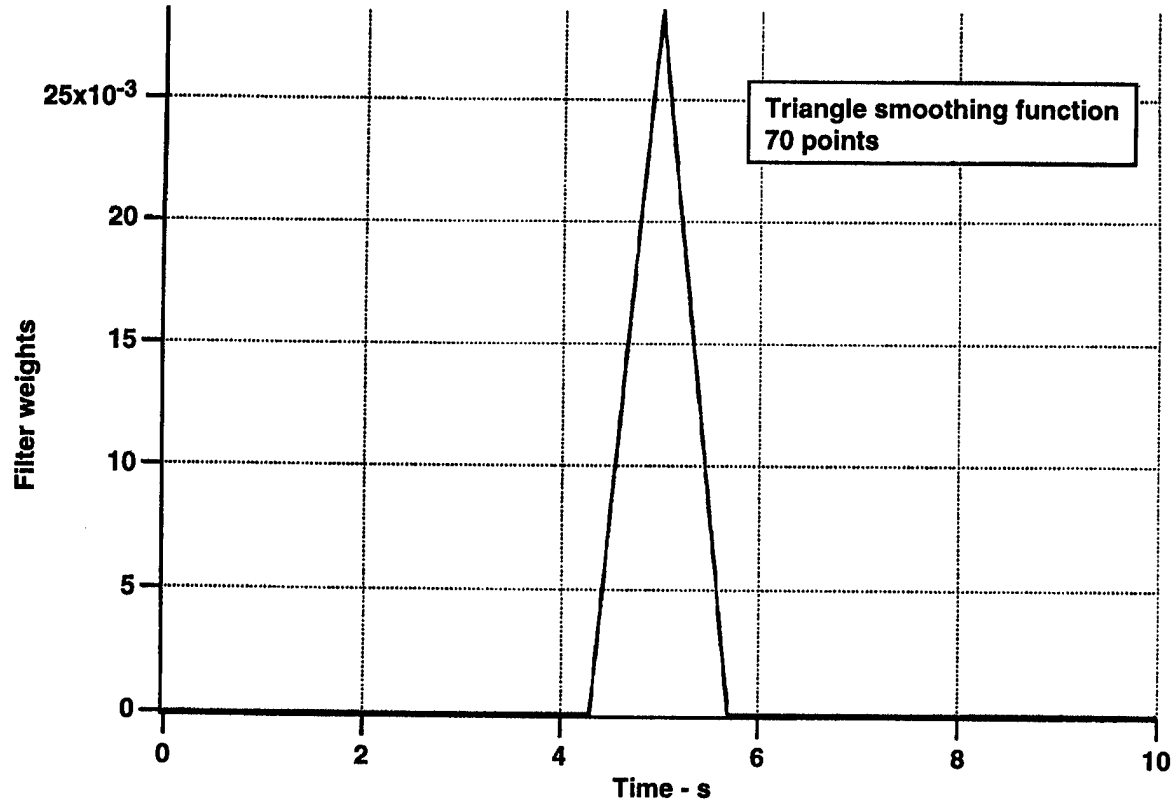

Figure 4.9
Filter coefficients for smoothing – 1.4-s filter.

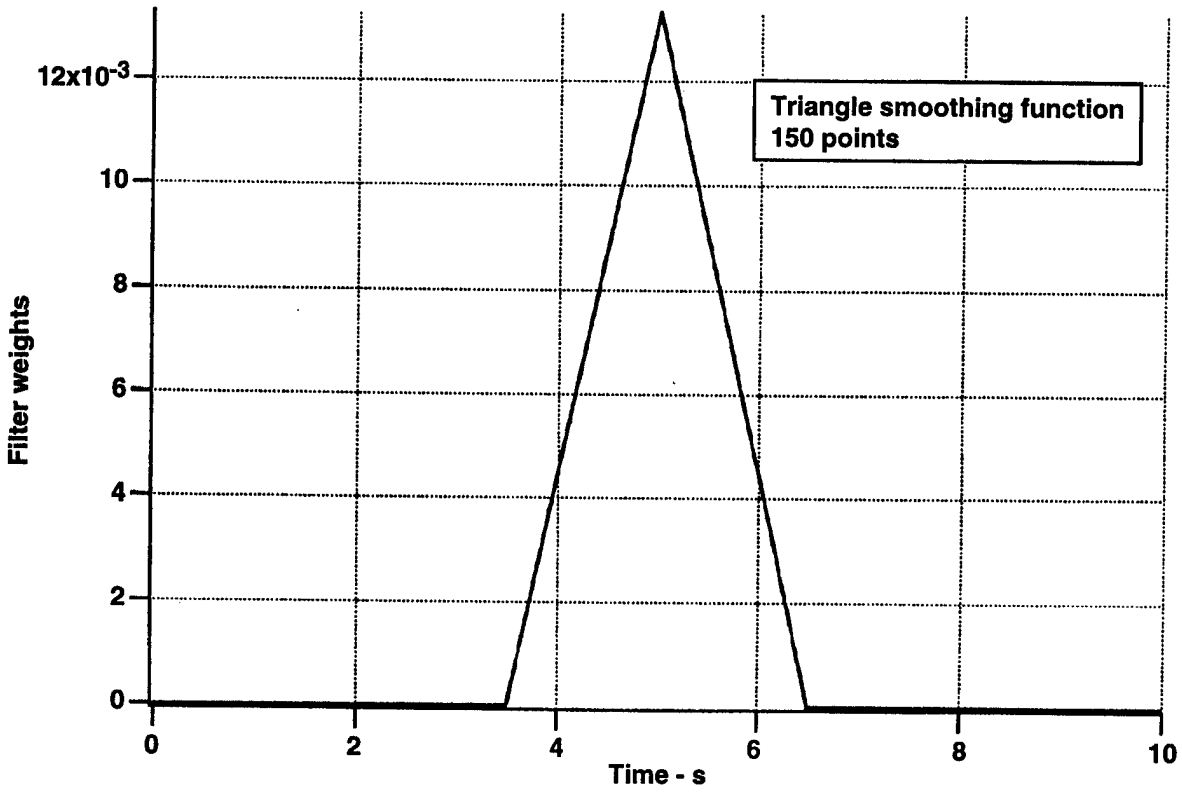

Figure 4.10
Filter coefficients for smoothing – 2.8-s filter.

ARL:UT
AS-97-116
RLR - rfg
4-97

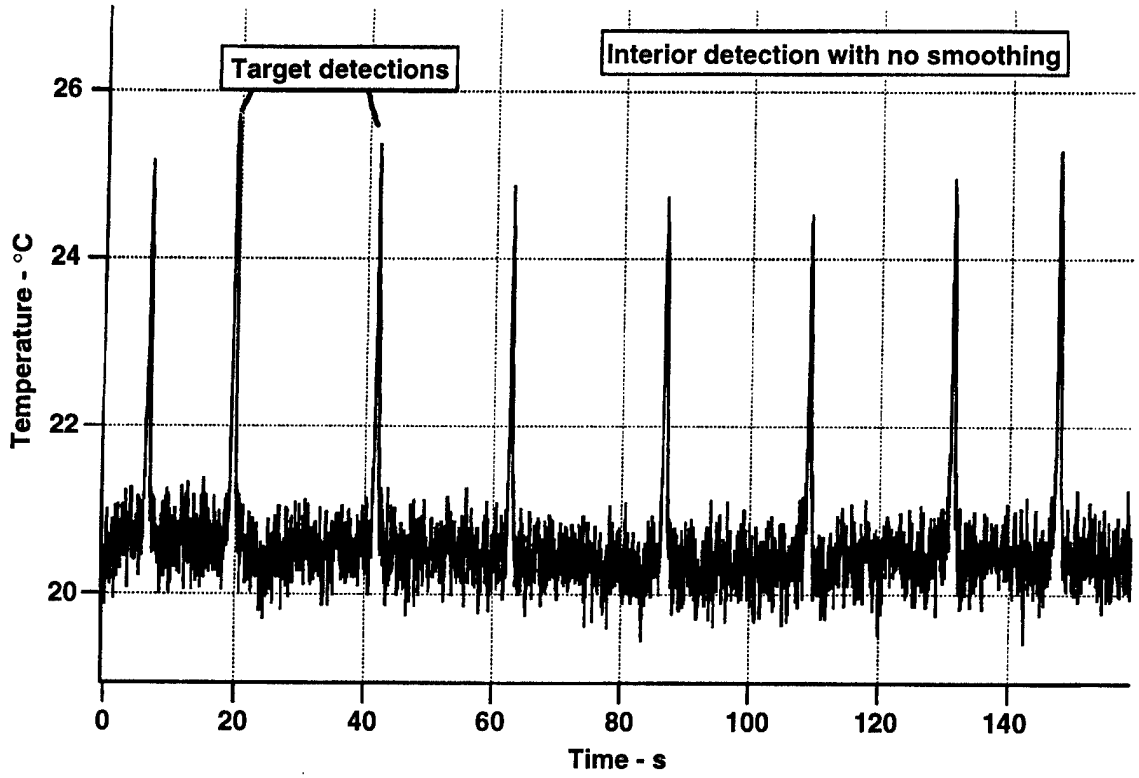

Figure 4.11
Sensor data with 1.4-s triangle filtering applied.

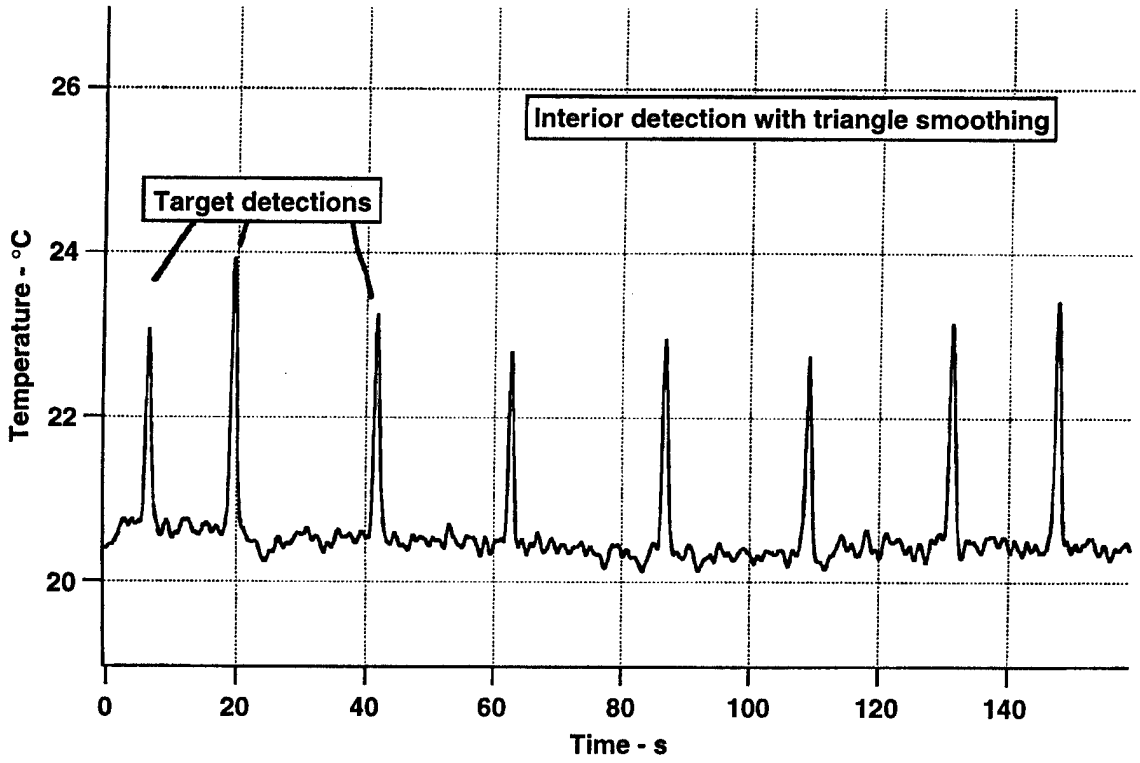

Figure 4.12
Raw sensor data.

Passive millimeter wave sensor with unfiltered output of reflector antenna for detection of a target at 25-ft range in an interior environment. Target passing in the field of view of the sensor is positive-going spike at approximately 20-s intervals.

ARL:UT
AS-97-117
RLR - rfg
4-97

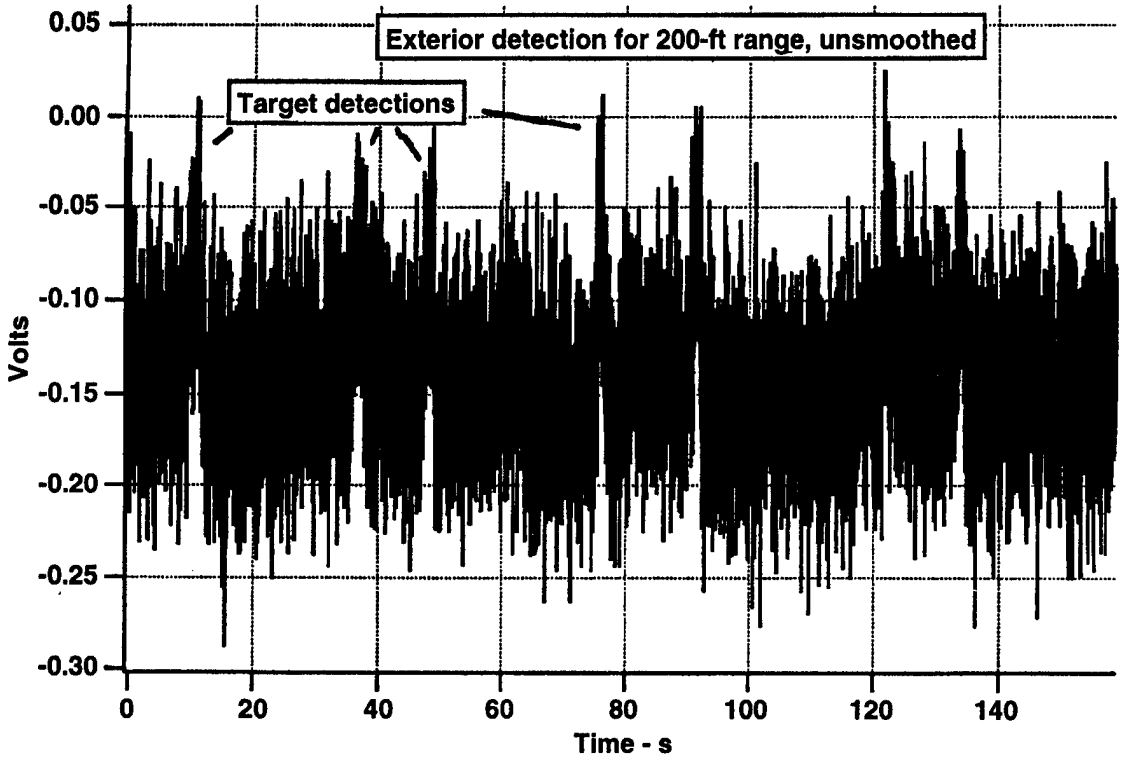

Figure 4.13
Raw sensor data.

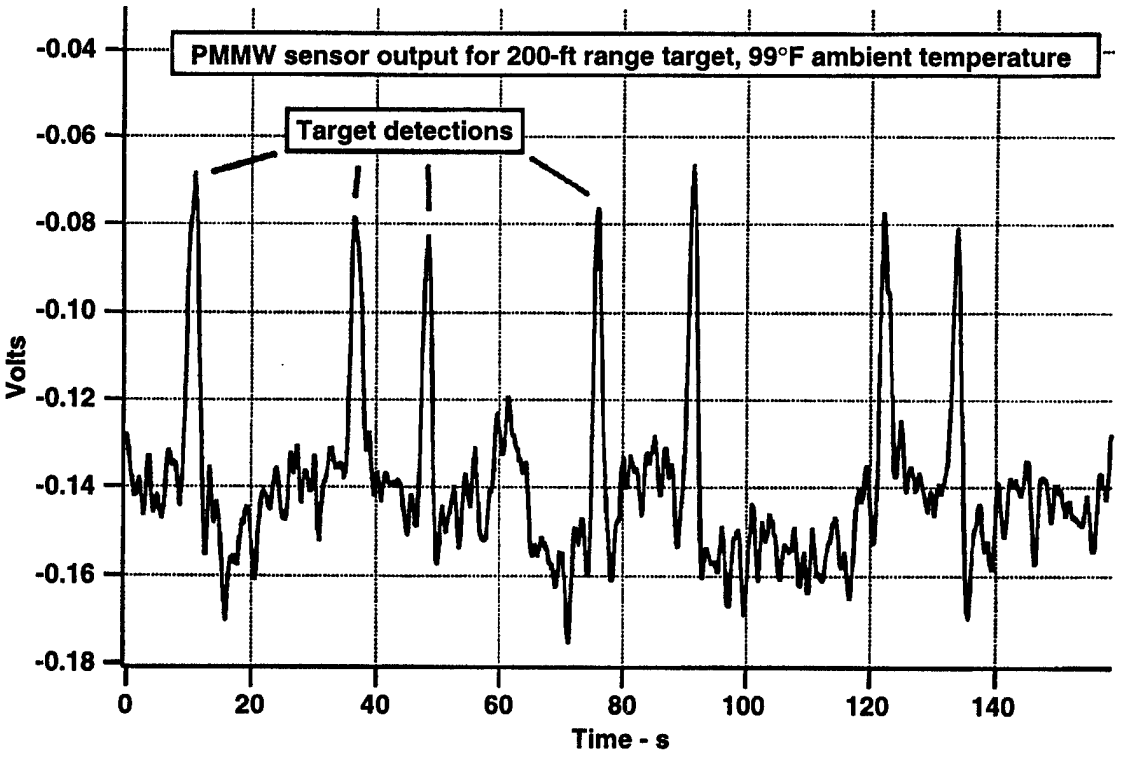

Figure 4.14
Sensor data with 1.4-s triangle filtering applied.

Passive millimeter wave sensor with lens antenna in exterior environment at 99°F and target range of 200 ft.

ARL:UT
AS-97-118
RLR - rfg
4-97

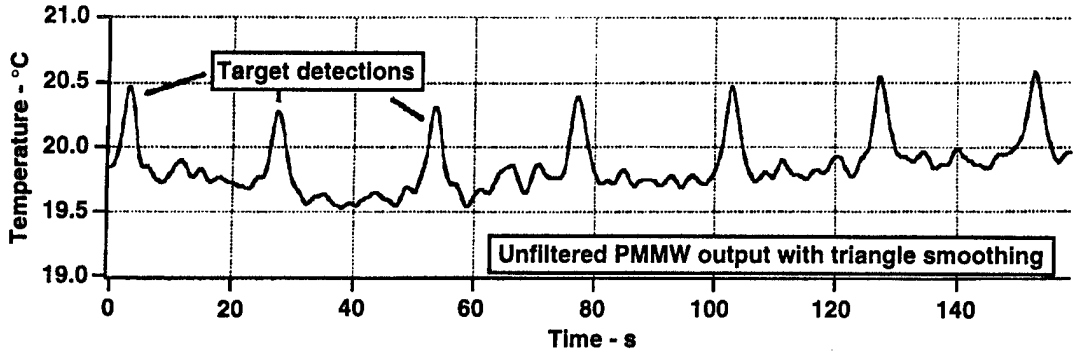

Figure 4.15
Passive millimeter wave sensor unfiltered output.

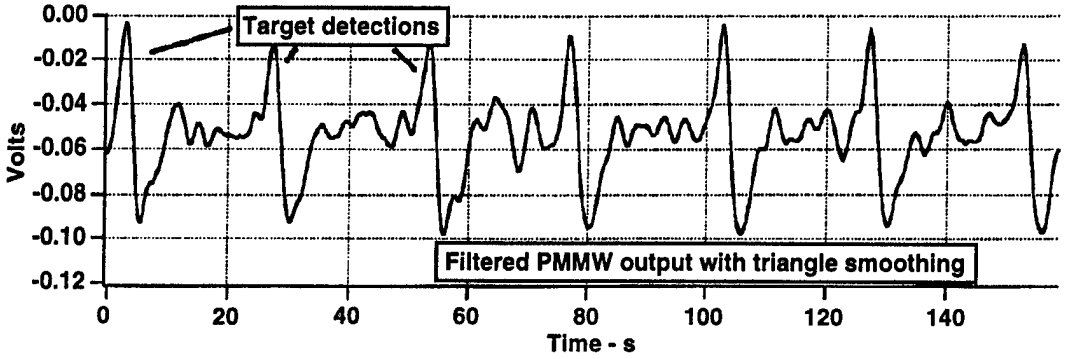

Figure 4.16
Passive millimeter wave sensor filtered output.

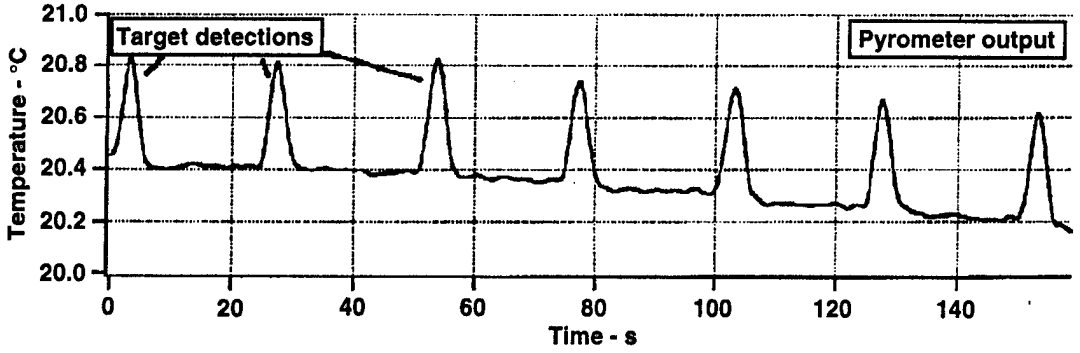

Figure 4.17
Pyrometer output.

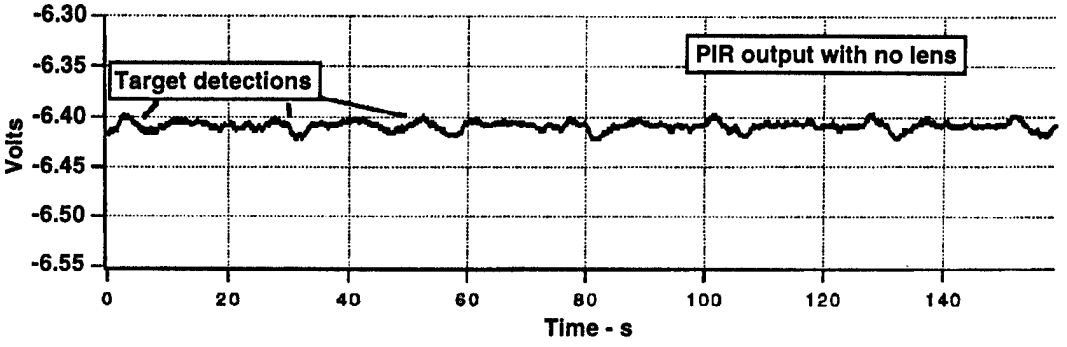

Figure 4.18
Passive infrared sensor output.

Output of the three sensors for the short range interior environment tests at a target range of 25 ft with a standard gain horn on the PMMW sensor and no lens on the PIR. All data except for the PIR data have been smoothed by a 2.8-s triangle smoothing filter. Target passing in the field of view of the sensor is positive-going spike at approximately 20-s intervals. The response of the PIR and the filtered PMMW sensor have a positive-going and a negative-going response for a single detection.

ARL:UT
AS-97-119
RLR - rfg
4-97

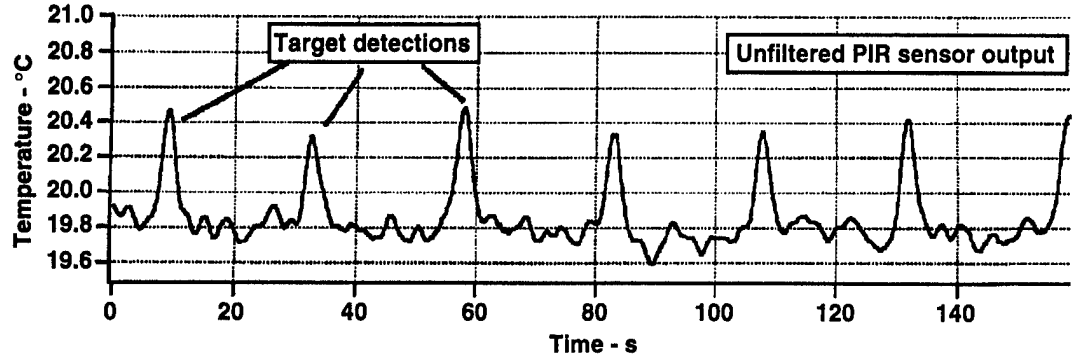

Figure 4.19 Passive millimeter wave sensor unfiltered output.

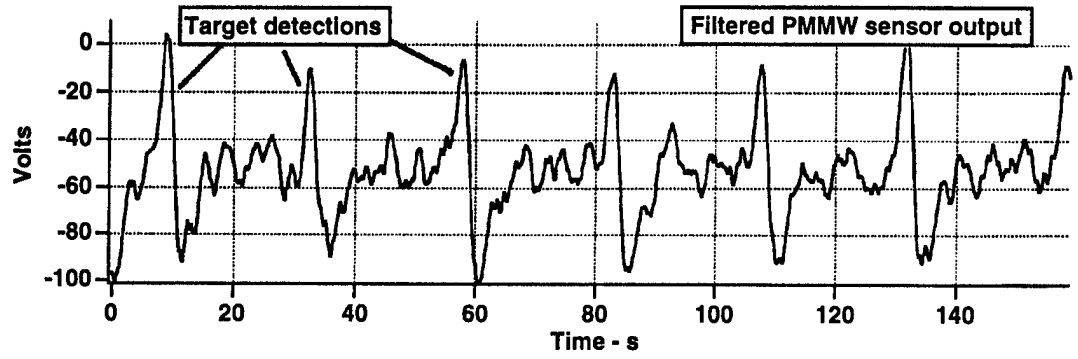

Figure 4.20 Passive millimeter wave sensor filtered output.

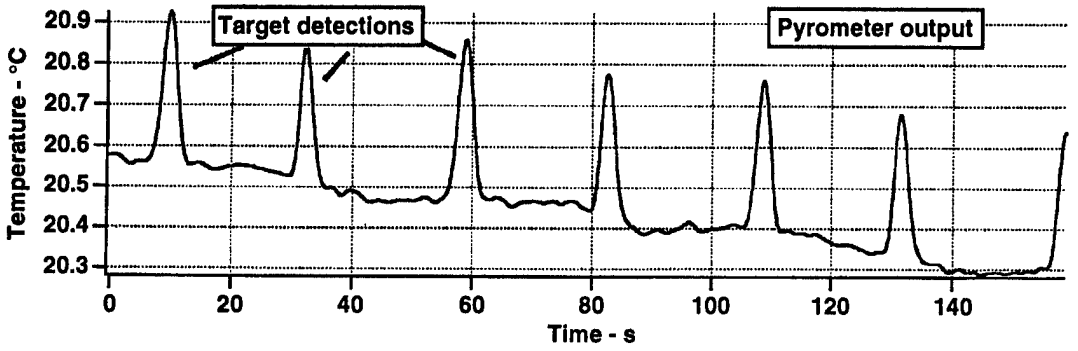

Figure 4.21 Pyrometer output.

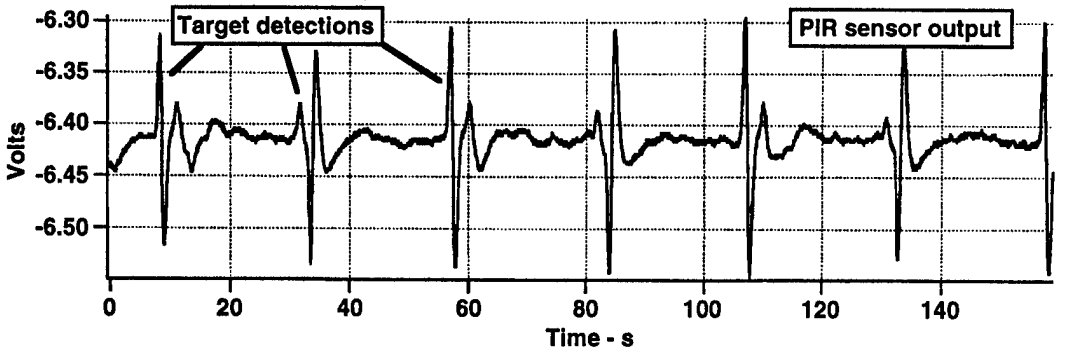

Figure 4.22 Passive infrared sensor output.

Output of the three sensors for the short range interior environment tests at a target range of 25 ft with a standard gain horn on the PMMW sensor and a standard "fly's eye" lens on the PIR. All data except for the PIR data have been smoothed by a 2.8-s triangle smoothing filter. Target passing in the field of view of the sensor is positive-going spike at approximately 20-s intervals. The response of the PIR and the filtered PMMW sensor have a positive-going and a negative-going response for a single detection.

ARL:UT
AS-97-120
RLR - rfg
4-97

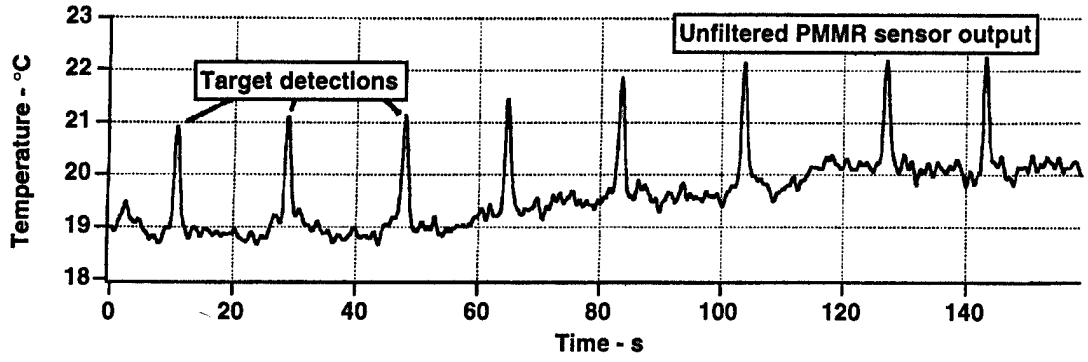

Figure 4.23
Passive millimeter wave sensor unfiltered output.

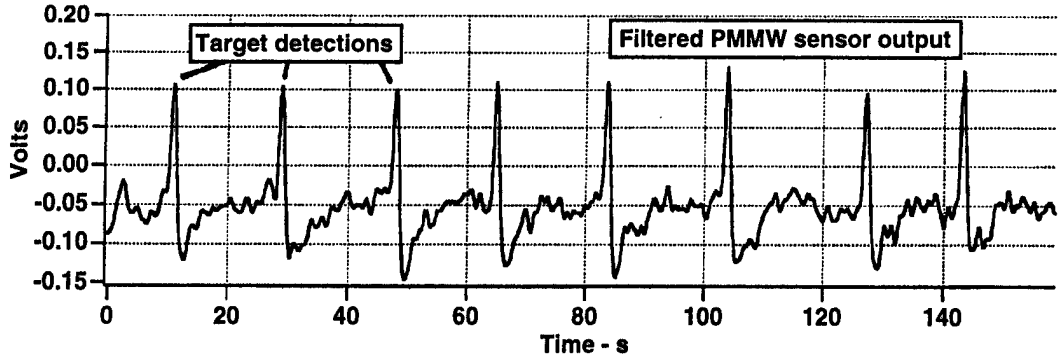

Figure 4.24
Passive millimeter wave sensor filtered output.

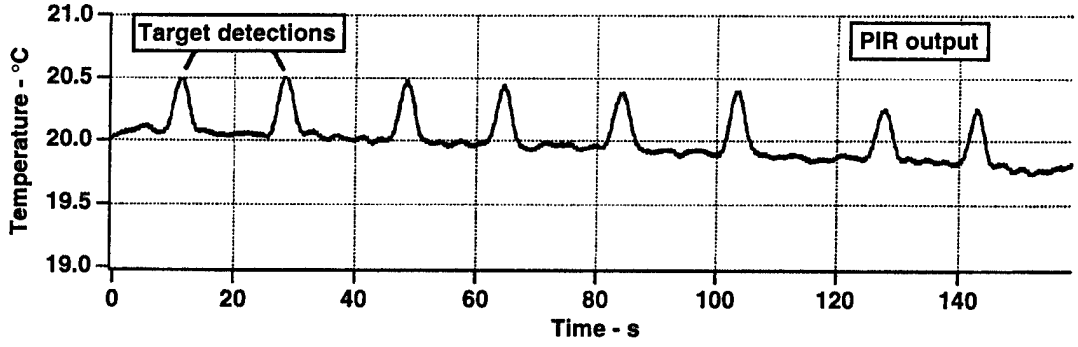

Figure 4.25
Pyrometer output.

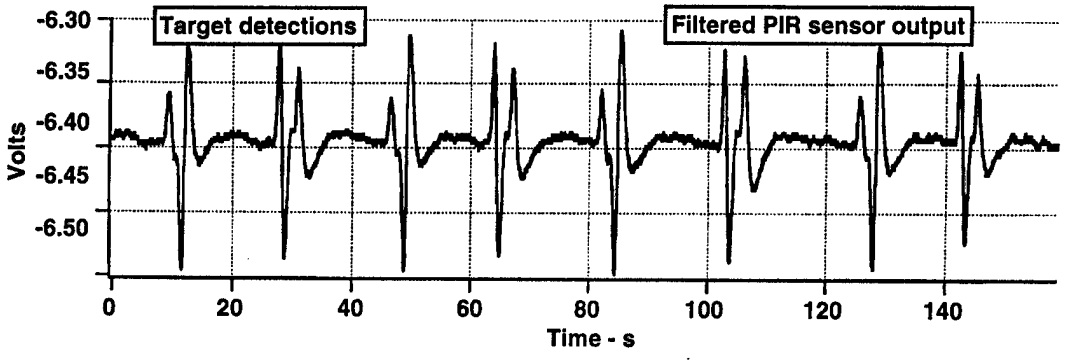

Figure 4.26
Passive infrared sensor output.

Output of the three sensors for the short range interior environment tests at a target range of 25 ft with a reflector antenna on the PMMW sensor and a standard "fly's eye" lens on the PIR. PMMW data have been smoothed by a 1.4-s triangle smoothing filter. Target passing in the field of view of the sensor is positive-going spike at approximately 20-s intervals. The response of the PIR and the filtered PMMW sensor have a positive-going and a negative-going response for a single detection.

ARL:UT
AS-97-121
RLR - rfg
4-97

Table 4.2
Summary of short range interior test SNR values.

	PIR sensor without lens	PMMW sensor with horn antenna	PIR sensor with lens	PMMW sensor with reflector antenna
Normal walking	3-4	5-6	40-45	25-30
Run tests	No data	No data	2	12-15

Figures 4.15 through 4.18 show the output of the PMMW sensor and the PIR sensor with no lens in the PIR sensor. Under these conditions, the target is not well detected by the PIR. This is worth noting because the beam pattern of the antenna makes a substantial contribution to the overall performance of both the PIR sensor and the PMMW sensor. The peak signal level of the PIR with no lens is around 5 mV to 7 mV, or 2 to 4 standard deviations of sensor noise. The temperature shift that the target makes on the PMMW sensor is about 0.6°C, which is 5 or 6 standard deviations of sensor noise on the unfiltered output. The analog filters remove the background drift but otherwise do not improve the SNR for the standard gain horn antenna. This is because the time constants chosen for the filters are better suited for a narrow beam and hence a faster changing signal. The same filter time constants worked very well and were near optimum for the PIR sensor. The temperature shift registered by the pyrometer is about 0.3°C to 0.4°C.

The pyrometer and the standard gain horn have similar beam patterns. Figures 4.19–4.22 show the output of the three sensors when the lens is put into the sensor and show that the lens is a major enhancement to the performance of the PIR sensor. The testing was primarily conducted with the lens in place, since this is the optimum configuration for the sensor. The drive apparent on the dc output of Figs. 4.15–4.22 can be easily removed via a high-pass filter. The actual analog filter that was designed for the sensor was approximately one order of magnitude too high in frequency cutoff to be effective. Figures 4.27 and 4.28 show the effect of removing the low frequency components below 0.01 Hz. The filtering was accomplished by performing a fast Fourier transform (FFT) on the data and removing the lowest frequency components. This effectively high-pass filters the data that have a cut-off frequency of 0.01 Hz.

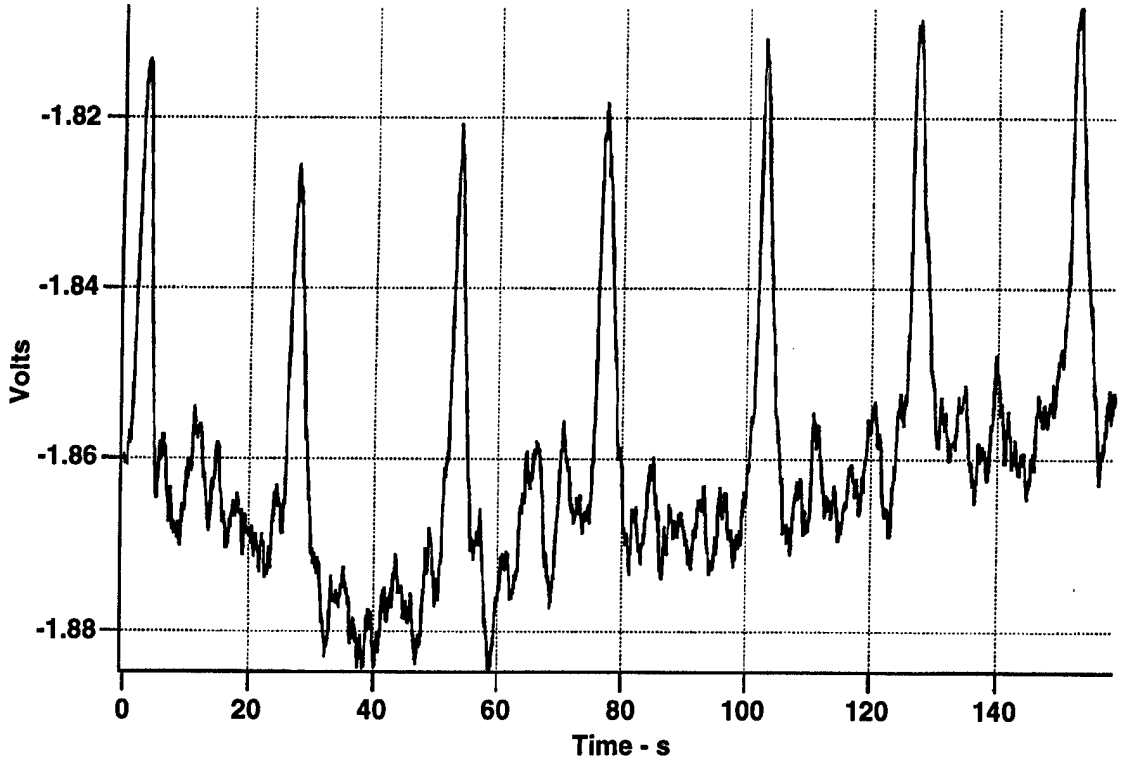

Figure 4.27
Standard gain horn, dc-coupled data from the passive millimeter wave sensor, smoothing only.

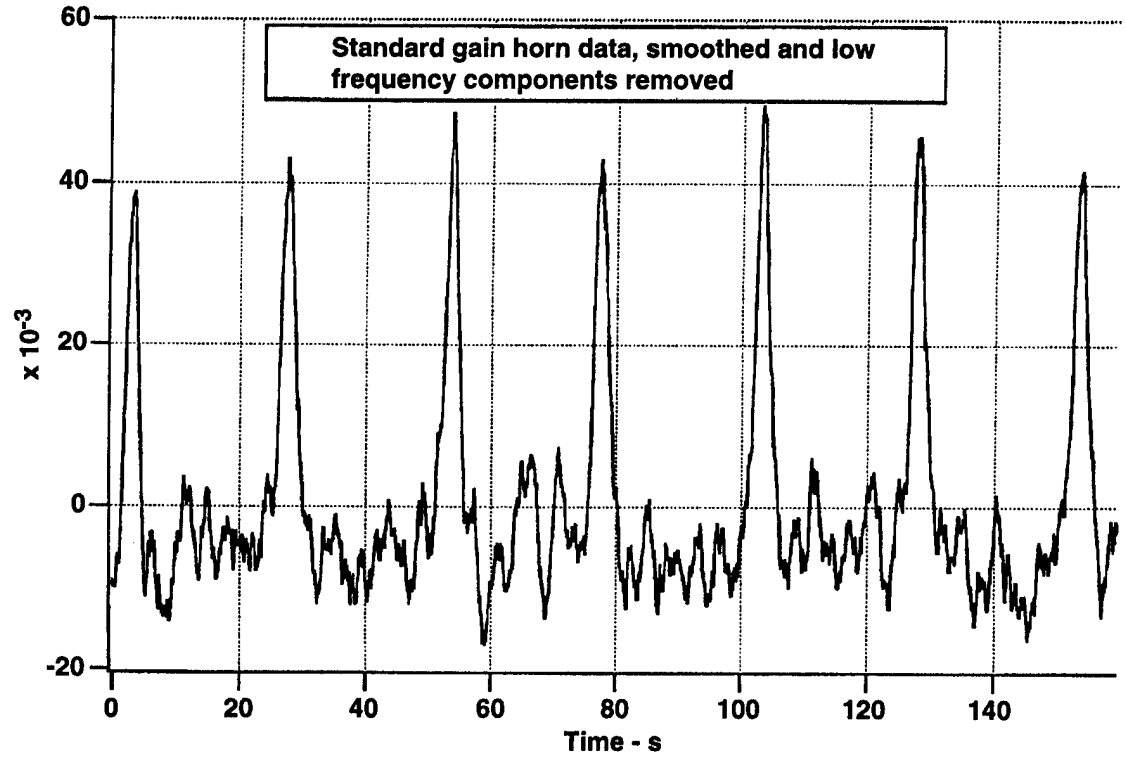

Figure 4.28
Standard gain horn, dc-coupled data from the passive millimeter wave sensor, with high-pass filtering at 0.01 Hz and smoothing.

Output of the PMMW sensor for the short range interior environment test with the standard gain horn antenna, smoothed by 2.8-s triangle smoothing filter. Target passing in the field of view of the sensor is positive-going spike at approximately 20-s intervals.

ARL:UT
AS-97-122
RLR - rfg
4-97

The next test was to change the standard gain horn to a reflector antenna. This had an effect similar to adding the lens to the PIR sensor. The results shown in Figs. 4.23–4.26 show improvement in the signal strength for the PMMW sensor similar to that obtained by putting a lens in front of the PIR sensor. It is important to note that the average temperature shift seen at the antenna is about 4°C to 5°C for the reflector antenna in which the target nearly fills the beam spot, while the temperature shift at the standard gain horn antenna, which has a spot size of 11 m^2 at 25 ft, shows only about a 0.6°C shift. The PIR has a lens that allows coverage of zones while keeping the total beam spot area relatively small. This is accomplished with the creation of narrow fingered beams, each of which are focused on one pyroelectric element. Unfortunately, at the time of this testing, an antenna with this type of beam pattern was not available, although such antennas can be fabricated.[13]

Figures 4.29 and 4.30 show the effect of different types of clothing on the received signal level. The pyrometer is used because it produces a calibrated absolute radiometric output. Note that the temperature difference between the target and the background is about 7°C and is barely affected by interposing the shirt or the heavy coat. The infrared signature in contrast is substantially affected even by the shirt. It will be shown later that the radiation from the head of the target is a large contributor to the overall signature detected by the PIR, while the whole body is detected by the PMMW sensor. Figures 4.31–4.34 show the output of the PMMW sensor and the PIR sensor in two walk-by tests. The target is dressed in normal clothing in the top traces. The lower two traces were taken when the subject was wearing a coat. Note that the PIR signature decreased slightly by about 14 percent of the average peak level, while the PMMW signature has increased slightly. The average signal strength on the PMMW sensor was about 5 percent larger when the subject was wearing a coat. This is possibly because the retained body heat warmed the skin, which is what the PMMW sensor detected. Ironically, a common evasive tactic, wearing a coat, caused the subject to become more visible on the PMMW sensor. A second test was conducted in which the subject again performed a normal walk-by experiment while wearing a coat and then adding a head covering of a piece of urethane packing foam. Urethane packing foam was observed to effectively block the infrared radiation, but seemed more transparent to the millimeter wave

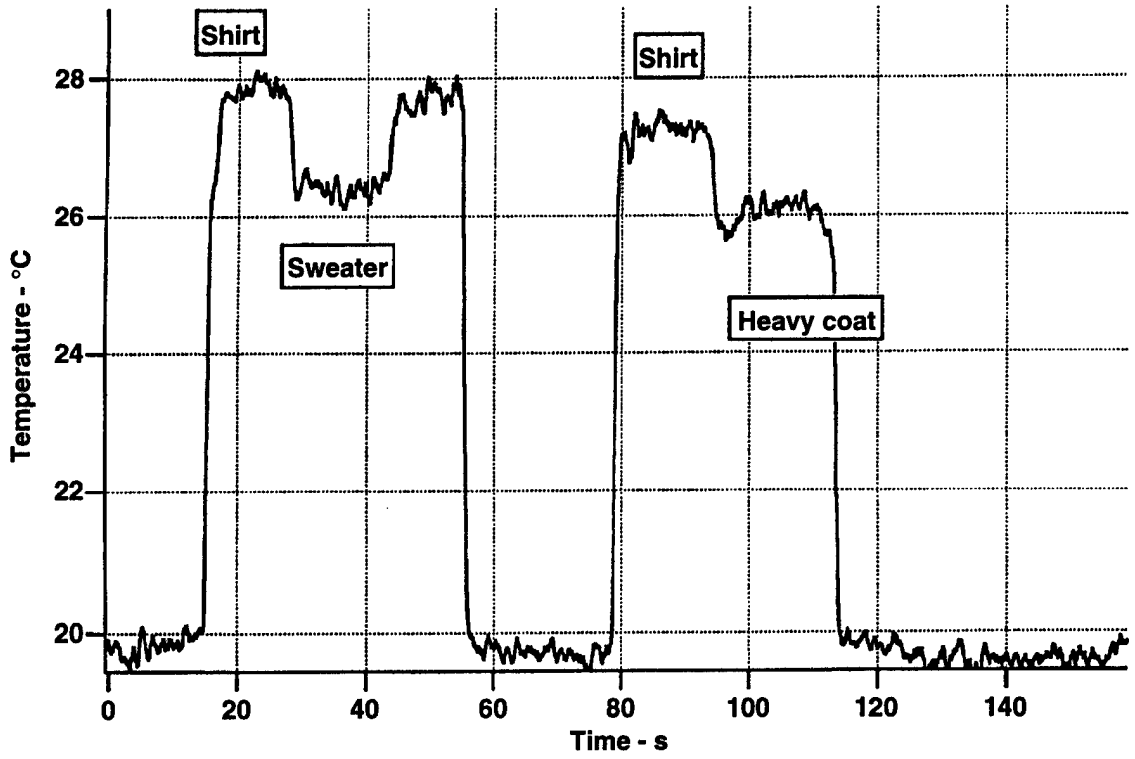

Figure 4.29
Unfiltered output of the passive millimeter wave sensor.

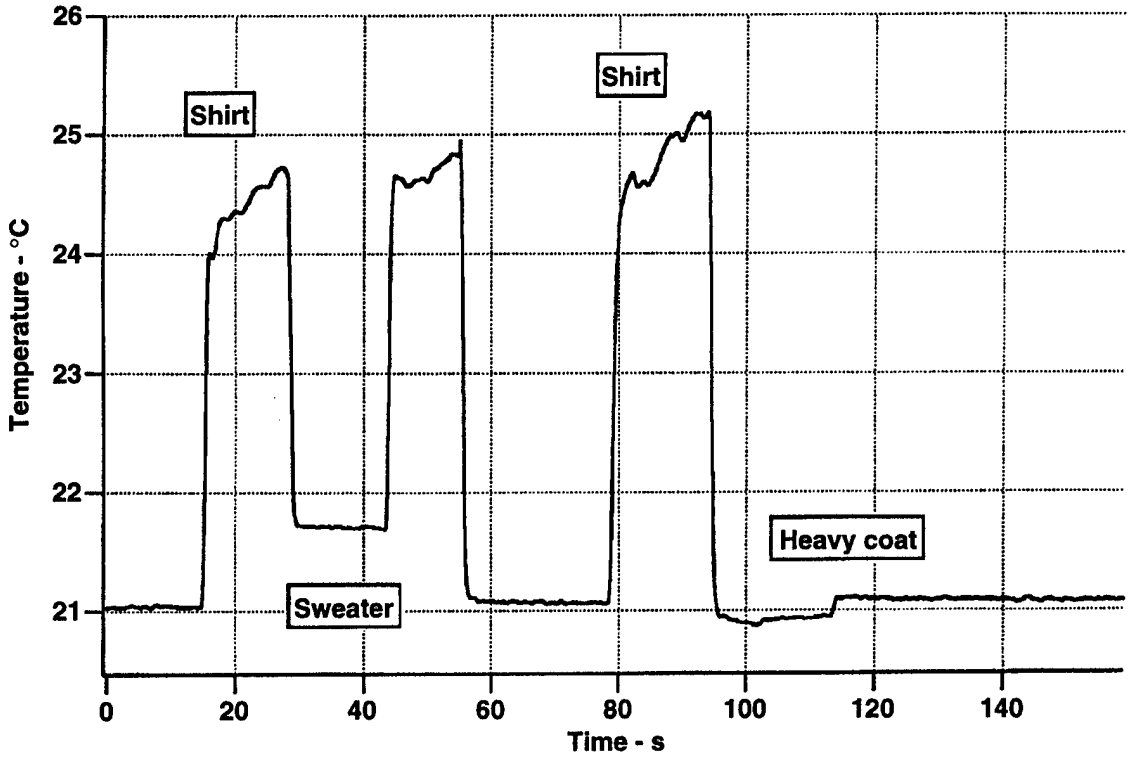

Figure 4.30
Pyrometer output.

Sensor outputs with a target moving into the field of view of both sensors simultaneously. Different articles of clothing were then interposed between the target and the sensors of the pyrometer and the PMMW. The sequence on the sensors is background, target with light shirt, target with light shirt and heavy sweater, target with light shirt, background, target with light shirt, target with light shirt and heavy coat.

ARL:UT
AS-97-123
RLR - rfg
4-97

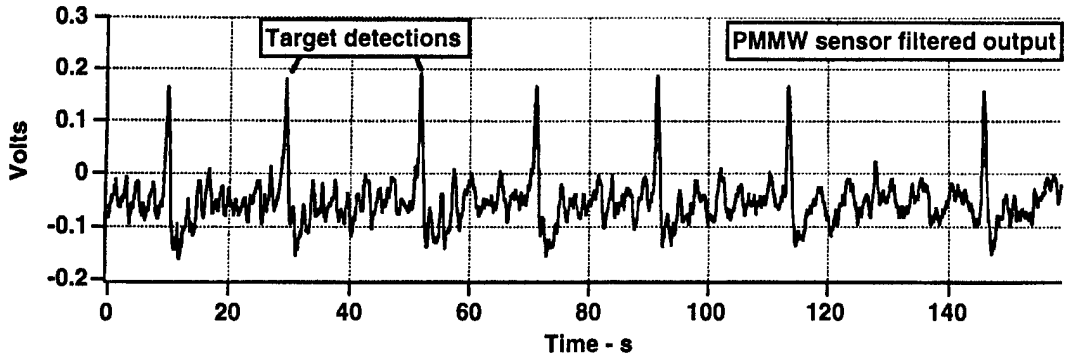

Figure 4.31
Target in normal clothing – passive millimeter wave sensor filtered output (test 1).

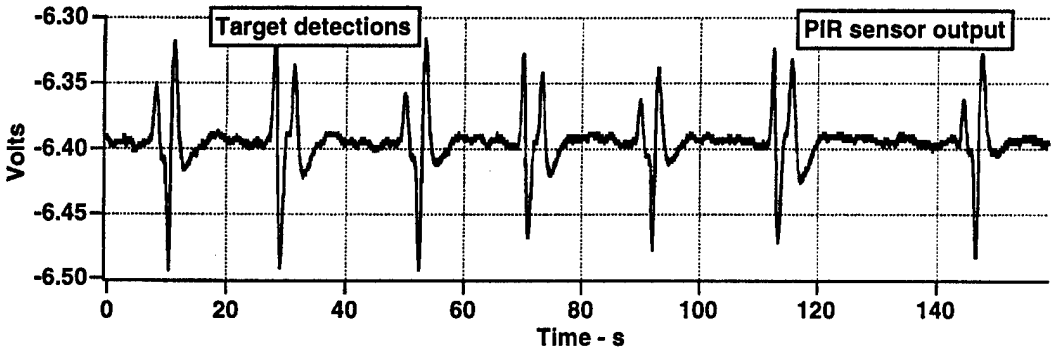

Figure 4.32
Target in normal clothing – passive infrared sensor output (test 1).

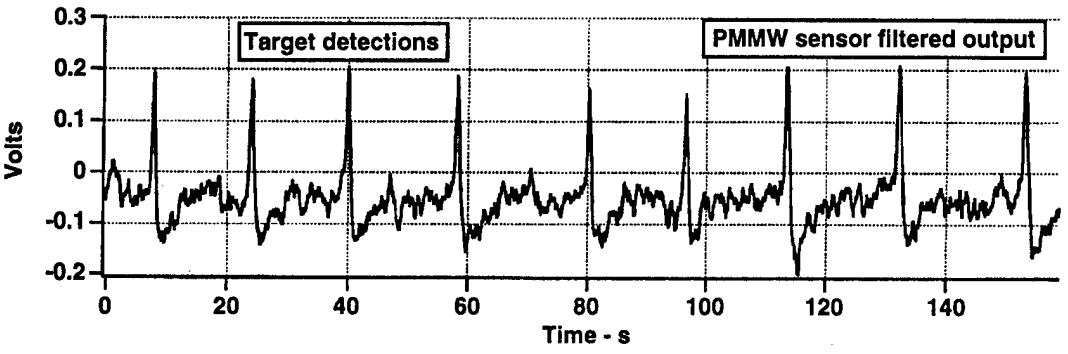

Figure 4.33
Target wearing down coat – passive millimeter wave sensor filtered output (test 2).

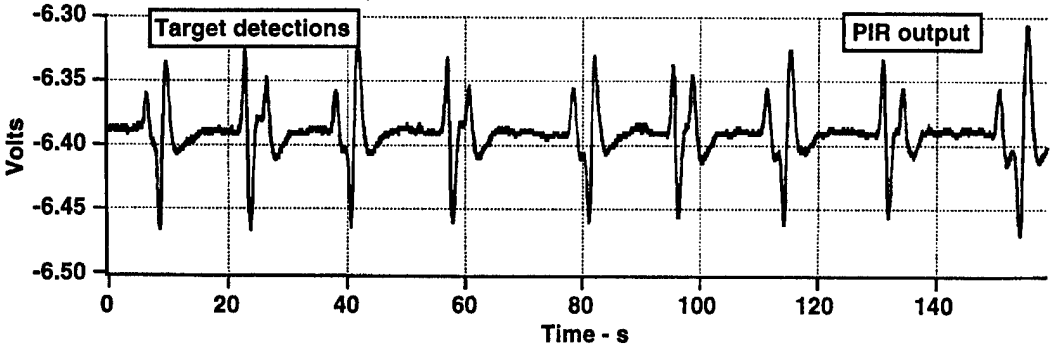

Figure 4.34
Target wearing down coat – passive infrared sensor output (test 2).

Short range interior test with target clothed normally (test 1) and with target wearing a heavy coat (test 2). PMMW sensor with reflector antenna and PIR with lens. PMMW data have been filtered with a 1.4-s triangle filter. Target passing in the field of view of the sensor is positive-going spike at approximately 20-s intervals. The response of the PIR and the filtered PMMW sensor have a positive-going and a negative-going response for a single detection.

ARL:UT
AS-97-124
RLR - rfg
4-97

radiation. The results of these two tests are compared in Figs. 4.35–4.38. Note that in the bottom trace, the signature on the PIR is much smaller. The reduction in target signal strength is about a factor of 3.7. The PMMW signature is reduced only by about 10 percent. This substantial reduction in signal strongly suggests that the PIR is primarily responding to radiation from the target's head.

Figures 4.39 and 4.40 compare close range tests conducted to assess the time response sensitivity of the sensor. The first crossings shown are walk-bys. The target took approximately 4 s to cross the field of view of the sensor during a normal walk-by. The smaller signals were produced when the target ran across the field of view of the sensor. This took approximately 1.5 s. It was not a full run, since the room was too small to allow that much speed. The typical reduction in target strength varied with the speed of the target, but reductions of 20 to 1 over the walking test were typical. Furthermore, the alarm in the PIR was not triggered during the run-by tests. The PMMW sensor, in contrast to the reflector antenna, showed only a 2 to 1 reduction in signal strength. The resulting SNR for the PIR was then down to about 2, while the PMMW sensor was still around 6. The SNR for the PIR was not high enough to reliably detect a target, while the PMMW sensor still was high enough for low false alarm rate detection. The PIR signal was checked at a point before reaching the analog filters to ensure that the dramatic reduction in signal observed was not due to the choice of post-detection filter time constants. The signal reduction appeared to be due to the response of the pyroelectric element itself and not the external circuitry.

Because ranges over about 25 ft are difficult to find in rooms, the tests for greater range were conducted in a long hallway. The hallway was more than 300 ft long. The testing was conducted during low traffic periods. However, some traffic was unavoidable, which made testing somewhat more difficult. Figures 4.41–4.44 show the typical detections made with a target range of 50 ft. The PIR sensor did not detect the target, but the PMMW sensor with the reflector antenna had no trouble detecting the target. The detections were performed while the target walked across the hallway. The hallway width was about 5 ft. The ambient temperature was around 20°C. Even though the PIR did not detect

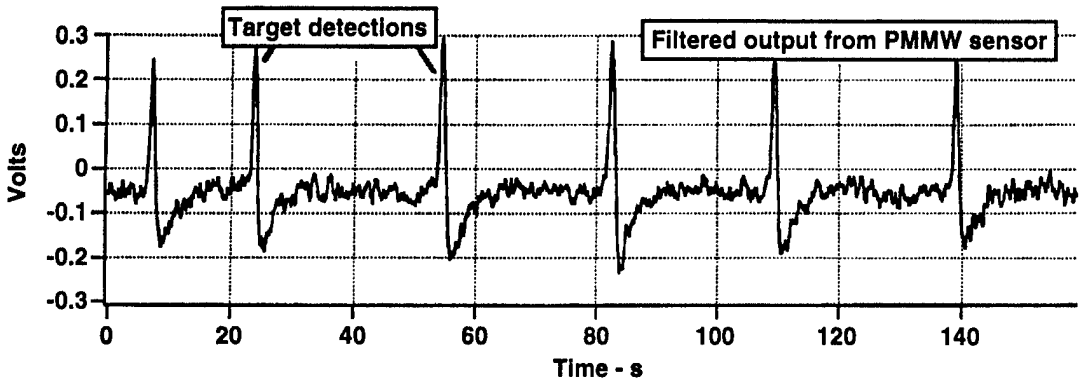

Figure 4.35
Target with no head cover – passive millimeter wave sensor filtered output (test 1).

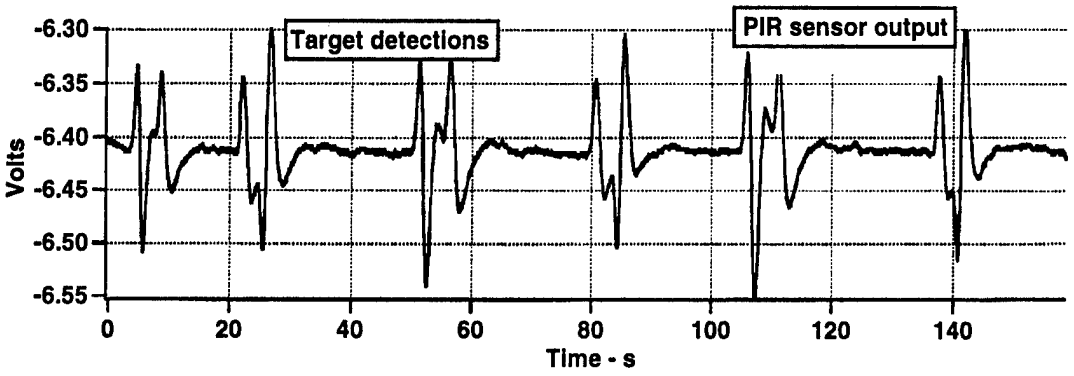

Figure 4.36
Target with no head cover – passive infrared sensor output (test 1).

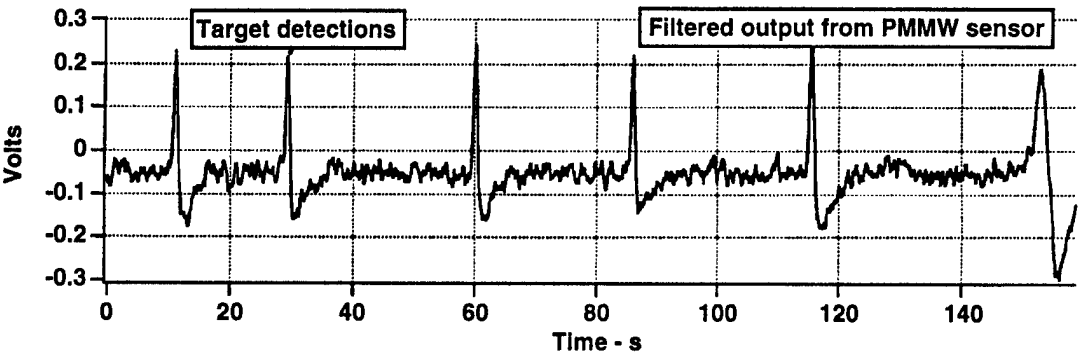

Figure 4.37
Target with head cover – passive millimeter wave sensor filtered output (test 2).

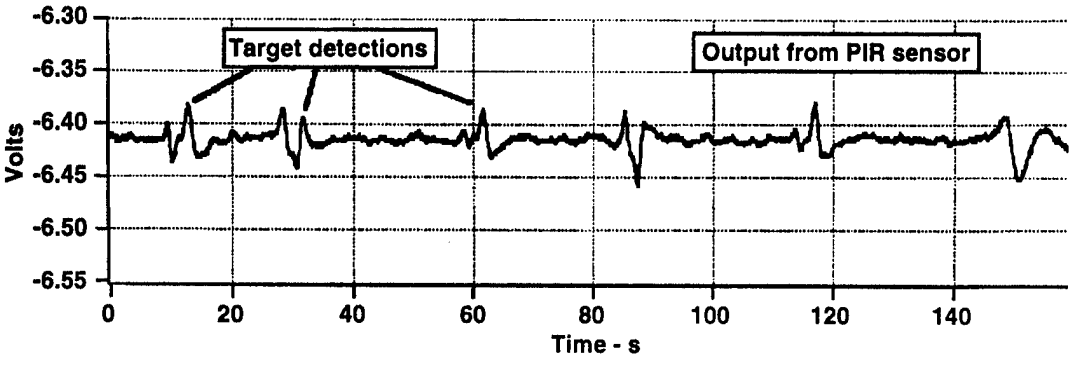

Figure 4.38
Target with head cover – passive infrared sensor output (test 2).

Short range interior test with target wearing a heavy coat without head cover (test 1) and with head cover (test 2); PMMW sensor with reflector antenna and PIR with lens. PMMW data have been filtered with a 1.4-s triangle filter.

ARL:UT
AS-97-125
RLR - rfg
4-97

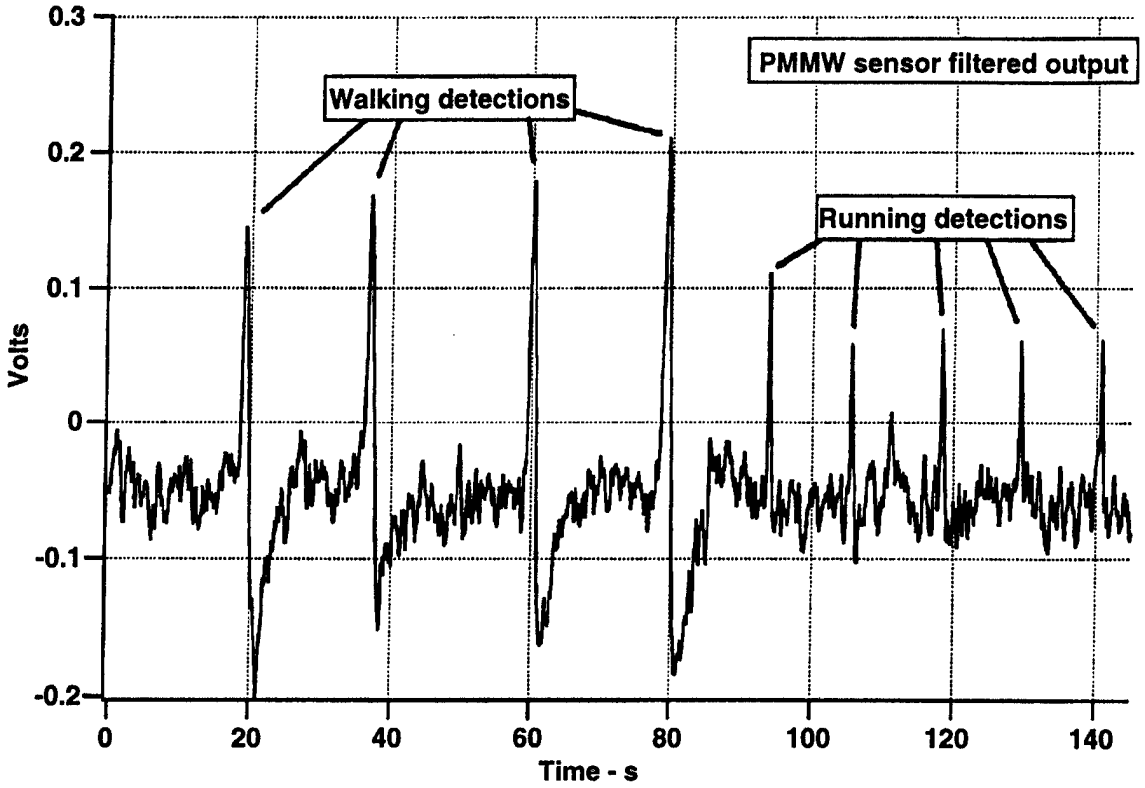

Figure 4.39
Passive millimeter wave sensor filtered output.

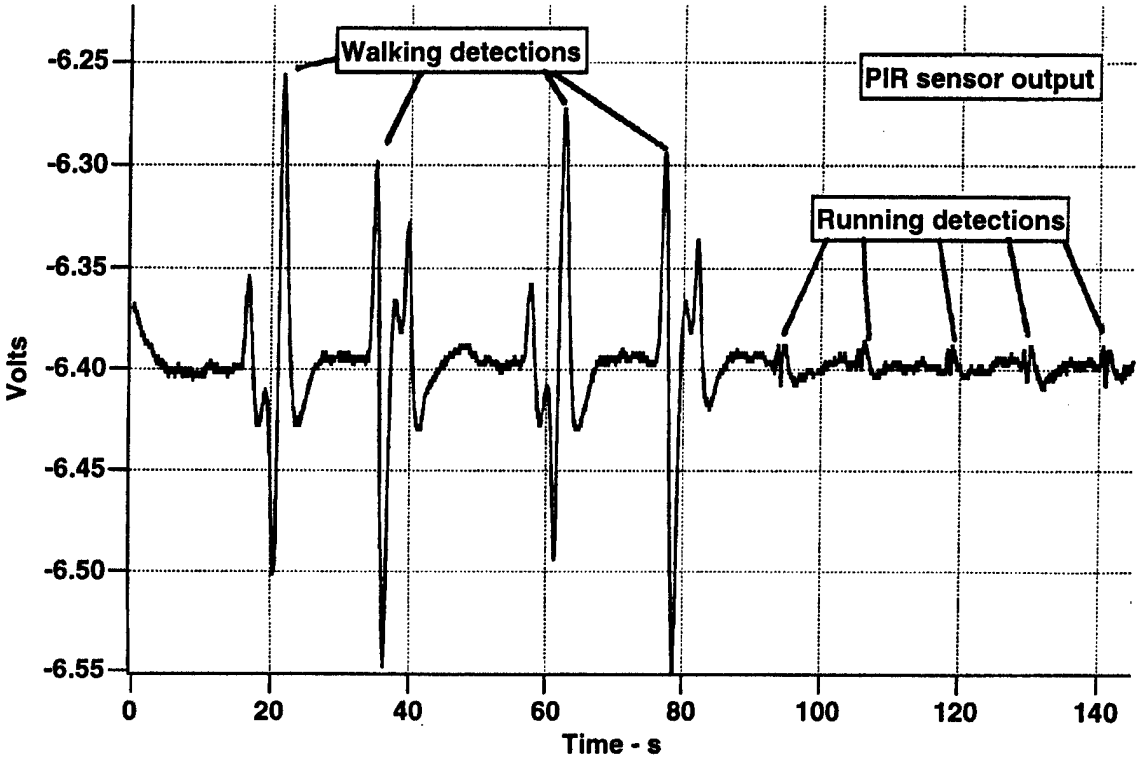

Figure 4.40
Passive infrared sensor filtered output.

Short range interior walk-by/run-by test with target wearing normal clothing. First four detections were with the target moving at a normal walking pace, taking about 4 s to cross the target area. The next five detections were with the target moving at a fast walk, taking about 2 s to cross the field of view. PMMW data were smoothed with a 1.4-s triangle filter.

ARL:UT
AS-970-126
RLR - rfg
4-97

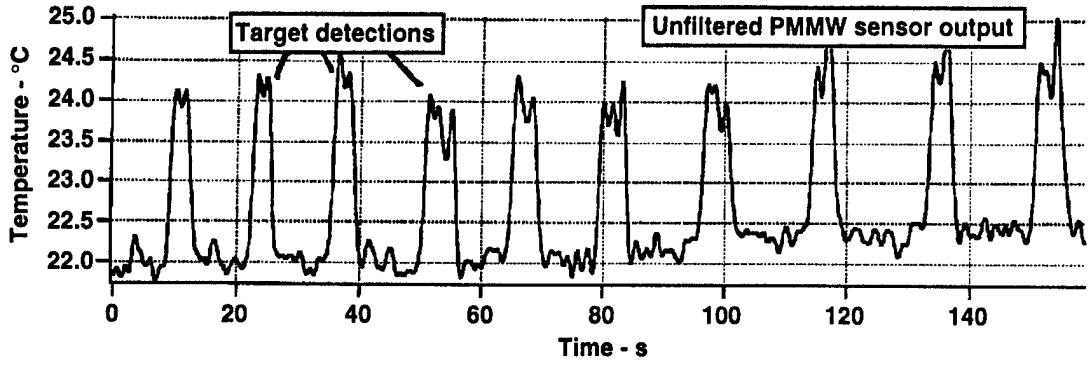

Figure 4.41 Passive millimeter wave sensor unfiltered output.

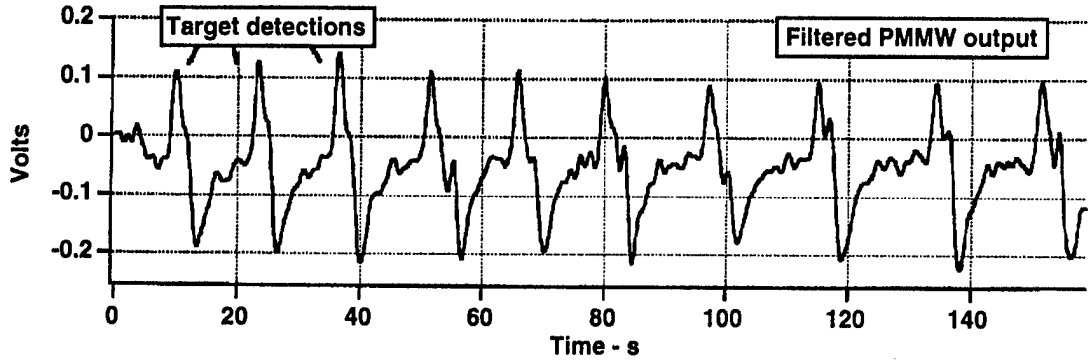

Figure 4.42 Passive millimeter wave sensor filtered output.

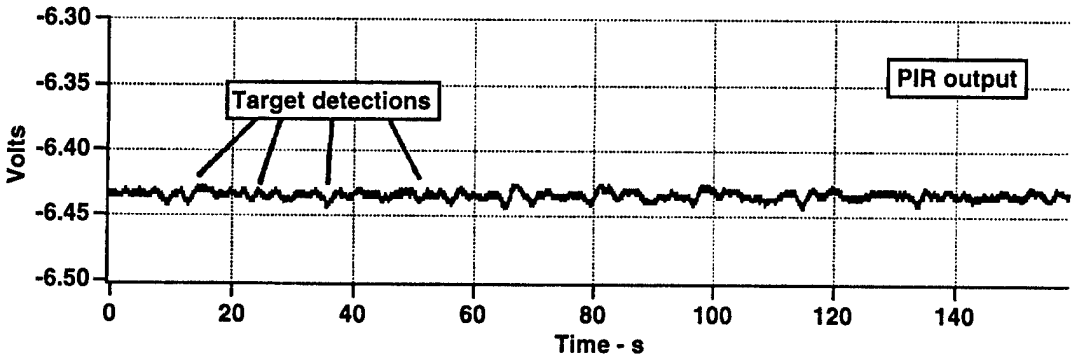

Figure 4.43 Passive infrared sensor output.

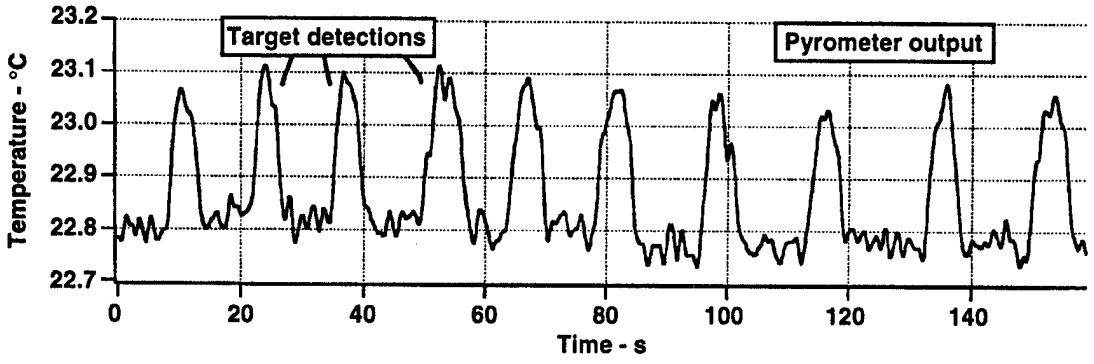

Figure 4.44 Pyrometer output.

Long range interior test with sensors looking down a long (300-ft) hallway. PMMW sensor data were smoothed with a 1.4-s triangle filter. Pyrometer sensor data were smoothed with a 2.8-s triangle filter. Target range is 50 ft, and the target is walking across the hallway at a normal pace. Target passing in the field of view of the sensor is positive-going spike at approximately 15-s intervals. The responses of the PIR and the filtered PMMW sensor have a positive-going and a negative-going response for a single detection.

ARL:UT
AS-97-127
RLR - rfg
4-97

the target, the pyrometer did. This difference is probably due to the single beam of the pyrometer that points more or less down the hall, whereas the PIR lens produces a fan-type beam.

Figures 4.45–4.52 show detections at 75 and 115 ft, respectively. The pyrometer shows detections at 75 ft. Even though the detections on the PMMW at 115 ft are visible, the temperature shift registered by the sensor is about 1°C, which is only about 3 to 4 standard deviations above the noise.

Referring back to Fig. 3.4, we can look at the receiver operating curves (ROCs) for the different SNR values obtained in these tests. If we want a P_d of about 0.9 or better with a false alarm rate of 10^{-7} or better (a minimum of one false alarm in 4 months, assuming a 1-s sampling interval), then the lowest SNR we can accept is 5. By examining Table 4.2, we can see that the PMMW sensor meets this requirement with either the horn antenna or the reflector antenna. However, the reflector antenna meets this criterion with a comfortable margin and will probably work over a wider range of environmental conditions. The PIR sensor without the lens would not meet this criterion, but with the lens, it would be met comfortably against a normal walking target. The PIR would could not, however, be used in the configuration used here to reliably detect a running target with the stated desired probabilities of false alarm and detection. Tables 4.3 and 4.4 show that the PMMW could also meet this requirement with the reflector antenna at a range of 75 ft in the hall tests. The PIR sensor could not be used even at 50 ft.

4.4 BLOCKAGE TESTS

One important feature of the PMMW sensor is its ability to "see" through many common materials such as Sheetrock, Styrofoam, and plywood. This has important applications when it is desirable to conceal the sensor. This capability is also useful at a distance for determining whether personnel are behind walls, wooden doors, or inside a building.

The test revealed that the PMMW sensor could detect targets through various substances that block a normal PIR sensor. Figures 4.53 and 4.54 show

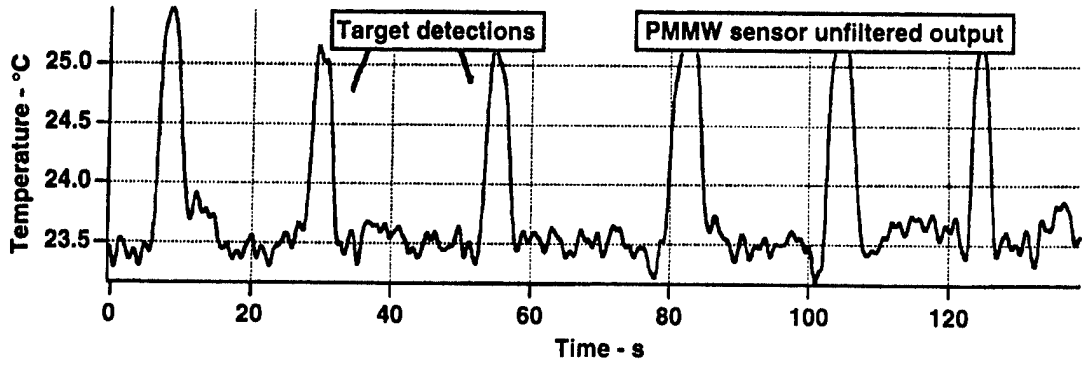

Figure 4.45
Passive millimeter wave sensor unfiltered output.

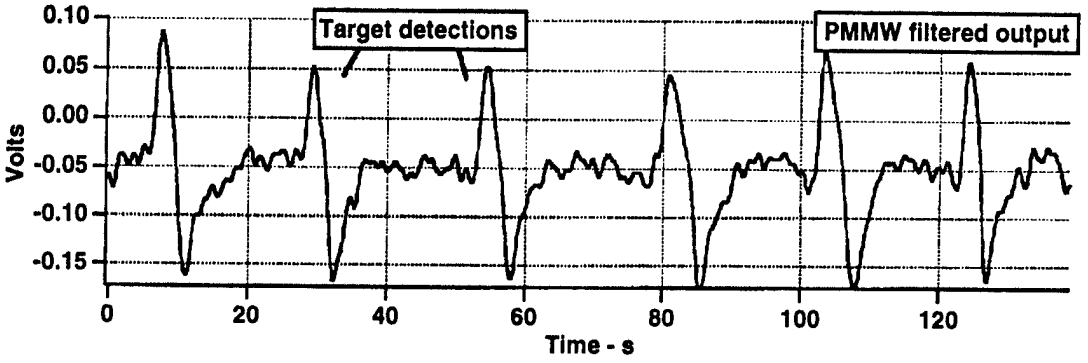

Figure 4.46
Passive millimeter wave sensor filtered output.

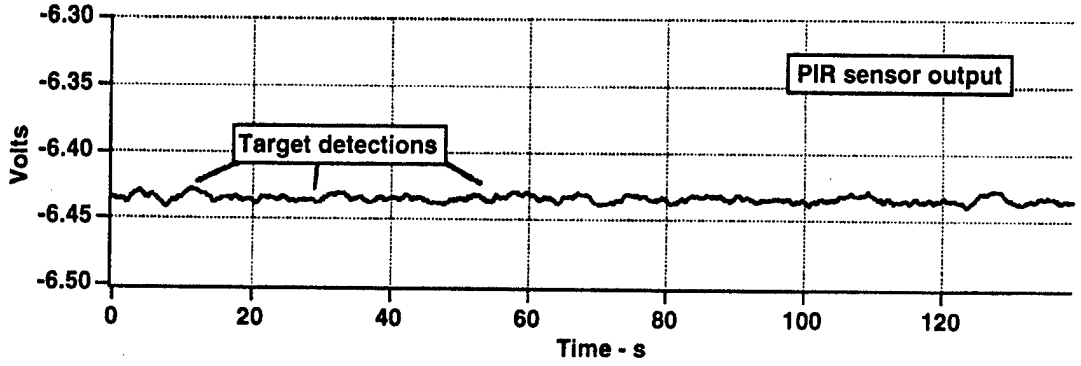

Figure 4.47
Passive infrared sensor output.

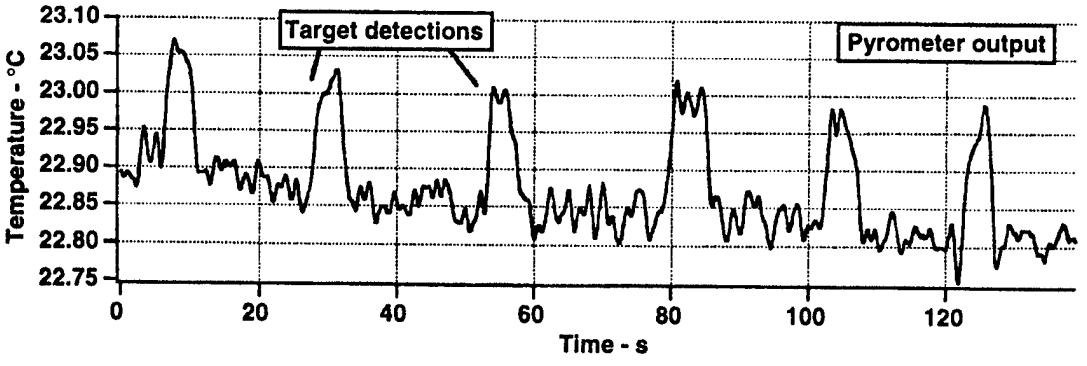

Figure 4.48
Pyrometer output.

Long range interior test with sensors looking down a long (300-ft) hallway. PMMW sensor data smoothed with a 1.4-s filter. Pyrometer data smoothed with a 2.8-s triangle filter. Target range is 75 ft, and the target is walking across the hallway at a normal pace. Target passing in the field of view of the sensor is positive-going spike at approximately 20-s intervals. The responses of the PIR and the filtered PMMW sensor have a positive-going and a negative-going response for a single detection.

ARL:UT
AS-97-128
RLR - rfg
4-97

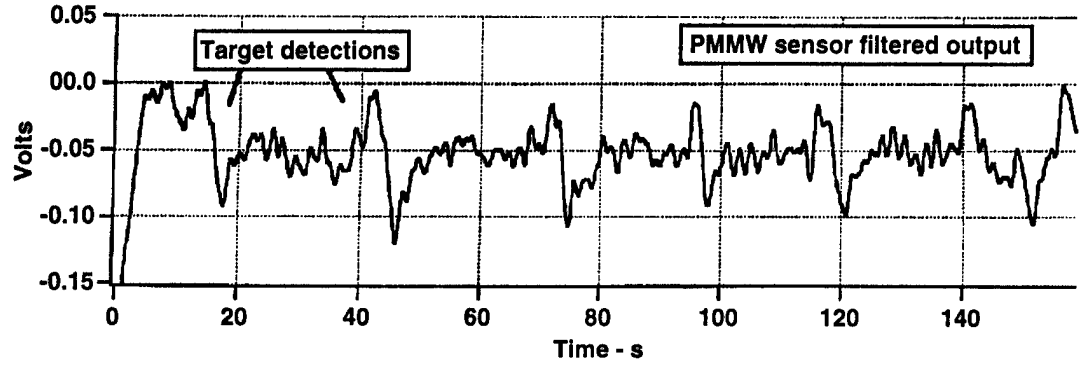

Figure 4.49
Passive millimeter wave sensor unfiltered output.

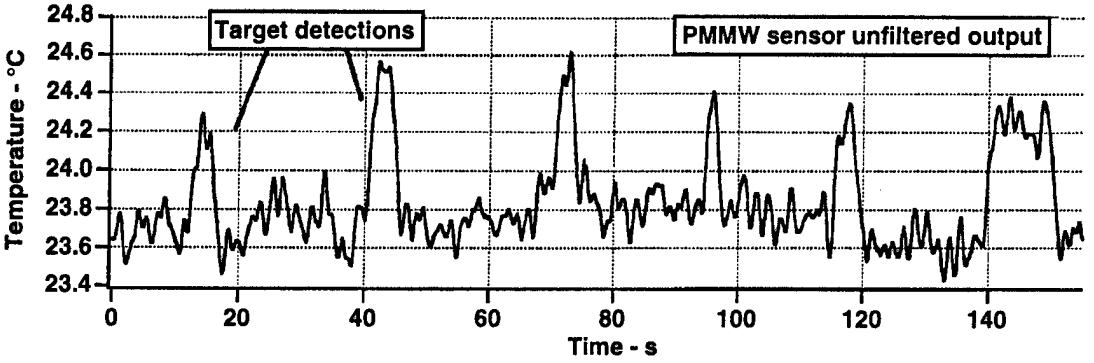

Figure 4.50
Passive millimeter wave sensor filtered output.

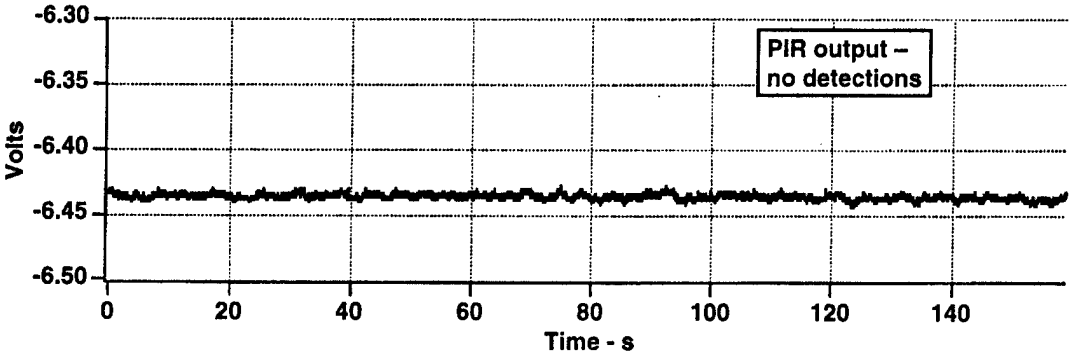

Figure 4.51
Passive infrared sensor output.

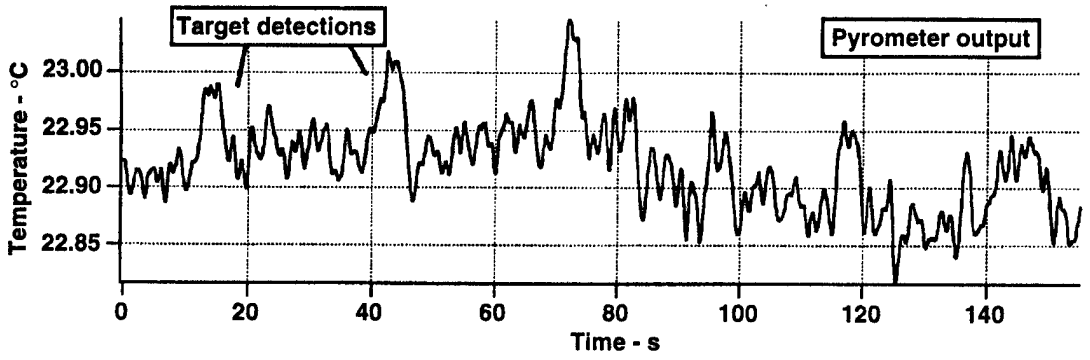

Figure 4.52
Pyrometer output.

Long range interior test with sensors looking down a long (300-ft) hallway. PMMW sensor data smoothed with a 1.4-s filter. Pyrometer data smoothed with a 2.8-s triangle filter. Target range is 115 ft, and the target is walking across the hallway at a normal pace.

ARL:UT
AS-97-129
RLR - rfg
4-97

Table 4.3
PMMW detections.

Range	No analog filter/ smoothed	SNR	Analog filter/ smoothed	SNR
50 ft	0.134 V	13.0	0.134 V	10.0
75 ft	0.085 V	9.4	0.10 V	7.7
115 ft	0.03 V	3.0	0.048 V	3.7

Table 4.4
PIR detections.

Range	Analog filtered output	SNR
50 ft	0.007 V	3.88
75 ft	0.0045 V	2.5
115 ft	No detectable signal	0.0

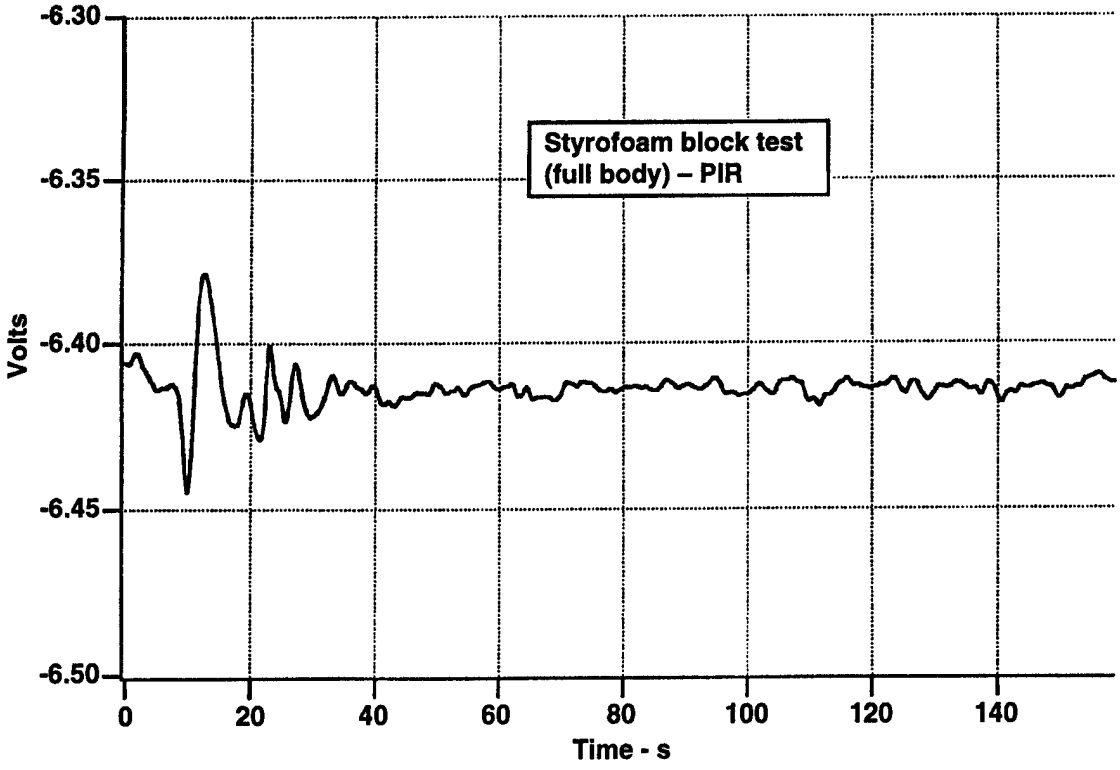

Figure 4.53
Passive infrared sensor output.

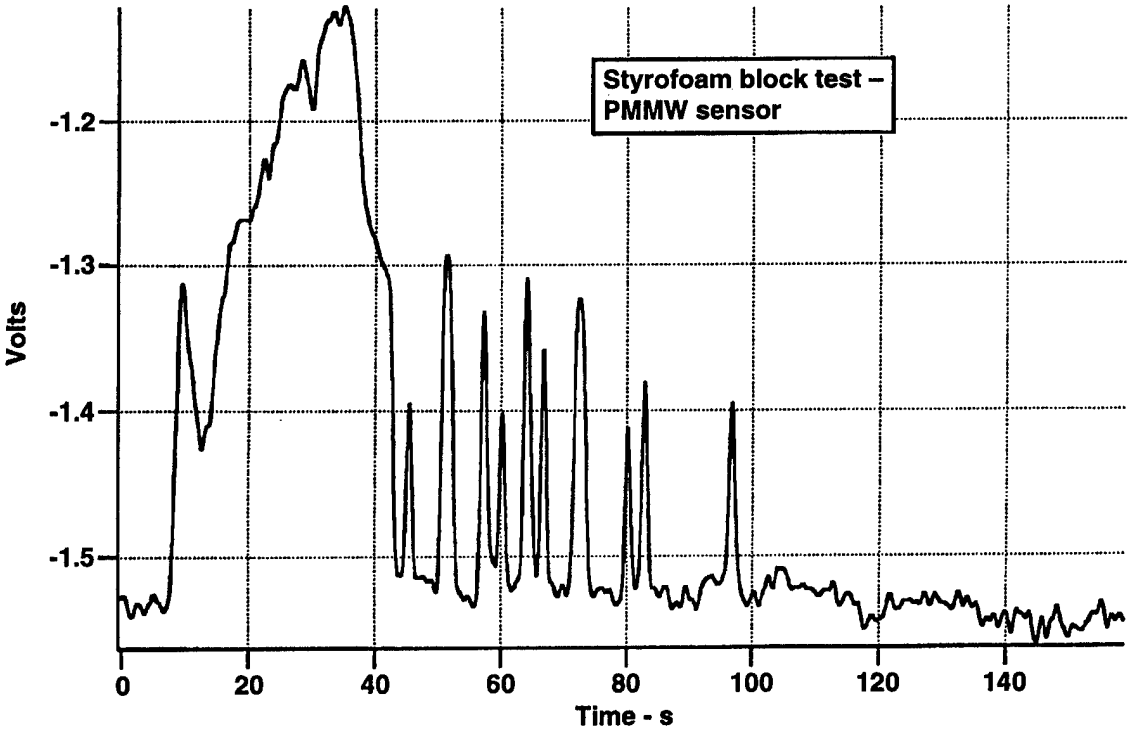

Figure 4.54
Passive millimeter wave sensor output. Large positive-going spike is the target advancing on the sensor with Styrofoam in front of the sensor. Smaller spikes are the target moving laterally back and forth in front of the sensor.

Short range interior test with target advancing on sensors with a large sheet of Styrofoam held between target and sensors. The initial signal is the target and Styrofoam moving into the field of the sensors, advancing on the sensor, and the Styrofoam being place in front of both sensors. The PIR sensor alarm was not triggered. The walk-by detections are at 25 ft.

ARL:UT
AS-97-130
RLR - rfg
4-97

the outputs of the PIR and the PMMW sensor when a piece of Styrofoam is placed in front of both sensors. The PIR sensor is completely blinded by the Styrofoam, while the PMMW sensor has no difficulty detecting targets through it. Essentially, the Styrofoam is transparent to the millimeter wave radiation. It was also found that if the Styrofoam was held in front of the target and moved up very close to the PIR sensor, the target could be blinded without setting off the sensor.

Figures 4.55 and 4.56 show a similar test with 5/8-in.-thick Sheetrock. The PMMW sensor can detect a target a substantial distance through the Sheetrock while again the PIR sensor is completely blocked. This is a very interesting feature because this means that the sensor could be placed behind a wall and detect activity on the other side of the wall.[14] Thus, the sensor would be completely concealed. Figures 4.57 and 4.58 show essentially the same result with 1/2-in.-thick plywood.[15] Typical building materials are, therefore, relatively transparent to the sensor, and the sensor can be completely concealed behind normal drywall. If the sensor sees too far through the walls, then the threshold could be changed to accommodate the desired reduced detection range.

4.5 EXTERIOR RESULTS

Several tests were conducted outside to assess the capability of the PMMW sensor in an exterior environment. Theoretically, the PMMW sensor should have a good detection range in the exterior environment, and this was confirmed by test results. It was also confirmed that the PMMW sensor was considerably more sensitive to targets than were either the PIR sensor or the pyrometer. Even more remarkably, the PMMW sensor detected targets at a range of as much as 200 ft when the exterior temperature was about 37°C (99°F). The ambient temperature during these tests was actually warmer than the surface temperature of the target. These test results suggest that the PMMW sensor is much less affected by ambient conditions in an exterior environment than are the other sensors.

Figures 4.59 and 4.60 show the output of the pyrometer and the PMMW sensor pointed at a garage door that is initially closed. At about 70 s from the beginning of the trace, the door is opened and the sensors are then pointed at the exterior environment. The air temperature of the exterior environment during

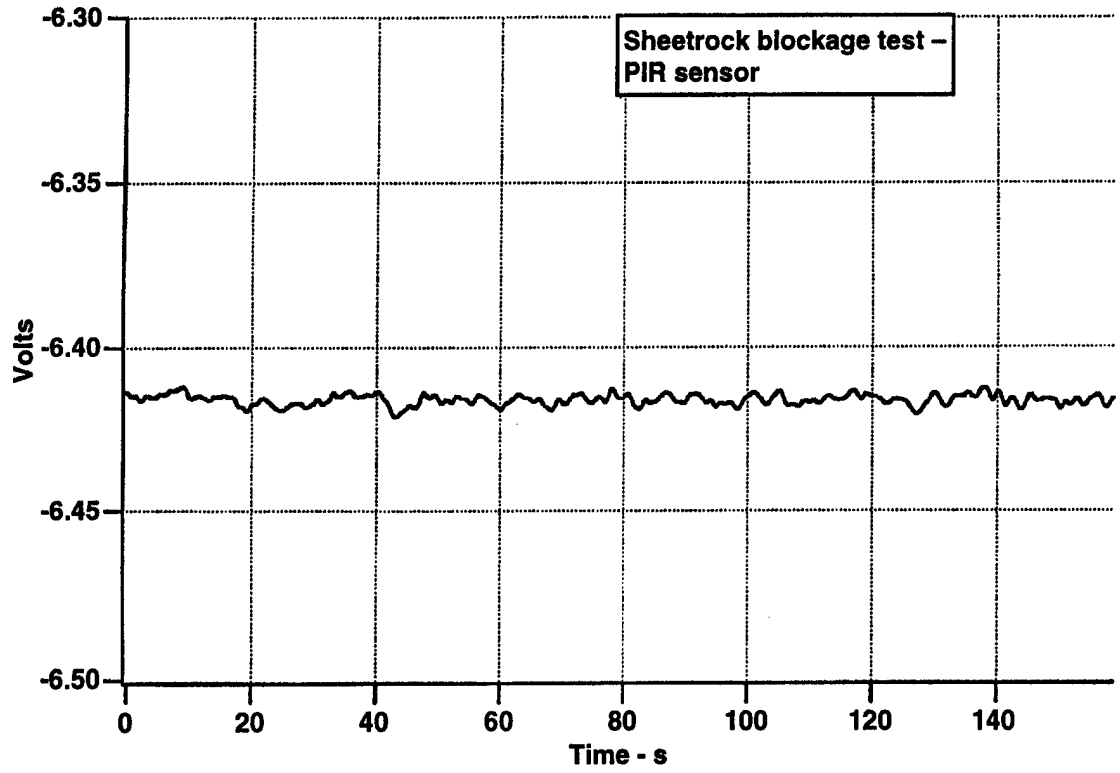

Figure 4.55
Passive infrared sensor output (no detections).

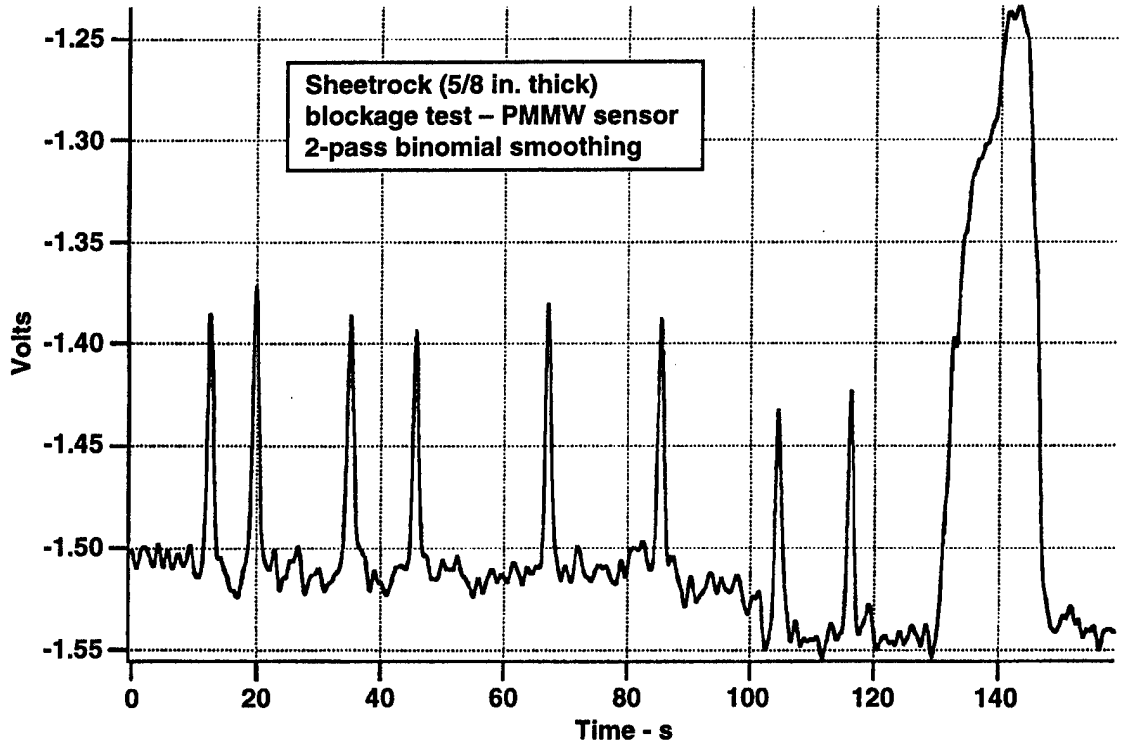

Figure 4.56
Passive millimeter wave sensor output. Positive-going spikes and the one large spike at 140 s are the target advancing radially on the sensor.

Short range interior test with 5/8-in.-thick Sheetrock in front of sensors. Target range is 25 ft. The last detection is a radial approach.

ARL:UT
AS-97-131
RLR - rfg
4-97

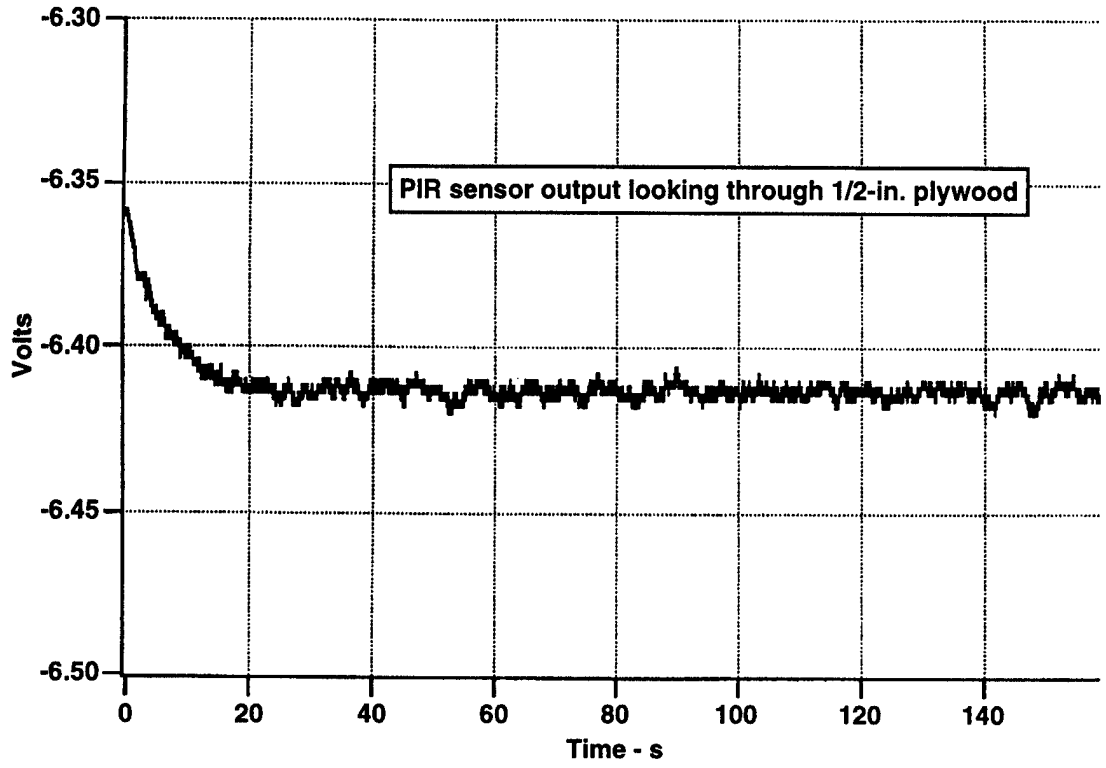

Figure 4.57
Passive infrared sensor output (no detections).

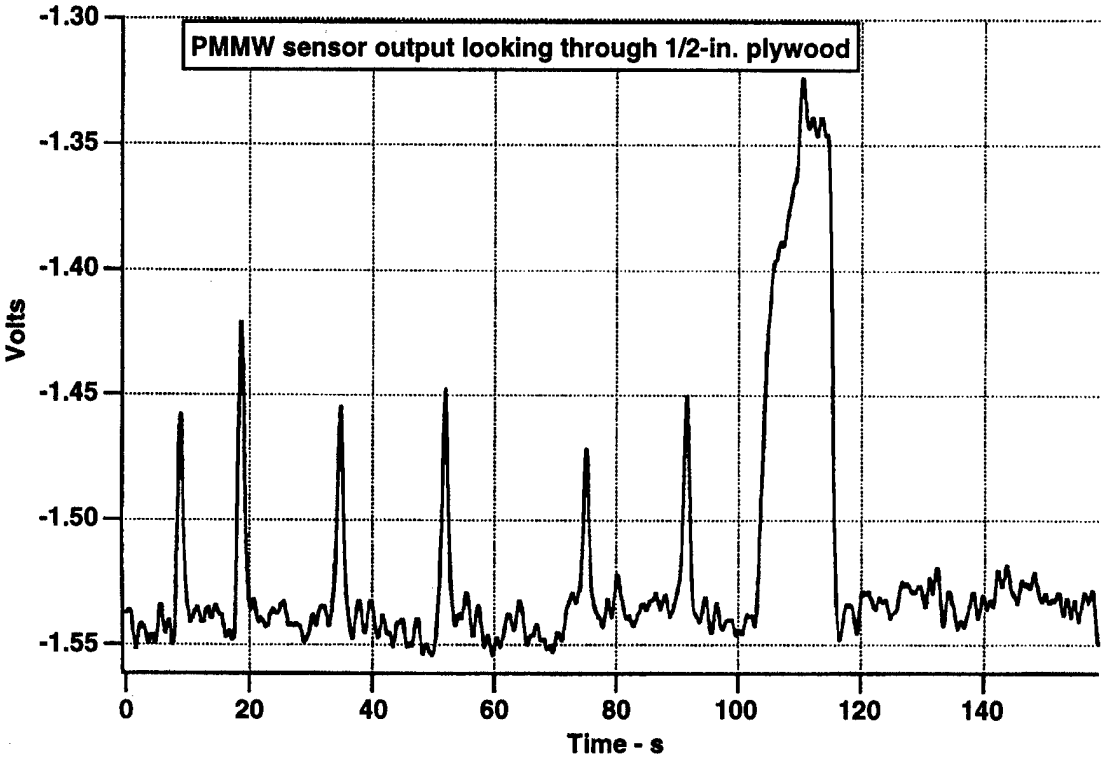

Figure 4.58
Passive millimeter wave sensor output. Positive-going spikes are the target passing in front of the covered area at 25-ft range; the large spike at about 110 s is the target advancing radially toward the sensor.

Short range interior test with 1/2-in. plywood in front of sensors. Target range is 25 ft. The last detection is a radial approach.

ARL:UT
AS-97-132
RLR - rfg
4-97

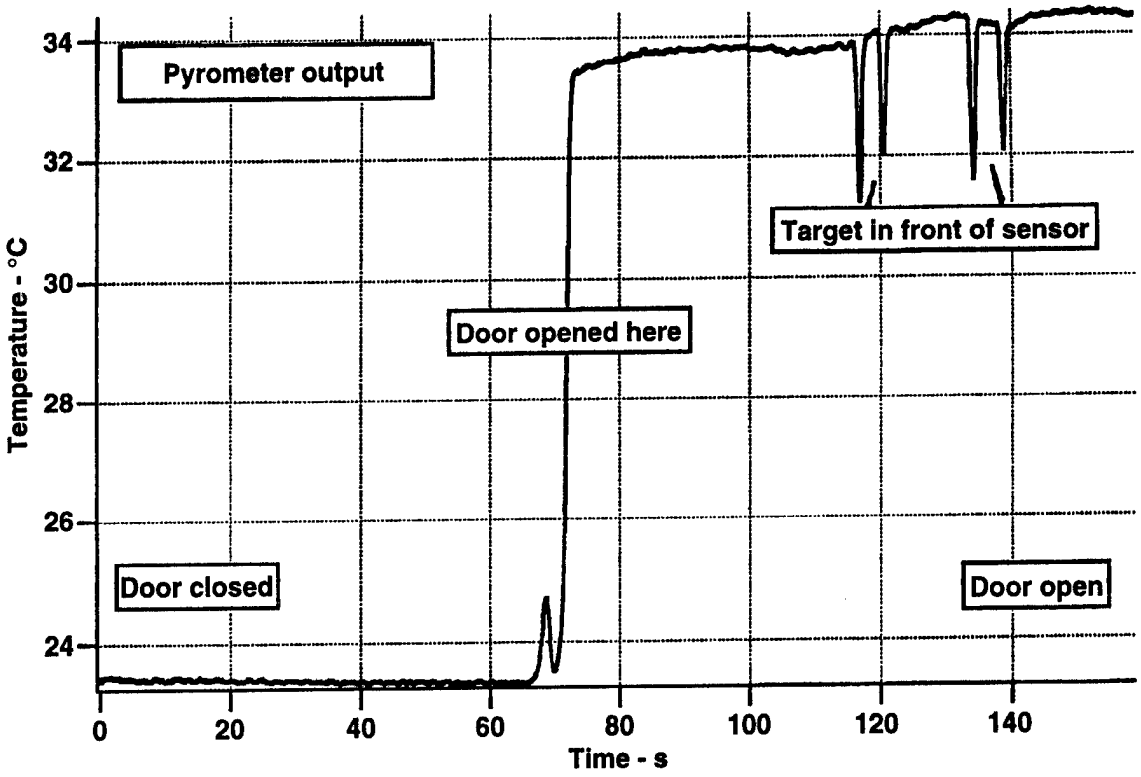

Figure 4.59
Pyrometer output. Target detections are negative-going spikes at about 120 and 140 s (four detections). Detection range is 2 ft.

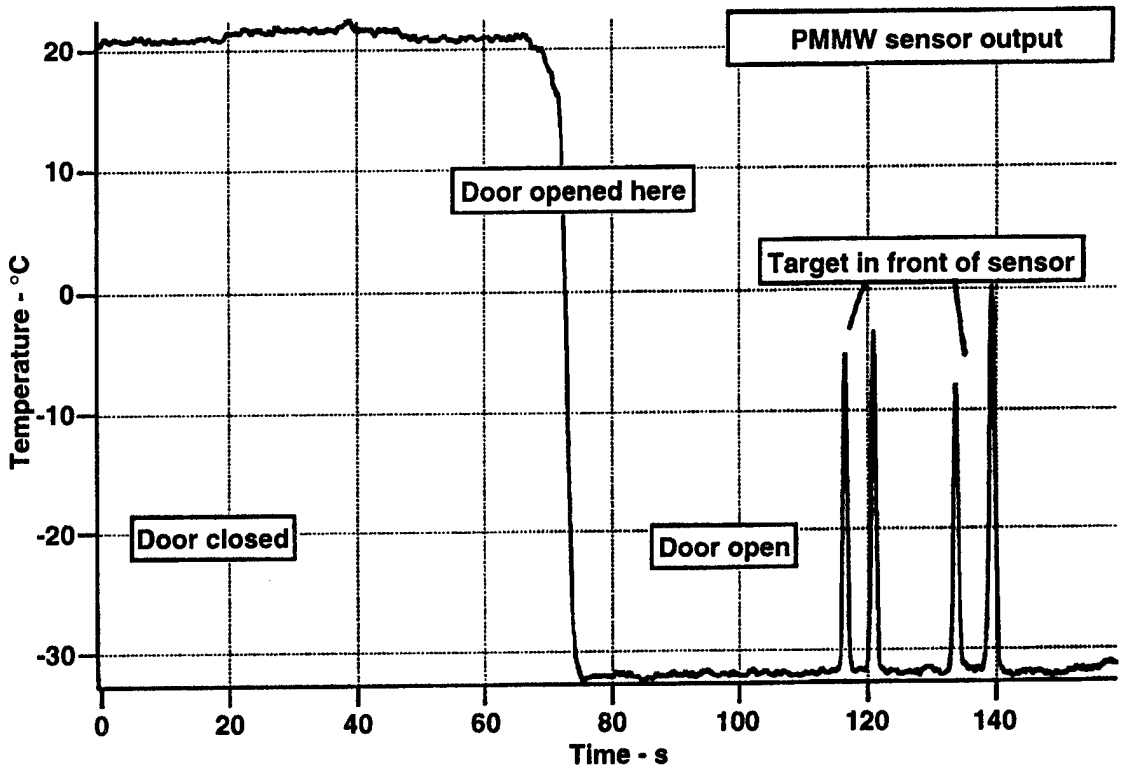

Figure 4.60
Passive millimeter wave sensor output. Target detections are positive-going spikes at about 120 and 140 s (four detections). Detection range is 2 ft.

Sensors located inside and looking at an overhead door, which is initially closed. The door is opened at 70 s. Interior ambient temperature is 21°C; exterior temperature is 36°C.

ARL:UT
AS-97-133
RLR - rfg
4-97

this test is 37°C (99°F), while the interior temperature is about 21°C (70°F). This data set clearly shows the difference in the behavior between the PMMW sensor and the pyrometer. As these data show, the infrared sensor output increases almost proportionately to the ambient temperature outside when the door is opened. The radiometric background temperature seen by the PMMW sensor, in stark contrast, drops roughly by 50°C. The spikes in the traces on both sensors are due to a target walking in front of the sensors at a range of about 5 ft. The infrared pyrometer output shows that the radiometric temperature of the target is actually less than the background temperature. The PMMW sensor, however, indicates that the radiometric temperature of the target is much warmer, by about 25°C, than the background temperature. This peculiar result is due to the fact that the sky is nearly transparent to outer space. The background radiometric temperature of the sky at 27 GHz is about 20 K. The sky temperature at infrared frequencies is close to ambient temperature (290 K to 300 K). At millimeter wave frequencies, the emissivity of terrestrial environment is less than 1. The emissivity of a human target is roughly 0.8, so the human target will appear warmer than the background if the emissivity of the background is less than that of the human. Because the actual temperature of the human is nearly 300 K warmer than the radiometric sky temperature, small differences in emissivity between the human target and the background can make large differences in apparent temperature contrast.

Figures 4.61–4.64 show a target detection at 100 ft. At this range, the target shows up quite well on the PMMW sensor, while neither the PIR sensor nor the pyrometer could detect the target. The temperature shift produced at the sensor antenna was about 9°C at 100-ft range. The target was more than 20 standard deviations above the noise level of the PMMW sensor, while it was not detectable on either of the infrared sensors.

Figures 4.65–4.68 show the detection of the target at a range of 160 ft (49 m), and at approximately 150 s, a truck passed in front of the sensor, producing a very large signal at a range of about 80 ft. Note that the spike is negative, indicating that the truck appeared to be a very cold object. This is because the metal from the truck is reflecting the sky temperature into the sensor, which is much lower than the ambient temperature. The truck showed up on the PIR and the pyrometer as a warm object. Note also that the signature is much smaller

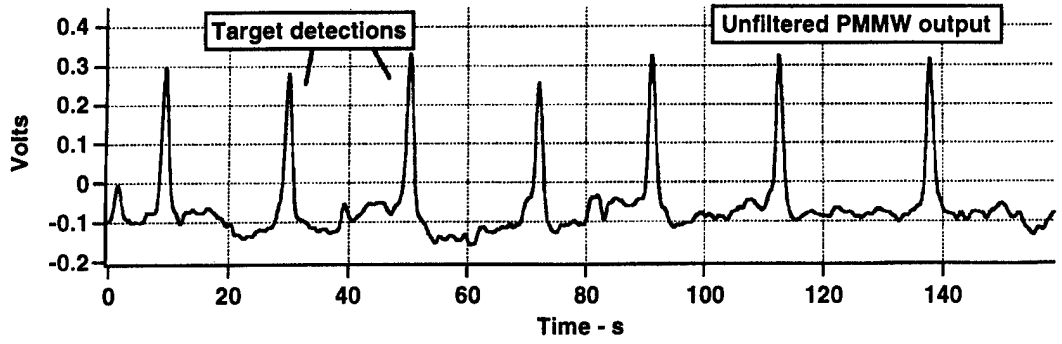

Figure 4.61
Passive millimeter wave sensor unfiltered output – ac-coupled with 200-s time constant. Target detections are positive-going spikes at approximately 20-s intervals.

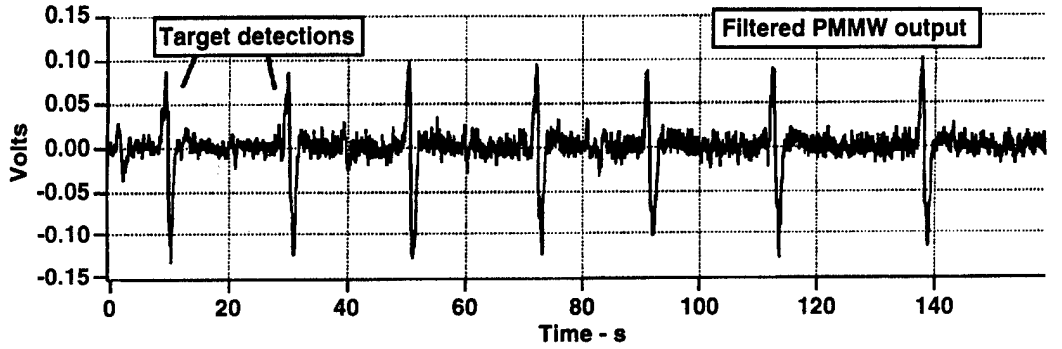

Figure 4.62
Passive millimeter wave sensor filtered output. Target detections are positive- and negative-going spikes at approximately 20-s intervals.

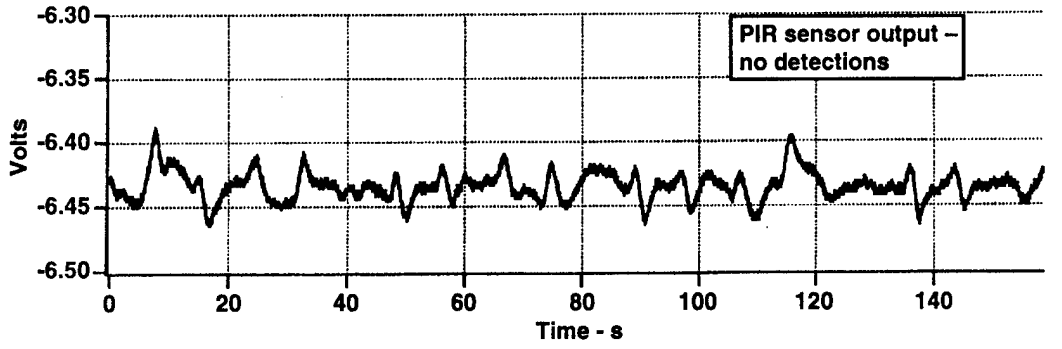

Figure 4.63
Passive infrared sensor output (no detections).

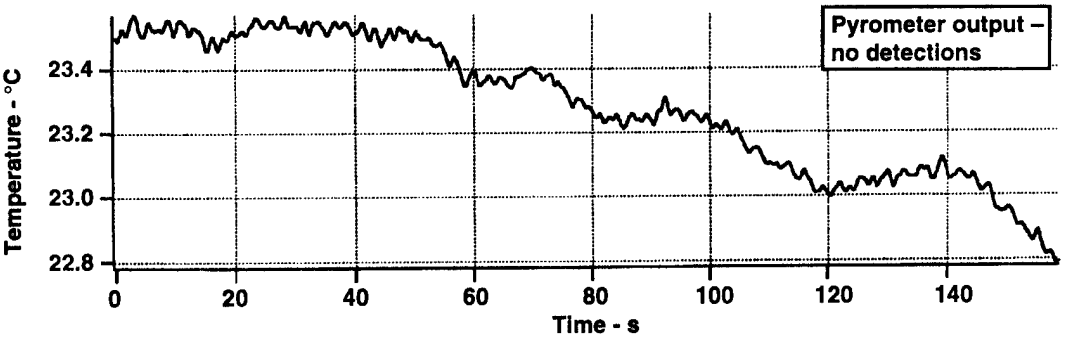

Figure 4.64
Pyrometer output (no detections).

Exterior sensor test with target at 100-ft range. Note that there are no discernible detections on either the pyrometer or the PIR sensor. The reflector antenna is used with the PMMW sensor. Pyrometer and unfiltered PMMW outputs are smoothed with 1.4-s triangle filter.

ARL:UT
AS-97-134
RLR - rfg
4-97

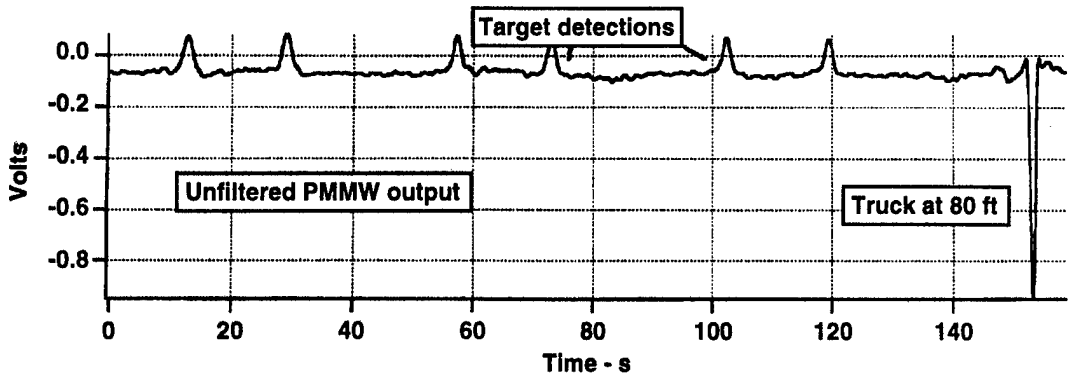

Figure 4.65
Passive millimeter wave sensor unfiltered output – ac-coupled with 200-s time constant. Target detections are positive-going spikes, and the truck passing 80 ft in front of the sensor is the large negative-going spike at about 150 s.

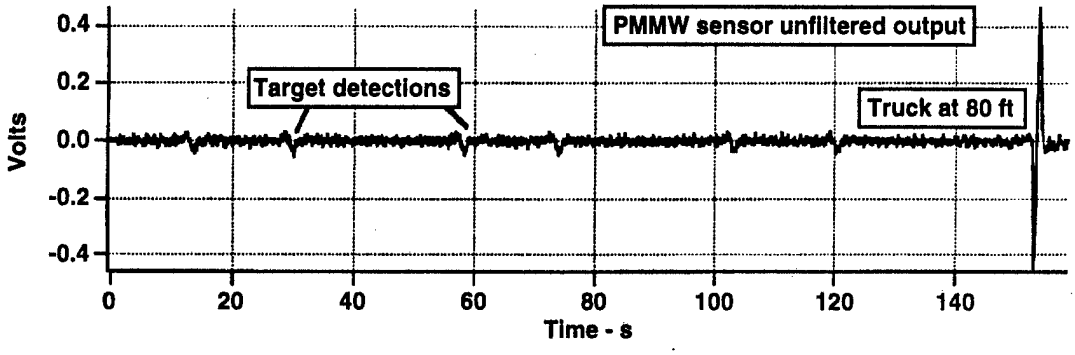

Figure 4.66
Passive millimeter wave sensor filtered output. Target detections are positive- and negative-going spikes, and the truck passing 80 ft in front of the sensor is the large, initially negative-going spike at about 150 s.

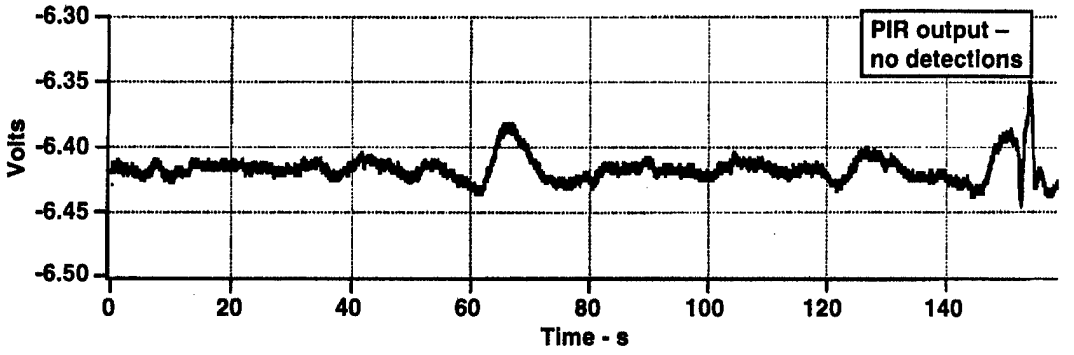

Figure 4.67
Passive infrared sensor output (no detections).

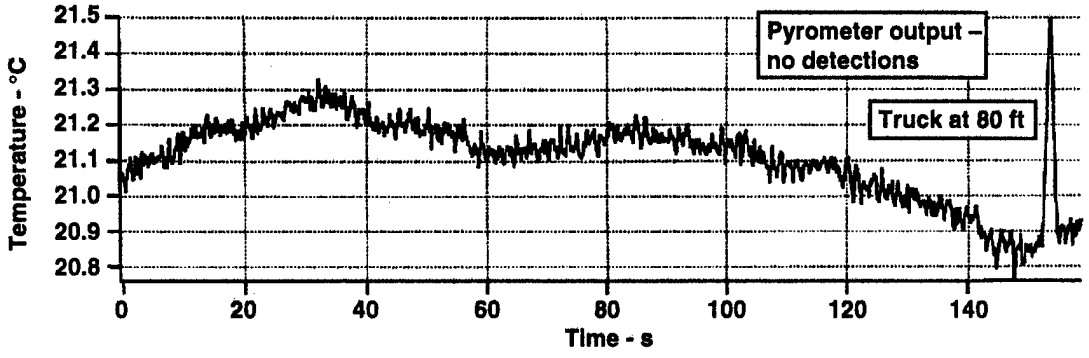

Figure 4.68
Pyrometer output. No target detections except for the truck (positive-going spike) at 150 s.

Exterior sensor test with target at 160-ft range. The only discernible detection on the pyrometer or the PIR is the truck at 80 ft. The reflector antenna is used with the PMMW sensor. Pyrometer and unfiltered PMMW outputs are smoothed with 1.4-s triangle filter.

ARL:UT
AS-97-135
RLR - rfg
4-97

than the signature on the PMMW sensor. Figure 4.65 shows that the target was about 13 standard deviations above the sensor noise. Figures 4.69 and 4.70 show exterior sensor test data from Figs. 4.65–4.68, rescaled to show target detections with the target at the 160-ft range. The truck is barely visible on the PIR sensor, and the target is not visible. The fluctuations on the PIR sensor are random and not related to target detection.

Figures 4.71–4.74 show the output of the sensor with the target at 200-ft range. Again, strong reliable detections were achieved. Again, as in all three of the previous cases, neither the PIR sensor nor the pyrometer detects the target. On the PMMW sensor, the target shows up at this range at about 10 standard deviations above the noise. This is a very strong detection, and the limit of detection could be further. However, the ability to detect a target while maintaining a low probability of false alarm requires an SNR greater than unity. The probability of false alarm for a target signal that is 10 standard deviations above the noise is less than 10^{-12}, or if the sensor noise and background noise has a Gaussian distribution, then probability of a false alarm is less than one false alarm in 10^4 years. It seems that the environment or the overall lifetime of the sensor may well play a more significant role in the false alarm rate than does the sensor noise.

The results of these tests are summarized in Table 4.5 (see page 71) for the exterior sensor tests. The results of the PIR and the pyrometer tests are not included because no detections were made at any range with either of these sensors. The PMMW sensors, in contrast, were able to detect targets at 200 ft with a high SNR. The ambient temperature was about 23°C.

Figures 4.75 and 4.76 show a remarkable set of detections made at a range of 200 ft when the exterior ambient air temperature was about 99°F. This set of data was made in the late afternoon when the temperatures were maximum. The infrared pyrometer shows a background temperature of about 36°C, which corresponds to 97°F. The infrared pyrometer showed no detections beyond a few feet in front of the sensor. This data clearly show that the sensitivity of the PMMW sensor appears to depend on different environmental variables than does the PIR sensors.

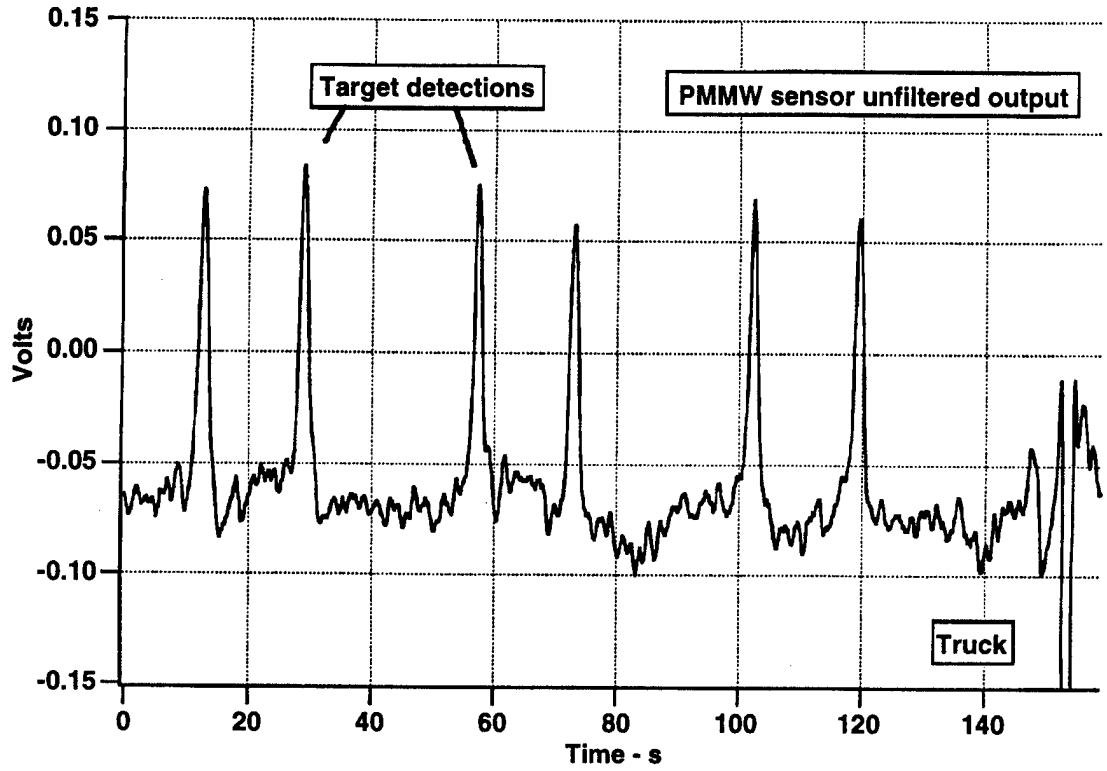

Figure 4.69
Exterior detection, passive millimeter wave sensor, unfiltered output.

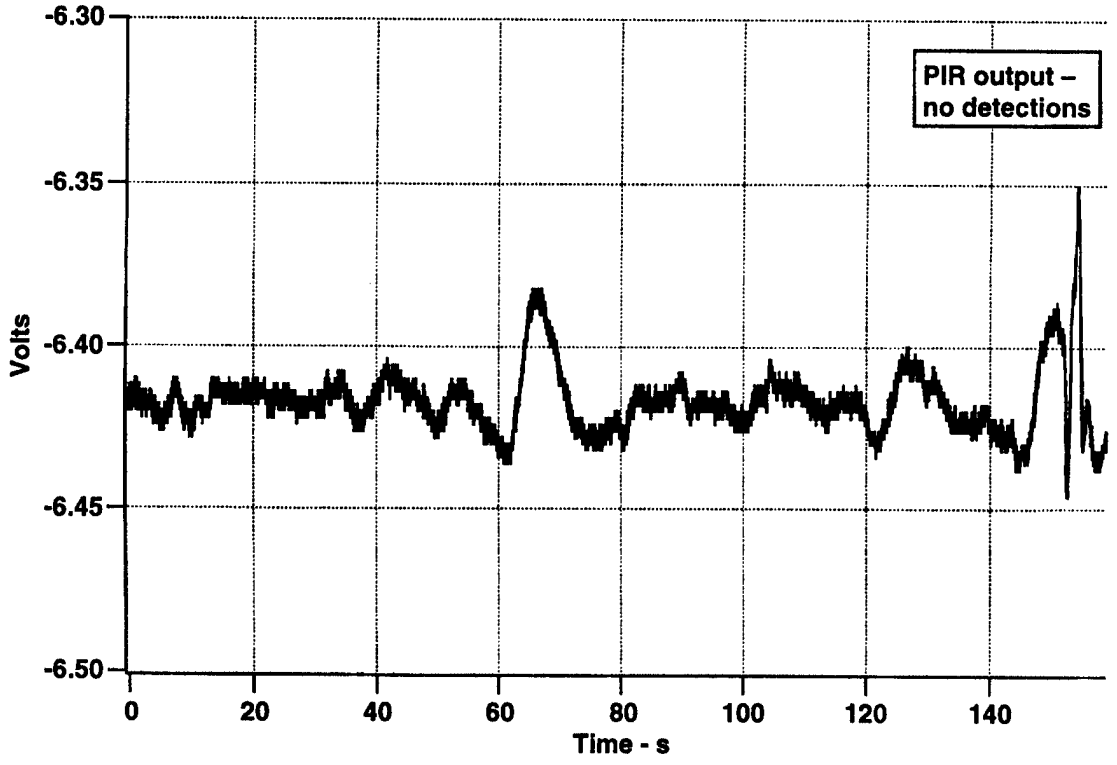

Figure 4.70
Passive infrared filtered ouput.

Exterior sensor test data shown in Figs. 4.65 and 4.67 but rescaled to show target detections with target at 160-ft range.

ARL:UT
AS-97-136
RLR -rfg
4-97

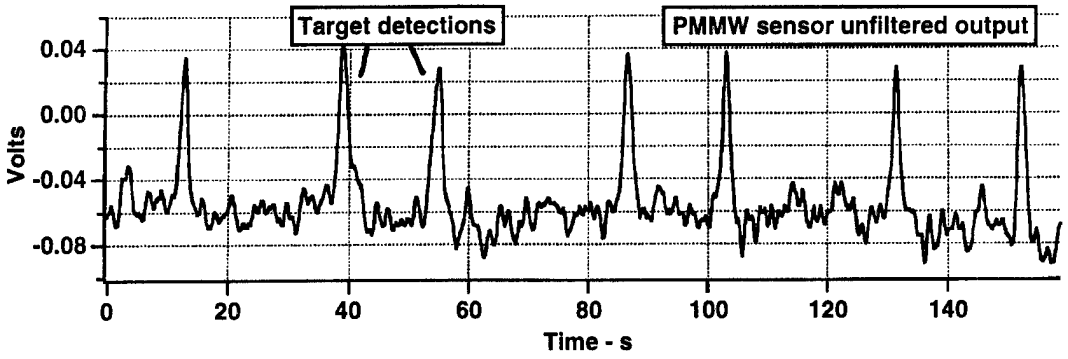

Figure 4.71
Passive millimeter wave sensor unfiltered output – ac-coupled with 200-s time constant. Target detections are positive-going spikes at approximately 20-s intervals.

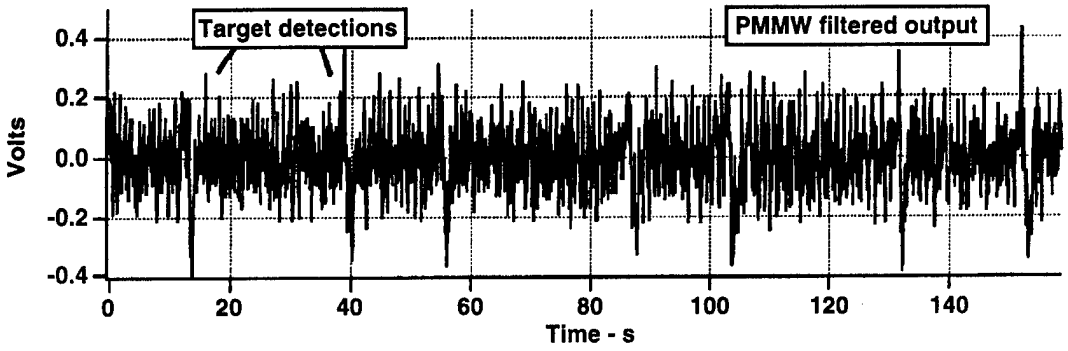

Figure 4.72
Passive millimeter wave sensor filtered output. Target detections are positive- and negative-going spikes at approximately 20-s intervals.

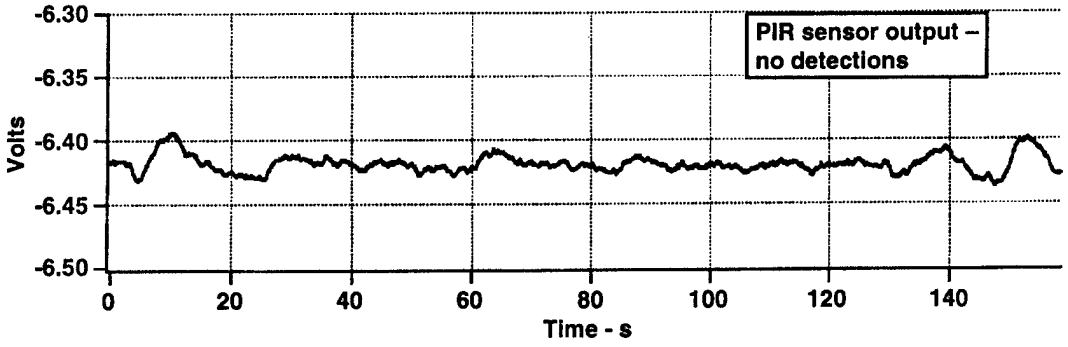

Figure 4.73
Passive infrared sensor output (no detections).

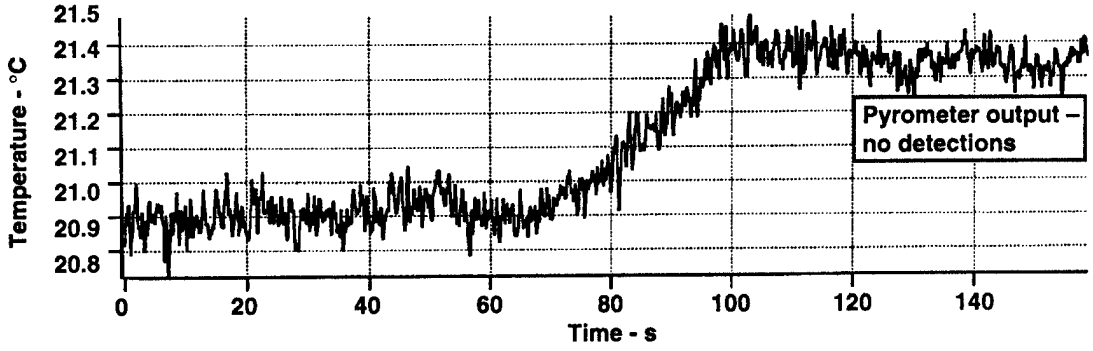

Figure 4.74
Pyrometer output (no detections).

Exterior sensor test with target at 200-ft range. The reflector antenna is used with the PMMW sensor. Pyrometer and unfiltered PMMW outputs are smoothed with 1.4-s triangle filter.

ARL:UT
AS-97-137
RLR - rfg
4-97

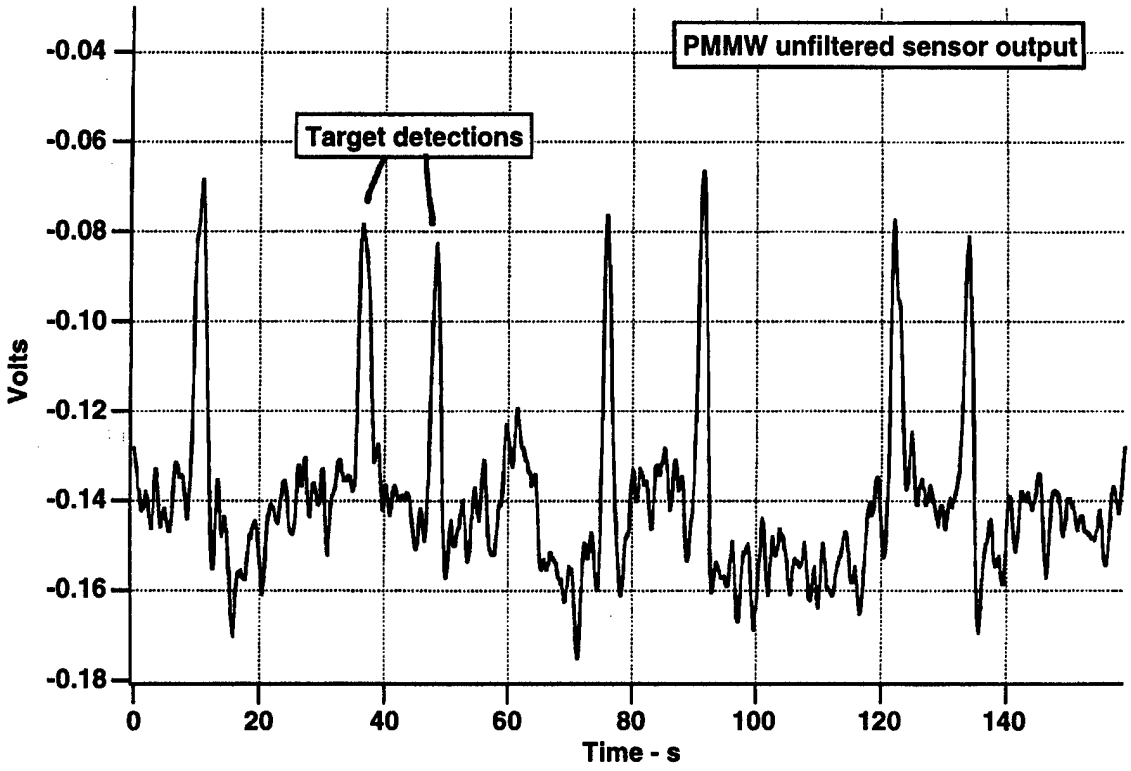

Figure 4.75
Passive millimeter wave sensor unfiltered output – ac-coupled with 200-s time constant. Target detections are positive-going spikes.

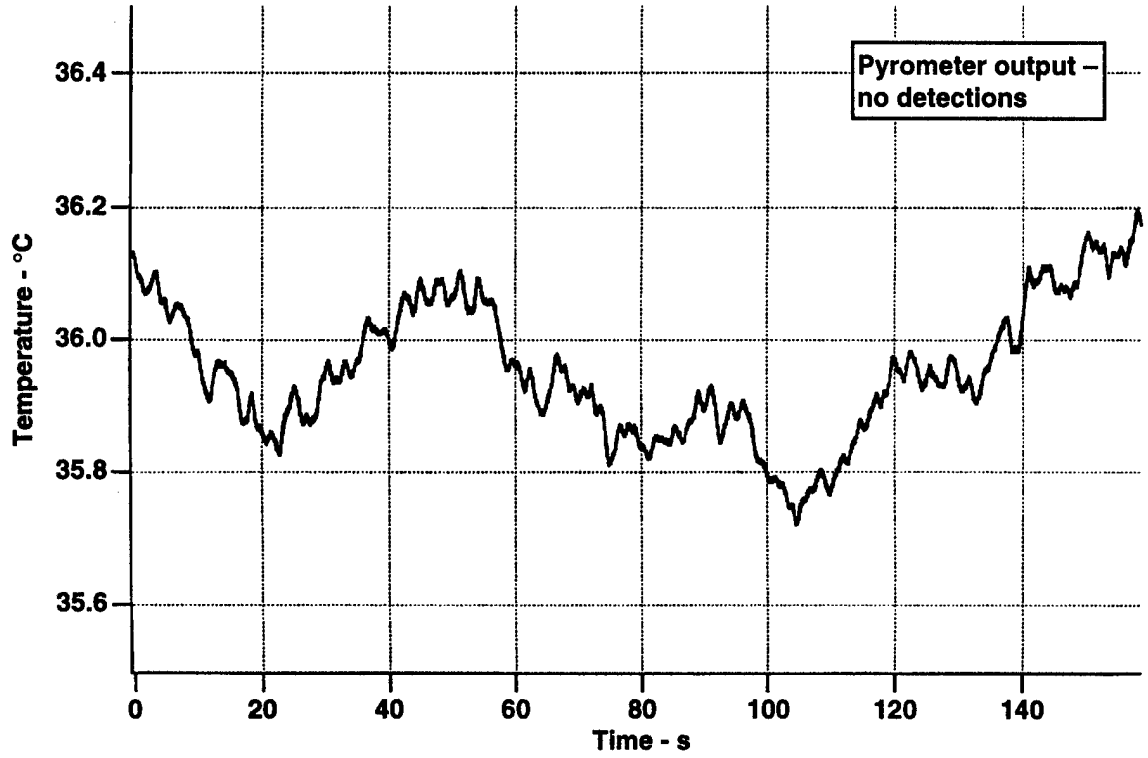

Figure 4.76
Pyrometer output (no detections).

Exterior sensor test with target at 200-ft range and ambient temperature at 99°F, 36°C. The lens antenna is used with the PMMW sensor. Pyrometer and unfiltered PMMW outputs are smoothed with 1.4-s triangle filter.

ARL:UT
AS-97-138
RLR - rfg
4-97

Although the ultimate range of this sensor in an exterior environment appears to be considerably greater than that of the infrared sensor, it is difficult to predict with this limited data what the maximum usable limit will be. The sensor itself can be improved considerably, but the actual range at which reliable detections can be made in the complex exterior environment depends on many factors that need further investigation. Tables 4.5 and 4.6 show the differences in performance between the PMMW sensor and the PIR sensor. From Table 4.5, we can see that the PMMW sensor makes reliable detections even at the 200-ft range. If we again use the criteria that we want a P_d of 0.9 with a maximum P_f of 10^{-7}, we see from Table 4.5 and the ROC curves in Fig. 3.4 that, even at 200 ft, the PMMW sensor can detect a target with an SNR value well in excess of the required SNR value of 5. In fact, the SNR value is 9.8, which is nearly double the SNR value required.

4.6 SUMMARY OF RESULTS

The results of these tests show superior performance by the PMMW sensor in an exterior environment. The PIR sensor performed better in the interior environment while the target was at a normal walking speed and was taking no evasive measures. On the other hand, the PMMW sensor performed better when the target was trying to avoid detection either by running, by putting on heavy clothing, or by blocking the sensor with material such as Styrofoam.

Table 4.5
Exterior PMMW detection at 23°C ambient temperature.

Range	RC high-pass filter with only 0.001-Hz corner freq.	SNR
100 ft	0.320 V	25.0
160 ft	0.170 V	13.0
200 ft	0.128 V	9.8

Table 4.6
Probability of false alarm for PIR exterior detections with the threshold set to the signal level (23°C ambient temperature).

Range	Signal strength	SNR
100 ft	No observable signal	0
160 ft	No observable signal	0
200 ft	No observable signal	0

This page intentionally left blank.

5. CONCLUSIONS

This report documents the development and test of a passive millimeter wave sensor (PMMW). The PMMW sensor prototype fabricated in this work showed definite advantages over the current passive infrared (PIR) sensors. Test results showing superior performance were obtained in five areas:

(1) Superior detection range was demonstrated by the PMMW sensor in the exterior environment; detection ranges of 200 ft with high SNRs were achieved (SNR > 9).

(2) The PMMW sensor is not affected nearly as strongly as is the PIR sensor by exterior environmental fluctuations; detection ranges of 200 ft were achieved even in ambient temperatures of 37°C (99°F).

(3) The PMMW sensor demonstrated the ability to sense targets through clothing as well as wall materials such as Sheetrock, plywood, and Styrofoam.

(4) The PMMW sensor demonstrated the ability to sense through heavy clothing, and hence sense the whole body; this is an important advantage for long range detection.

(5) The PMMW sensor demonstrated superior response time to a target moving rapidly across the field of view of the sensor.

The tests were conducted comparing a high quality intrusion detection PIR sensor, an infrared pyrometer, and the PMMW sensor. It is important to note that the infrared sensors were not low cost sensors. The PIR intrusion sensor cost more than $300, and the pyrometer was about $500. The PMMW sensor that was used for these tests was made from the inexpensive printed circuit board technology and will allow production of low cost sensors when made in quantity. The estimated cost of these sensors is in the $100 to $500 price range, depending on the sensor parameters. In addition, it was demonstrated that the total power radiometer is a valid mode of operation for this type of sensor. The PMMW sensor made good target detections when the PIR sensor made good target detections. In addition to the superior exterior performance, the PMMW sensor, as previously stated, made better detections when evasive techniques were being used against PIR sensors. At close ranges (inside the metal building during the short range tests), the PIR sensor had a higher SNR, provided that no evasive measures were being used. However, for the longer range tests, and

especially in the exterior environment, the PMMW sensor made detections where the PIR sensor did not. Because of the different phenomenologies of the PMMW and PIR sensors, it may be possible for colocated sensors to discriminate between different types of targets, such as humans and animals, and to reduce the nuisance alarm rates of the system.

A factor in assessing the cost of covering an area with a PMMW sensor is how much area coverage is available for a given sensor. A security sensor must cover a certain area to be useful for locating intruders. The PIR sensor used in this test had the usual fan-type lens pattern, which produces a number of fingers pointing in different directions. This is a good pattern for covering a room or a wide open area. Unfortunately, the antennas that we had for the sensor were single beam antennas and were not designed, as the PIR lens was, to provide good "trip wire" coverage over a large area. As can be seen in the data, the standard gain horn, which has a moderately wide beam, had about half as strong a signal as the reflector antenna. The PIR lens, in contrast, forms a number of widely spaced narrow beams, which are focused on the pyroelectric element. This allows a large area to be covered while not causing the total beam width to be so large that the sensitivity is compromised.

The same technique could be used for the PMMW sensor. It is conceivable to design and build at low cost an antenna that produces a "lobed" beam pattern, which would have an effect similar to that of the lens on the PIR sensor.[13] This will allow several narrow beams to be focused over a large area without requiring that the antenna beam be continuous across the area, which would be undesirable because the target needs to cause the signal to go up and down as it moves through the beams. The patterns that can be produced by millimeter wave antennas will have somewhat broader beams, but they should be acceptable for this application.

The future development of this sensor will need to focus on the packaging and the choice of sensor parameters for the desired application. Some further work is also needed to refine the down-converter module and improve its performance. It will be especially important to determine the frequency of operation because the penetration ability, detection ability, and false alarm performance of the sensor will all be affected by this factor. Fortunately, because

millimeter wave propagation is primarily by line-of-sight and so much spectrum is available at millimeter wave frequencies, electronic interference of the sensor is not expected to be a major problem, even as millimeter wave systems become more numerous. It should be possible to equip the sensor with a filtering circuit that will prevent the sensor from indicating an alarm if it is detecting an rf signal from a radar or a communications transmitter. The circuit could also trigger an indicator that the sensor is detecting electronic interference.

The test results shown in this report indicate that the PMMW sensor is an effective and covert interior sensor, which can provide the capabilities of sensing through walls, sensing through heavy clothing, and sensing rapidly moving targets. Our tests also show that the PMMW sensor will be an extremely effective exterior detection sensor, which may provide good performance even under conditions in which conventional infrared sensors do not function well.

This page intentionally left blank.

REFERENCES

1. N. Nagano et al., "Monolithic Ultra-Broadband Transimpedance Amplifiers Using AlGaAs/GaAs Heterojunction Bipolar Transistors," IEEE Trans. Microwave Theory Tech., **42**(1), 2–10 (Jan. 1994).

2. Huei Wang et al., "Monolithic V-Band Frequency Converter Chip Set Development Using 0.2 mm AlGaAs/InGaAs/GaAs Pseudomorphic HEMT Technology," IEEE Trans. Microwave Theory Tech., **42**(1), 11–17 (Jan. 1994).

3. W. G. Fink, "Intelligent Transportation Systems," IEEE Microwave and Millimeter Wave Monolithic Circuits Symposium Digest, Orlando, Florida, 3 (May 1995).

4. M. P. Pavio, "Low-Cost High-Volume RF Products: Dream, Anticipation, or Reality?," IEEE Microwave and Millimeter Wave Monolithic Circuits Symposium Digest, Orlando, Florida, 7-10 (May 1995).

5. T. Otsuji, Y. Imai, and E. Sano, "Lightwave Communication ICs beyond 10 Gb/s - Design and Measurement Challenges," IEEE Microwave and Millimeter Wave Monolithic Circuits Symposium Digest, Orlando, Florida, 11–14 (May 1995).

6. R. L. Rogers, "Passive Millimeter Wave Sensors for Security Applications," Applied Research Laboratories Technical Report No. 91-15 (ARL-TR-91-15), Applied Research Laboratories, The University of Texas at Austin (1991).

7. F. T. Ulaby, R. K. Moore, and A. K. Fung, *Microwave Remote Sensing: Active and Passive*, Vol. 1 (Addison-Wesley, 1981).

8. N. Skou, *Microwave Radiometer Systems: Design and Analysis* (Artech House, Dedham, Massachusetts, 1989).

9. R. H. Dicke, "The Measurement of Thermal Radiation at Microwave Frequencies," Review of Scientific Instruments, **17**(7), 268–275 (1946).

10. R. K. Hoffman, *Handbook of Microwave Integrated Circuits* (Artech House, Norwood, Massachusetts, 1987), pp. 351-388.

11. S. A. Maas, *Microwave Mixers*, 2nd ed. (Artech House, Boston, Massachusetts, 1993), pp. 176–180.

12. H. L. Van Trees, *Detection and Estimation and Modulation Theory, Part 1* (John Wiley and Sons, New York, 1968), pp. 17–45.

13. A. Ip and D. R. Jackson, "Radiation from Cylindrical Leaky Waves," IEEE Trans. Antennas Prop., **38**(4), 482–488 (April 1990).

14. C. D. Govan, "A Wide-Band Frequency-Tunable Dicke Radiometer and Microwave Radiometric Measurements," Applied Research Laboratories Technical Report No. 95-9 (ARL-TR-95-9), Applied Research Laboratories, The University of Texas at Austin (1995).

15. G. I. Torgovnikov, *Dielectric Properties of Wood and Wood-Based Materials* (Springer-Verlag, Berlin, 1993).

15 April 1997

DISTRIBUTION LIST
ARL-TR-97-3
Final Report under Contract N00039-91-C-0082,
TD No. 04A1003, Passive Millimeter Wave Sensor

Copy No.	
	Defense Special Weapons Agency 6801 Telegraph Road Alexandria, VA 22310-3398
1 - 2	Attn: ISST
3 - 5	OPSFPS
6	OPS
7	OPO
	Defense Technical Information Center 8725 John J. Kingman Rd., STE 0944 Ft. Belvoir, VA 22060-6218
8 - 9	Attn: DTIC/OCP
	Office of Assistant Secretary of Defense Pentagon Washington, DC 20301
10	Attn: ODASD (I&S) (CI & SP)
	Commander-in-Chief U.S. Central Command MacDill Air Force Base, FL 33608-7001
11	Attn: CCJ3
12	CCPM
	Headquarters U.S. European Command Unit 30400, Box 1000 APO AE 09128
13	Attn: ECJ5D
	Under Secretary of Defense (ACQ) 3140 Defense Pentagon Washington, DC 20301-3140
14	Attn: ODDR&E/S&TS/LW

Distribution List for ARL-TR-97-3 under Contract N00039-91-C-0082, TD No. 04A1003 (cont'd)

Copy No.

	Director U.S. Nuclear Command and Control System Support Staff Skyline #3, Suite 500 5201 Leesburg Pike Falls Church, VA 22041-3202
15	Attn: LTCOL David S. Powell
	Defense Advanced Research Project Agency 3701 North Fairfax Drive Arlington, VA 22203-1714
16	Attn: EAO
17	STO D Flank
18	Library
	Headquarters Department of the Army 4401 Ford Ave., Suite 225 Alexandria, VA 22302-1432
19 - 20	Attn: DAMO-ODL-S
	Director Night Vision and Electronic Sensors Directorate Physical Security Equipment Attn: AMSEL-RD-NV-TIS-PS 10221 Burbeck Road Fort Belvoir, VA 22060-5806
21	Attn: AMSAT-D-WCP
	Commander U.S. Army Military Police School Fort McClellan, AL 36205
22	Attn: ATZN-MP-TS
23	ATZN-MP-CD
24	ATZN-MP-DE
25	ATZN-MP-TB

Distribution List for ARL-TR-97-3 under Contract N00039-91-C-0082, TD No. 04A1003 (cont'd)

Copy No.

	Commander U.S. Army Nuclear and Chemical Agency 7150 Heller Loop Suite 101 Springfield, VA 22150-3198
26	Attn: MONA-SU
	CNO (NO9N3) 901 M Street SE Bldg. 111, WNY Washington, DC 20388-5024
27	Attn: Code 24B
	Naval Facilities Engineering Services Center 560 Center Drive Port Hueneme, CA 93043-4328
28	Attn: ESC66
	Naval Surface Warfare Center Bldg. 300, Hwy. 362 Crane, IN 47522
29	Attn: Code 2064/Larry D. Hembree
	Director Office of Chief Naval Operations 2000 Navy Pentagon Department of the Navy Washington, DC 20350-2000
30	Attn: NO9N
	Commander Space and Naval Warfare Systems Command 2451 Crystal Drive Arlington, VA 22245-5200
31	Attn: PME-121-3
	Commander in Chief U.S. Atlantic Command Norfolk, VA 23511
32	Attn: J324

Distribution List for ARL-TR-97-3 under Contract N00039-91-C-0082, TD No. 04A1003 (cont'd)

Copy No.

Headquarters
U.S. Marine Corps
Washington, DC 20390
33 Attn: POS-30
34 POS-20
35 POS-16

Air Force Materiel Command
Wright-Patterson AFB, OH 45433
36 Attn: AFMC/SP

Department of the Air Force
Washington, DC 20330
37 Attn: AF/RDST

Headquarters
Electronic Systems Division
Hanscom AFB, MA 01731
38 Attn: AVJR

HQ ACC/SP
Department of the Air Force
220 Sweeney Blvd.
Suite 112
Langley AFB, VA 23665-2796
39 Attn: HQ ACC/SP

Military Airlift Command AMC/SP
Scott AFB, IL 62225
40 Attn: SP

Headquarters
PACAF/LGWSN
Hickam AFB, HI 96853-5001
41 Attn: SP

Headquarters
USAF/SF
Pentagon, Room BF939B
Washington, DC 20330-5100
42 Attn: USAF/SFO
43 USAF/SFX

Distribution List for ARL-TR-97-3 under Contract N00039-91-C-0082, TD No. 04A1003 (cont'd)

Copy No.

Headquarters
USAFE/SP
APO New York 09094-5001
44 Attn: USAFE/SPP
45 USAFE/SPO

Department of Energy
GTN
Washington, DC 20545
46 Attn: DASMA, DP-20
47 NN-513.4

Sandia National Laboratories
Attn: Mail Services
P.O. Box 5800
Albuquerque, NM 87185-0459
48 Attn: J. W. Kane/MS 0768

Computer Science Corporation
7405 Alban Station Court
Suite B200
Springfield, VA 22150-2318
49 Attn: Richard A. Swanson

Kaman Sciences Corporation
Attn: FCDSWA/DASIAC
1680 Texas Street, SE
Kirtland AFB, NM 87117-5669
50 Attn: DASIAC

Vitro Corporation
4002 Lincoln Drive West
Marlton, NJ 08503
51 Attn: Thomas J. Whittle

The University of Texas Pan-American
Engineering Department
1201 W. University Dr.
Edinburg, TX 78539
52 Attn: Heinrich D. Foltz

53 David L. Fisher, ARL:UT

Distribution List for ARL-TR-97-3 under Contract N00039-91-C-0082, TD No. 04A1003 (cont'd)

Copy No.	
54	John M. Huckabay, ARL:UT
55	Robert L. Rogers, ARL:UT
56	Library, ARL:UT
57 - 67	Reserve, Advanced Sonar Division, ARL:UT